Reaction Kinetics, Catalyst Development, and Reaction Networks for Hydrothermal Hydrodeoxygenation

by

Jacob G. Dickinson

A dissertation submitted in partial fulfillment
of the requirements for the degree of
Doctor of Philosophy
(Chemical Engineering)
in the University of Michigan
2014

Doctoral Committee:

Professor Phillip E. Savage, Chair
Associate Professor Suljo Linic
Professor Melanie S. Sanford
Professor Levi T. Thompson

To my fiancé, Chloe

Acknowledgements

This dissertation would not have been possible without the guidance, support, and input from many people.

I would like to thank my family for their support during my graduate studies. My fiancé Chloe, has been a fantastic partner during this journey. She has always helped me keep a healthy perspective on graduate school. My brother, George, and sister-in-law, Kyle, have also made my time in graduate school significantly more enjoyable. Last, my parents, Chris and Sharon, were critically important in my completion of this degree. Beyond their support, they often provided sage advice. For example, when picking an advisor, my Dad suggested choosing the person I thought I would work with the best, rather than picking an advisor based on the projects being offer. This is fantastic advice, and I am fortunate to have received it and followed it.

My father's advice led me to working with Phil Savage. I am extremely gratefully for his guidance throughout graduate school. As an advisor, Phil managed to strike a great balance between allowing me the freedom to think and test my own ideas, while teaching and guiding me through the process. Phil has two qualities, in particular, that I would be proud to emulate. First, he was never the rate-limiting step in my work. If I needed a piece of lab equipment or a chemical, I was always told to just order it. When I was writing a paper, Phil never took more than a few days to edit it, and editing my papers was often no small task. Second, Phil encourages an active debate and lively discussion. This includes disagreeing with his ideas. He was always willing to share his perspective and ideas on a subject, and work with me on pursuing the best path forward.

Additionally, members of the Savage lab were instrumental in my completion of this degree. There are too many to name, but, in particular, I would like to thank Peter Valdez and Thomas Yeh. Peter was always helpful troubleshooting issues in the lab and bouncing ideas off of. Also, I truly enjoyed the time Peter and I spent in our office discussing work, politics, or the latest internet craze. Thomas was especially helpful when discussing catalysis questions and helping perform catalyst characterization, such as TEM. Thomas always has a way of keeping the mood light and making me laugh.

My greatest surprise in graduate school was the spectacular friends I made. I have lived with Nick Cilfone and Alex Thompson for more than three years and I have enjoyed every minute of it. Their wit, humor, and generally childish behavior were a welcome relief after a long day. Without their help and friendship, I would have struggled greatly during graduate school. Phil Christopher, Ramsey Zeitoun, Mike Nelson, and Adam Holewinski were also great friends during grad school.

I would like to thank the departmental support staff. In particular, Kelly Raickovich, Susan Hamlin, Claire O'Connor, and Laurel Neff were always beyond helpful when issues arose. Without their help I would have spent a great deal of time dealing with daily administrative tasks rather than completing the work required for my degree.

I thank the National Science Foundation for a graduate research fellowship and grant EFRI-0937992 which provided the financial support to make this work possible.

Table of Contents

List of Figures

List of Tables

Abstract

This dissertation examines issues related to producing a hydrocarbon biocrude from wet algal biomass. It first reports on the hydrothermal liquefaction (HTL), a high-temperature (>250 °C) and high-pressure (>40 bar) aqueous treatment, of *Nannochloropsis* sp. to produce a bio-oil. Determining the elemental and molecular composition of the bio-oil, aqueous, gaseous, and solid products produced by HTL at 350 °C revealed how these product compositions are affected by the choice of solvent used to extract the bio-oil. Hexadecane and decane provided the highest gravimetric yields of bio-oil (39 wt% each). Furthermore, quantifying 19 individual molecular components in the bio-oil showed that many of the heteroatoms (N, S, and O) were present in free fatty acids and heterocyclic molecules.

The removal of oxygen from the bio-oil increases the energy density and stability of the oil, while decreasing the viscosity. Studying the effect of process variables on hydrothermal hydrodeoxygenation (HDO) of benzofuran over Pt/C at 380 °C provided the reaction network and kinetics for benzofuran HDO. The kinetic analysis revealed that benzofuran had an inhibitory effect on the dehydration of ethylphenol to ethylbenzene.

Studying the hydrothermal HDO of o-cresol in a flow reactor at 380 °C showed that Pt/C, Raney Ni, and 10 wt% Raney NiCu were stable under the hydrothermal reaction conditions, but only Pt/C and Raney NiCu were selective for the production liquid hydrocarbons. The Raney NiCu catalyst increased the liquid hydrocarbon yield by a factor of 3.4 when compared with the unmodified Raney Ni.

Raney NiCu catalysts doped with more than 10 wt% Cu showed a significant decrease in gasification activity and an increase in liquid oxygenated products, but no

change in the desired liquid hydrocarbons. The addition of acid sites to the NiCu catalysts, either by supporting NiCu on Al_2O_3 or by calcining the Raney Ni catalyst to convert Al in the catalyst to Al_2O_3, increased the liquid hydrocarbon yield significantly. In flow reactions, two catalysts, calcined 5% Raney NiCu and 10%, 0.5% NiCu/Al_2O_3, achieved a high (~70%) and stable yield of liquid hydrocarbons. These catalysts provided the highest known stable yields of liquid hydrocarbons for hydrothermal HDO.

Chapter 1

Introduction

This chapter provides a broad and general introduction to the field of biofuels. This includes a discussion about the need for biofuels, the biomass feedstocks used, and the conversion technologies employed.

1.1 The need for biofuels

Biofuels are fuels that can replace fuels refined from petroleum with little or no change to the current energy infrastructure and are derived from renewable biomass. It is essential that biofuels are fungible for petroleum-derived fuels because of the significant infrastructure present worldwide for the processing, transportation, and consumption of petroleum. Through the years, proponents of biofuels have cited numerous reasons for their development. At present, in the United States, the primary drivers of biofuel development are renewable fuel standards. These renewable fuel standards were developed and implemented to reduce CO_2 emissions from fuels and to develop a domestic energy source. The rapid growth of shale gas since the mid 2000's and a stable supply of heavy crude oil from Canada have eliminated many concerns of an unstable supply of petroleum. Therefore, the current goals of the renewable fuel standards are to reduce green house gas emissions, such as CO_2. Predictions of future biofuel market penetration are difficult, but in 2011 the U.S. Energy Information Administration projected that biofuels

would account for 11% of the U.S. supply of transportation fuels by 2035 [1] and the 2013 outlook predicted a roughly 75% increase in biofuel production by 2040 when compared with 2011 [2].

1.2 Biomass feedstocks

A diverse array of biomass feedstocks are used to produce biofuels and renewable chemicals. First-generation biofuels are produced from easily transformable biomass sources such as corn (i.e., sugars) and soybeans (i.e., oils). Biofuels produced from these crops have come under scrutiny for several reasons. First, in general, first-generation biofuel feedstocks are food crops. The production of biofuels from food crops can decrease the supply of these crops, thereby increasing the price. This is often referred to as the "fuel vs. food" controversy. Second, first-generation biofuels require arable land, fresh water, and fertilizer to grow. Recent research suggests that land use change, (i.e., converting grasslands and forests into farmland to produce biomass feedstocks) can potentially increases the greenhouse gas emissions when compared to burning petroleum [3].

Second-generation biofuels address many of these concerns by using lignocellulosic biomass feedstocks such as wood and agricultural wastes to minimize the effects of land use change and food competition. Unfortunately, the conversion of second-generation biomass into usable fuels is significantly more complicated than the conversion of first-generation biomass. The conversion of second-generation biomass into fuels will be discussed in more detail in section 1.3.

Third-generation biofuels are typically derived from microalgae and are in the early stages of development. Microalgae based biofuels have several major advantages over first-

and second-generation biofuels. Microalgae have high growth rates, can grow in a variety of water sources, have a limited food versus fuel controversy, and do not require arable land for growth. Even with these benefits, several major challenges remain to producing commercially viable algal biofuels such as selecting an efficient bioreactor, developing a high yield microalgal strain, efficiently providing CO_2 for growth, and converting the microalgae into bio-oil [4, 5].

1.3 Biomass conversion

Upon the growth and collection of biomass, a conversion technology must be employed to break down the biomass macromolecules into fuel range molecules. The most common conversion technologies are fermentation, gasification, pyrolysis, and hydrothermal liquefaction (HTL). Fermentation is the use of yeast or bacteria to produce ethanol or higher alcohols from sugars, while gasification is the thermal decomposition of biomass into gaseous products. Gasification produces gasses that can be directly combusted or processed further via Fischer-Tropsch synthesis to liquid fuels. Both of these processes are active areas of research.

Pyrolysis is a biomass liquefaction technique where dry biomass is rapidly (< 5 s) heated to ~500 °C to produce a bio-oil. Pyrolysis is commonly used on dry lignocellulosic biomass to produce a mixture or solution of bio-oil and water (20-30 wt%). Typical pyrolysis bio-oils have a high viscosity (30-200 cp.) and a low higher heating value (~22.5 MJ/kg) because of their high oxygen content (45 wt%).

Hydrothermal liquefaction (HTL) is a high-temperature (~350 °C) and high-pressure (~165 bar) aqueous phase processing technique to valorize biomass. HTL is best

suited for high moisture content biomass, such as microalgae, because HTL obviates the biomass-drying step necessary in pyrolysis. Elimination of the biomass-drying step significantly reduces the energy inputs necessary to process the biomass into fuel. HTL of microalgae has received significant attention in literature recently. In general, HTL of microalgae produces a bio-oil (~10 wt%) and water (~90 wt%) mixture that can be difficult to separate due to the hydrophilic nature of the oxygen (5-15 wt% of the bio-oil) containing functional groups [6]. Nonetheless, this bio-oil is energy dense (~35 MJ/kg) and transfers the majority (50-65%) of the carbon from the microalgae to the bio-oil [7]. Between 15 and 40 wt% of the carbon from the microalgae resides in the aqueous phase [7, 8].

1.4 Hydrodeoxygenation

Hydrodeoxygenation (HDO) is an enabling technology for the production of fuels from biomass because HDO reduces the viscosity and increases the energy density and stability of bio-oils, making them a more suitable drop-in replacement for petroleum. [9-11]. HDO is a catalytic process, shown in fig. 1.1, where hydrogen is used to remove oxygen from organic molecules as water.

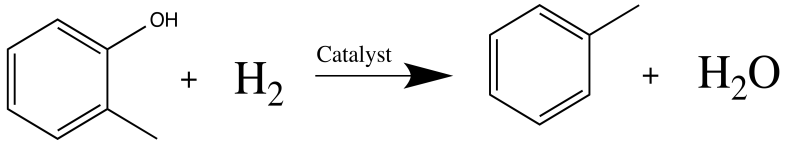

Figure 1.1. Example HDO reaction.

HDO is not used in the oil refining industry because crude oils have a low oxygen content, therefore a significant need exists to develop and optimize this process for bio-oil upgrading. HDO is analogous to other hydrotreating techniques such as

hydrodenitrogenation (HDN) and hydrodesulfurization (HDS) that are currently used in refineries to remove smog- and acid-rain-forming nitrogen and sulfur atoms from refined products. The typical operating conditions for HDN and HDS reactions are ~350 °C and ~30 bar with the reaction occurring over NiMo or CoMo catalysts supported on γ-Al_2O_3 [12].

1.5 Research scope and proposed work

HDO is presently and historically an active area of research. The first reports of HDO arrived from a desire to upgrade coal-derived liquids to petroleum-like transportation fuels [9]. More recently, HDO has focused on upgrading bio-oils from the fast pyrolysis of lignocellulose and the HTL of microalgae to drop-in replacement transportation fuels [10, 13-15]. The majority of HDO studies have examined vapor-phase reactions without water present. As was detailed in section 1.3, however, water is present in the reactor effluent after the initial liquefaction process is applied. Furthermore, even if the bio-oil is completely dewatered prior to HDO, the HDO reaction will produce water, as shown in fig. 1.1. Reaction stoichiometry indicates that HDO of a bio-oil containing 15 wt% oxygen prior to the reaction will form a bio-oil and water mixture containing 17 wt% water upon complete HDO. Therefore, water will be present, likely in high quantities during HDO.

HDO occurring in a high temperature aqueous (i.e., hydrothermal) environment has received relatively little attention in literature. Many common hydrotreating catalysts such as NiMo and CoMo oxidize under hydrothermal conditions [16], and common catalyst supports such as γ-Al_2O_3 and SiO_2 may be unstable under some hydrothermal conditions

[16-18]. Therefore, active and stable alternative catalysts must be developed and studied for use in hydrothermal HDO.

In addition to the development of hydrothermal HDO catalysts, the reaction networks and kinetics of active and stable hydrothermal HDO catalysts must be determined to provide information on product yields and selectivities. Determining catalytic reaction networks and kinetics for hydrothermal HDO also provides insights into rate limiting steps that can further spur catalyst development.

Last, work also must be performed to determine the molecular and elemental composition of bio-oils from the HTL of microalgae. As noted in sections 1.2 and 1.3, microalgal HTL bio-oils represent a new and active area of research that holds significant promise. Determining the composition of HTL microalgal bio-oils will ensure that the research performed on hydrothermal HDO is applicable to both pyrolysis bio-oils and microalgal HTL bio-oils.

The following chapters provide extensive background information on the objectives discussed above and discuss the progress made toward advancing these objectives. Chapter 2 provides background information on the molecular composition of bio-oils and the catalysts and reaction conditions used to upgrade these bio-oils. Chapter 3 outlines the materials, experimental methods, and reactors used throughout this dissertation. Chapter 4 discusses the work performed to understand the elemental and molecular makeup of microalgal bio-oils, and how the experimental methods used to obtain these oils affects their composition. Chapter 5 discusses the hydrothermal HDO of benzofuran, a model oxygenated molecule, and the associated reaction kinetics over Pt/C. Chapter 6 presents the results from testing the stability of Ni- and Pt-based catalysts for hydrothermal HDO of

o-cresol in a flow reactor. Chapter 7 provides an extensive analysis of the most promising catalysts from chapter 6, Raney NiCu, and discusses how yields and selectivities of this catalyst can be increased. Chapter 8 analyzes of the impacts of this dissertation and provides a description of further research areas that may provide impactful results.

References

1. U. S. E.I.A., Department of Energy (2011)
2. U. S. E.I.A., Department of Energy (2013)
3. T. Searchinger, R. Heimlich, R. A. Houghton, F. Dong, A. Elobeid, J. Fabiosa, S. Tokgoz, D. Hayes, T.-H. Yu, Science 319, (2008) 1238-1240.
4. P. E. Savage, J. A. Hestekin, Environmental Progress & Sustainable Energy 32, (2013) 877-883.
5. Y. Chisti, J. Biotechnol. 167, (2013) 201-214.
6. T. M. Yeh, J. G. Dickinson, A. Franck, S. Linic, L. T. Thompson, P. E. Savage, J. Chem. Technol. Biotechnol. 88, (2013) 13-24.
7. P. J. Valdez, J. G. Dickinson, P. E. Savage, Energy Fuels 25, (2011) 3235-3243.
8. D. C. Elliott, T. R. Hart, A. J. Schmidt, G. G. Neuenschwander, L. J. Rotness, M. V. Olarte, A. H. Zacher, K. O. Albrecht, R. T. Hallen, J. E. Holladay, Algal Research 2, (2013) 445-454.
9. E. Furimsky, Appl. Catal. A: Gen. 124, (2000) 470-477.
10. E. Furimsky, Catal. Today 217, (2013) 13-56.
11. H. Wang, J. Male, Y. Wang, ACS Catal. 3, (2013) 1047-1070.
12. R. Prins, Adv. Catal. 46, (2001) 399-464.
13. P. Duan, P. E. Savage, Appl. Catal. B: Environ. 104, (2011) 136-143.
14. P. Duan, P. E. Savage, Energy Environ. Sci. 4, (2011) 1447-1456.
15. P. Duan, P. E. Savage, Bioresour. Technol. 102, (2011) 1899-1906.
16. D. C. Elliott, L. J. Sealock Jr, E. G. Baker, Ind. Eng. Chem. Res. 32, (1993) 1542-1548.
17. R. M. Ravenelle, J. R. Copeland, W.-G. Kim, J. C. Crittenden, C. Sievers, ACS Catal. 1, (2011) 552-561.
18. J. Yu, P. E. Savage, Appl. Catal. B: Environ. 31, (2001) 123-132.

Chapter 2

Background

This chapter provides detailed background information about the composition of bio-oils, the HDO of benzofuran, a model oxygenated compound, and hydrothermal HDO. These detailed sections are followed by an analysis of the gaps in the literature to provide a context for the original work presented in chapters 4-7.

2.1. Composition of bio-oils

As introduced in chapter 1, bio-oils are produced from a variety of biomass sources and liquefaction techniques. Herein, we focus on two common bio-oil types: pyrolysis bio-oils from lignocellulosic sources and HTL bio-oils from microalgae. As will be shown later, these bio-oils contain similar characteristics that allow one, with careful selection of catalysts, reaction environment, and reactants, to conduct studies applicable to the upgrading of both types of bio-oil.

2.1.1. Pyrolysis bio-oils

Pyrolysis, or fast pyrolysis, is a liquefaction technology for the conversion of biomass, typically dry lignocellulosic biomass, into a bio-oil, that with additional treatment, can substitute for petroleum crude oil. Pyrolysis is typically performed between 450-

550 °C with short residence times of 0.5-5 s [1]. The liquid product from pyrolysis is high in water and oxygen content, as shown in table 2.1.

Table 2.1. Typical characteristics of pyrolysis bio-oils [1, 2].

Water content	20-30 wt%
pH	~2.5
Specific gravity	~1.20
Elemental analysis (moisture free, wt%)	
C	44-58%
H	5.5-7%
N	0-0.2%
S	<0.1%
O	35-40%
Ash	0-0.2%
Higher Heating Value (HHV)	22.5 MJ/kg
Viscosity (40 °C)	30-200 cp

The high oxygen content of these bio-oils results in a HHV of only 22.5 MJ/kg (Table 2.1). This value is low compared with the 45 MJ/kg HHV of crude oil, making pyrolysis bio-oils undesirable for standard refinement into transportation fuels. Furthermore, the high oxygen content of pyrolysis bio-oils makes them unstable for storage and potentially reactive during distillation [3]. The high oxygen content and resulting instability of pyrolysis bio-oils is due to the presence of primarily phenols, guiacols, furans, and esters [3, 4]. Examples of these molecules are shown in fig. 2.1. Table 2.1 and fig. 2.1 show the need for HDO of pyrolysis bio-oils to produce renewable, drop-in replacement bio-oils for petroleum because HDO will result in an oil with an increased HHV and stability [3, 5, 6].

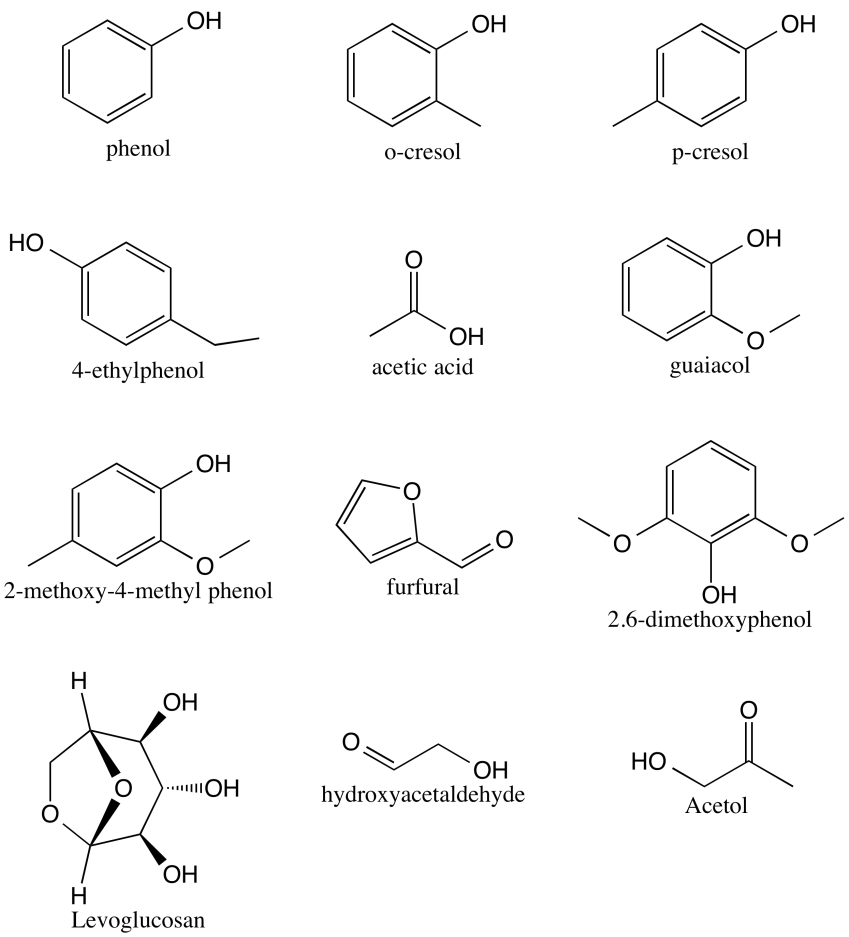

Figure 2.1. Common products in pyrolysis bio-oils [3, 4].

2.1.2 HTL bio-oils from microalgae

Unlike pyrolysis bio-oils, which were studied extensively, the elemental and molecular composition of microalgal bio-oils was not well known when this dissertation began. Since the start of this dissertation, many researchers have studied the effects of process variables, catalysts, and extraction procedures on the composition of microalgal bio-oils [7-24]. Below we provide an overview of these studies, but we note that work

presented in chapter 4, which studies the yield and composition of microalgal bio-oils, predates most of them.

HTL treats wet biomass (~20 wt% solids, ~80 wt% water) between 250 and 370 °C and at pressures exceeding the saturation pressure (40-210 bar) of water so that the majority of the water in the reactor remains in the liquid state. The typical properties of the bio-oil resulting from the HTL of microalgae are shown in table 2.2.

Table 2.2. Typical property ranges of microalgal bio-oils produced from HTL.

HTL reactor effluent	10-20 wt% bio-oil 80-90 wt% aqueous phase
Elemental analysis of microalgal bio-oils (wt%)	
C	70-75%
H	8-10%
N	5-7%
S	0.5-1.5%
O	5-20%
Bio-oil yield (g bio-oil/g solids loaded)	20-45%
HHV	33-37 MJ/kg
Viscosity (60 °C)	40-60 cP
Energy recovery to bio-oil	60-80%

Comparing the bio-oil properties between tables 2.1 and 2.2 reveals that microalgal bio-oils have a higher carbon, hydrogen, nitrogen and sulfur content than pyrolysis bio-oils and a lower oxygen content. These changes in elemental composition result in a HHV for microalgal bio-oils that is 10-15 MJ/kg higher than for pyrolysis bio-oils. This higher HHV is primarily a function of the lower oxygen content of these oils.

The molecular composition of microalgal bio-oils varies primarily based on the feedstock and conditions used for HTL. Fig. 2.2 shows common products in these bio-oils.

In general, the oxygen containing molecules are free fatty acids and phenols, and the nitrogen containing molecules are indoles, pyrroles, and long chain amides. Comparing the oxygen containing products in figs. 2.1 and 2.2 reveals that both bio-oils contain a variety of phenolic molecules, but the microalgal bio-oils do not contain a significant fraction of guaiacols. Furthermore, the microalgal bio-oils contain free fatty acids and nitrogen containing products, while these products did not appear in significant yields in the pyrolysis bio-oils.

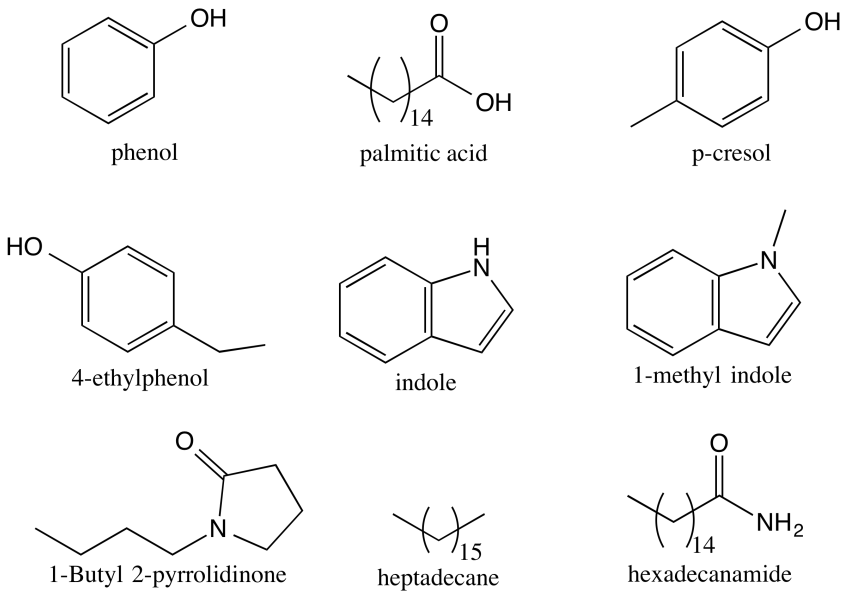

Figure 2.2. Common products in microalgae HTL bio-oils [9, 17].

Beyond the bio-oil produced from the HTL of microalgae, the aqueous co-product also contains carbon. The aqueous co-product and bio-oil are usually separated by solvent extraction. In general, the aqueous phase is enriched with nitrogen when compared with the microalga fed to the reaction, but this phase also contains 15 to 40 wt% of the carbon from the feed [20, 25]. This carbon is often bound in polar, oxygen- or nitrogen-containing

products such as acetic acid, ethanol, pyrrolidones, and polyols [26]. The significant carbon content of the aqueous co-product makes it a secondary source of energy that should be utilized when producing bio-oils.

2.2 Hydrothermal HDO

Removal of heteroatoms can be accomplished by conventional hydrotreating upon the separation of the bio-oil and water. Recent work has shown that this separation is not trivial for some algae species because the high heteroatom content in the bio-oil results from hydrophilic functional groups, as discussed in section 2.1, that can create an oil/water emulsion [9, 20, 23]. Furthermore, the aqueous reactor effluent contains products that can be used in fuels, and, if left in the aqueous phase, would require significant wastewater treatment. Last, as discussed in the introduction, section 1.4, even a moisture free bio-oil will produce water during HDO. Therefore, HDO will occur with water present. We will, in general, limit the discussion below to hydrothermal HDO studies. HDO has received significant attention in the literature and has been the focus of several extensive reviews focusing on conventional [3, 5, 6] and hydrothermal HDO [27, 28].

2.2.1 Noble metal catalysts

Dumesic and co-workers pioneered the conversion of sugars and biofuel byproduct molecules, such as ethylene glycol, to H_2 and alkanes [29-33]. Many of these studies have focused on aqueous-phase reforming of sugars with the goal of producing H_2, but the authors found that some metals, such as Ni, Rh, and Ru were more selective for alkane

production than gas formation [31]. Huber et al. examined the conversion of sorbitol over Pt and achieved a high gas phase hydrocarbon yield and found their catalyst to be stable over a six-day period [32]. Furthermore, they found that the liquid alkane yield was greater when they used a mixture of Pt/Al_2O_3 and SiO_2-Al_2O_3. This increase in liquid alkane yield was attributed to the presence of the solid acid (SiO_2-Al_2O_3) catalyst.

Similarly, Kunkes et al. converted sorbitol into monofunctional liquid organic products over a PtRe/C catalyst between 210 and 250 °C without added hydrogen. They speculated that the PtRe/C catalyst, which was stable for at least 1 month on stream, reformed a small portion of the sorbitol to produce the hydrogen necessary for the subsequent deoxygenation reactions [33]. In a similar study, Vispute et al. produced commodity chemicals (benzene, toluene, ethylbenzene, and ethylene) from the aqueous phase processing of water-soluble pyrolysis oil over Ru/C, Pt/C, and zeolite catalysts with added hydrogen [34, 35].

Lercher and co-workers have extensively examined the hydrothermal HDO of lignin derived phenolic molecules between 150 and 200 °C using Pd/C with H_3PO_4 or HZSM-5 [36-38] and achieved complete conversion and high selectivity (> 80%) to cycloalkanes. Interestingly, without the acid catalyst (i.e., H_3PO_4 or HZSM-5), no cycloalkanes were observed. In later studies, they combined the active metal, Pd, and acid catalysts into a single, bifuntional catalyst, Pd/HBEA, that produced primarily larger, oxygen-free hydroalkylation products from phenolic molecules [39].

Savage and coworkers have also made significant progress in catalytically converting bio-oils and bio-derived molecules into liquid hydrocarbons under

hydrothermal conditions [10, 40-46]. In general, these studies have taken place at higher temperatures (350 – 500 °C) and pressures (150 to 305 bar) than those examined by Dumesic and Lercher (~200 °C, ~25 bar). These studies revealed that Pt/C is an active and stable catalyst for the dexcarboxylation of palmitic acid. It is important to note, that unlike the work of Lercher et al., these reactions did not require an additional acid catalyst to perform deoxygenation.

The above reports illustrate that a hydrothermal environment can be effectively used to perform HDO on bio-oils to produce fungible petroleum-like crude oils, but they provide limited knowledge about the reaction kinetics, especially at high conversion. Furthermore, these studies have focused on using noble metal catalysts whose high cost and susceptibility to poisoning from nitrogen and sulfur make them undesirable [47].

2.2.2 Non-noble metal catalysts

Non-noble metal catalysts are desirable for hydrothermal HDO because they are significantly less expensive than noble metal catalysts, and they are less susceptible to poisoning from sulfur and nitrogen. This resistance to poisoning is especially important for microalgal bio-oils, compared with pyrolysis bio-oils, because the microalgal bio-oils contain higher concentrations of nitrogen and sulfur.

Reports of active non-noble metal catalysts for hydrothermal HDO are rare. Lercher and associates examined the use of Raney Ni with homogeneous (H_3PO_4 and acetic acid) or solid acid catalysts (Nafion/SiO_2) and determined that only the Raney Ni and Nafion/SiO_2 catalyst combination was effective at producing cycloalkanes from 4-n-propylphenol at

200 °C [48]. Again, the researchers determined that the use of the solid acid catalyst was essential for producing cycloalkanes, as conversions and selectivities were negligible without it. These researchers have also examined the use of Ni/HZSM-5 and Ni/γ-Al_2O_3-HZSM-5 bifunctional catalysts for phenol and phenolic monomer hydrothermal HDO and obtained a 100% yield of hydrocarbons between 200 and 250 °C [49, 50]. These researchers also performed a detailed kinetic analysis under differential reactor conditions and found that phenol hydrogenation, occurring on Ni particles, was the rate-limiting step in the reaction. They definitively showed that the hydrogenation reactions occurred on the Ni metal particles, and the dehydration reaction occurred within the HZSM-5 support on Brønsted acid sites. Unfortunately though, these catalysts showed substantial deactivation in catalyst recycle experiments, even with catalyst regeneration occurring between cycles, due to catalyst particle sintering, Ni leaching, and structural changes to the catalyst support [49].

2.2.3 HDO of benzofuran

In chapter 5, we examine the hydrothermal HDO of benzofuran over Pt/C. We chose 2,3-benzofuran as a model oxygenated compound, because, as shown in section 2.1, furans and phenolic compounds are prevalent in bio-oils. To the best of our knowledge, there are no previous benzofuran hydrothermal HDO studies; therefore, we will briefly examine previous studies in non-aqueous environments. The studies show that benzofuran deoxygenates through a pathway that includes phenols and alcohols [51-54].

Lee and Ollis examined the HDO of benzofuran over a sulfided $CoMo/\gamma\text{-}Al_2O_3$ catalyst in a trickle bed reactor between 220 and 340 °C and found that the major reaction intermediates were 2,3-dihydrobenzofuran and ethylphenol, and the HDO products were cyclohexane, cyclohexene, and ethane. Their kinetic analysis, which was performed under differential reactor conditions, also revealed that the hydrogenation of benzofuran to dihydrobenzofuran and the hydrogenolysis of dihydrobenzofuran to 2-ethylphenol proceeded at similar rates, while the HDO of ethylphenol was the rate-limiting step [53]. Edelman et al. expanded on this kinetic analysis using a sulfided $NiMo/\gamma\text{-}Al_2O_3$ from 300 to 400 °C with integral reactor conditions. They found that the HDO reaction was best modeled as -1 order in oxygenated compounds, and produced ethylbenzene, toluene, and benzene [55]. More recently, Bunch et al. performed a detailed characterization of both sulfided and reduced $NiMo/\gamma\text{-}Al_2O_3$ during the HDO of benzofuran. Interesting they determined that H_2S, the sulfiding agent, actually reduced the rate of benzofuran HDO. Furthermore, they proposed a reaction network that included both a direct deoxygenation pathway, where ethylphenol dehydrates to form ethylbenzene, and a hydrogenation pathway, where benzofuran is fully hydrogenated to octohydrobenzofuran before the dehydration reaction, for the production of hydrocarbons [51, 52]. Last, Romero et al. studied the HDO of benzofuran over both sulfided and reduced $NiMoP/Al_2O_3$ and determined that the presence of benzofuran and dihydrobenzofuran decreased the rate of ethylphenol HDO [54].

2.3 Literature analysis

Above, we examined the elemental and molecular compositions of bio-oils produced the pyrolysis of lignocellulosic biomass and the HTL of microalgae. Analysis of these bio-oils revealed that HDO is a necessary enabling technology to produce fungible bio-fuels from the aforementioned crude bio-oils. Furthermore, this analysis also revealed the need to perform the HDO in a hydrothermal environment. Examination of the literature for hydrothermal HDO showed that most researchers chose noble metal catalysts (i.e. Pt, Pd, Ru, and Rh) to perform HDO, because, as discussed in the introduction, common hydrotreating catalysts (NiMo and CoMo) and supports (γ-Al_2O_3 and SiO_2) may be unstable in hydrothermal conditions.

The current literature contains several knowledge gaps that are addressed in this dissertation. First, when this dissertation was started, little was known about the molecular composition of microalgal bio-oils. Of particular interest was whether the extraction and workup procedures used in previous HTL studies affected the yield and composition of the bio-oil. To address these shortcomings, and to obtain a greater understanding of microalgal bio-oil prior to performing hydrothermal HDO studies, we first examine the effects of various solvents on the yield and composition of microalgal bio-oils in chapter 4.

With a greater understanding of the composition of bio-oils, we next sought to determine the kinetics for the hydrothermal HDO of benzofuran over Pt/C. We chose benzofuran as a model compound because the analysis in chapter 4 shows that the much of the oxygen in the microalgal bio-oils is in heterocycles and phenolic molecules. Section 2.1 also showed that furans and phenols are common in pyrolysis bio-oils making this study

broadly applicable. Furthermore, when this study was conducted, the majority of hydrothermal HDO literature reacted sugars over noble metal catalysts at temperatures around 200 °C. The few researchers examining the hydrothermal HDO of phenolic molecules found that the reaction required the use of an acid catalyst in conjunction with the noble metal catalyst to obtain a high yield and conversion of liquid hydrocarbons (see section 2.2.1). To address this knowledge gap, we studied, in chapter 5, the hydrothermal HDO of benzofuran using a Pt/C catalysts at 380 °C and determined reaction network and kinetics.

Last, we desired to develop active and stable non-noble metal catalysts for hydrothermal HDO because of the high cost and susceptibility to poisoning of noble metals. Section 2.2.2 demonstrated that little research has been performed in this area, and the catalysts developed showed substantial deactivation in hydrothermal conditions despite the catalyst regeneration steps taken. Therefore, in chapter 6 we examine the activity and stability of several Ni based commercial catalysts in a flow reactor, and then develop an active and stable Raney NiCu catalyst. Chapter 7 expands on the work started in chapter 6. In chapter 7 we study of the effect of Cu loading on the selectivity and liquid hydrocarbon yield of a variety Raney NiCu catalysts. Also in this chapter, we show that the addition of acid sites to the Ni catalysts increases the hydrothermal HDO activity. The hydrothermal HDO catalysts developed in chapter 7 provide the highest stable yield of liquid hydrocarbons from non-noble metal catalysts yet reported.

References

1. A. V. Bridgwater, D. Meier, D. Radlein, Org. Geochem. 30, (1999) 1479-1493.
2. S. Czernik, A. V. Bridgwater, Energy Fuels 18, (2004) 590-598.
3. E. Furimsky, Appl. Catal. A: Gen. 124, (2000) 470-477.
4. C. A. Mullen, A. A. Boateng, N. M. Goldberg, I. M. Lima, D. A. Laird, K. B. Hicks, Biomass Bioenerg. 34, (2010) 67-74.
5. E. Furimsky, Catal. Today 217, (2013) 13-56.
6. H. Wang, J. Male, Y. Wang, ACS Catal. 3, (2013) 1047-1070.
7. K. Anastasakis, A. B. Ross, Bioresour. Technol. 102, (2011) 4876-4883.
8. P. Biller, A. B. Ross, Bioresour. Technol. 102, (2010) 215-225.
9. T. M. Brown, P. Duan, P. E. Savage, Energy Fuels 24, (2010) 3639-3646.
10. P. Duan, P. E. Savage, Ind. Eng. Chem. Res. 50, (2011) 52-61.
11. J. L. Faeth, P. J. Valdez, P. E. Savage, Energy Fuels 27, (2013) 1391-1398.
12. S. Inoue, Y. Dote, S. Sawayama, T. Minowa, T. Ogi, S. Yokoyama, Biomass Bioenerg. 6, (1994) 269-274.
13. U. Jena, K. C. Das, J. R. Kastner, Bioresour. Technol. 102, (2011) 6221-6229.
14. U. Jena, K. C. Das, Energy Fuels (2011) 111107111047004.
15. T. Matsui, A. Nishihara, C. Ueda, M. Ohtsuki, N. Ikenaga, T. Suzuki, Fuel 76, (1997) 1043-1048.
16. T. Minowa, S. Yokoyama, M. Kishimoto, T. Okakura, Fuel 74, (1995) 1735-1738.
17. A. B. Ross, P. Biller, M. L. Kubacki, H. Li, A. Lea-Langton, J. M. Jones, Fuel 89, (2010) 2234-2243.
18. S. Sawayama, T. Minowa, S. Y. Yokoyama, Biomass Bioenerg. 17, (1999) 33-39.
19. Z. Shuping, W. Yulong, Y. Mingde, I. Kaleem, L. Chun, J. Tong, Energy 35, (2010) 5406-5411.
20. P. J. Valdez, J. G. Dickinson, P. E. Savage, Energy Fuels 25, (2011) 3235-3243.
21. P. J. Valdez, M. C. Nelson, H. Y. Wang, X. N. Lin, P. E. Savage, Biomass Bioenerg. 46, (2012) 317-331.
22. P. J. Valdez, P. E. Savage, Algal Research 2, (2013) 416-425.
23. Y. F. Yang, C. P. Feng, Y. Inamori, T. Maekawa, Resources, conservation and recycling 43, (2004) 21-33.
24. S. Zou, Y. Wu, M. Yang, C. Li, J. Tong, Energy Environ. Sci. 3, (2010) 1073-1078.
25. D. C. Elliott, T. R. Hart, A. J. Schmidt, G. G. Neuenschwander, L. J. Rotness, M. V. Olarte, A. H. Zacher, K. O. Albrecht, R. T. Hallen, J. E. Holladay, Algal Research 2, (2013) 445-454.
26. L. Garcia Alba, C. Torri, D. Fabbri, S. R. A. Kersten, D. W. F. Brilman, Chemical Engineering Journal 228, (2013) 214-223.
27. D. E. Furimsky, Ind. Eng. Chem. Res. 52, (2013) 17695-17713.
28. T. M. Yeh, J. G. Dickinson, A. Franck, S. Linic, L. T. Thompson, P. E. Savage, J. Chem. Technol. Biotechnol. 88, (2013) 13-24.
29. J. Q. Bond, D. M. Alonso, D. Wang, R. M. West, J. A. Dumesic, Science 327, (2010) 1110-1114.

30. D. J. Braden, C. A. Henao, J. Heltzel, C. C. Maravelias, J. A. Dumesic, Green Chem. (2011)
31. R. R. Davda, J. W. Shabaker, G. W. Huber, R. D. Cortright, J. A. Dumesic, Appl. Catal. B: Environ. 43, (2003) 13-26.
32. G. W. Huber, R. D. Cortright, J. A. Dumesic, Angewandte Chemie International Edition 43, (2004) 1549-1551.
33. E. L. Kunkes, D. A. Simonetti, R. M. West, J. C. Serrano-Ruiz, C. A. Gärtner, J. A. Dumesic, Science 322, (2008) 417.
34. T. P. Vispute, G. W. Huber, Green Chem. 11, (2009) 1433-1445.
35. T. P. Vispute, H. Zhang, A. Sanna, R. Xiao, G. W. Huber, Science 330, (2010) 1222-1227.
36. C. Zhao, Y. Kou, A. A. Lemonidou, X. Li, J. A. Lercher, Angew. Chem. 121, (2009) 4047-4050.
37. C. Zhao, J. He, A. A. Lemonidou, X. Li, J. A. Lercher, J. Catal. 280, (2011) 8-16.
38. C. Zhao, J. A. Lercher, ChemCatChem 4, (2012) 64-68.
39. C. Zhao, D. M. Camaioni, J. A. Lercher, J. Catal. 288, (2012) 92-103.
40. P. Duan, P. E. Savage, Appl. Catal. B: Environ. 108-109, (2011) 54-60.
41. P. Duan, P. E. Savage, Appl. Catal. B: Environ. 104, (2011) 136-143.
42. P. Duan, P. E. Savage, Energy Environ. Sci. 4, (2011) 1447-1456.
43. P. Duan, P. E. Savage, Bioresour. Technol. 102, (2011) 1899-1906.
44. J. Fu, F. Shi, L. T. Thompson Jr, X. Lu, P. E. Savage, ACS Catal. 1, 227-231.
45. J. Fu, X. Lu, P. E. Savage, Energy Environ. Sci. 3, (2010) 311-317.
46. J. Fu, X. Lu, P. E. Savage, ChemSusChem 4, (2011) 481-486.
47. Y. Yu, O. Y. Gutiérrez, G. L. Haller, R. Colby, B. Kabius, J. A. Rob van Veen, A. Jentys, J. A. Lercher, J. Catal. 304, (2013) 135-148.
48. C. Zhao, Y. Kou, A. A. Lemonidou, X. Li, J. A. Lercher, Chemical Communications 46, (2010) 412-414.
49. C. Zhao, S. Kasakov, J. He, J. A. Lercher, J. Catal. 296, (2012) 12-23.
50. C. Zhao, J. A. Lercher, Angew. Chem. 124, (2012) 6037-6042.
51. A. Y. Bunch, U. S. Ozkan, J. Catal. 206, (2002) 177-187.
52. A. Y. Bunch, X. Wang, U. S. Ozkan, J. Mol. Catal. A: Chem. 270, (2007) 264-272.
53. C. L. Lee, D. F. Ollis, J. Catal. 87, (1984) 325-331.
54. Y. Romero, F. Richard, Y. Renème, S. Brunet, Appl. Catal. A: Gen. 353, (2009) 46-53.
55. M. C. Edelman, M. K. Maholland, R. M. Baldwin, S. W. Cowley, J. Catal. 111, (1988) 243-253.

Chapter 3

Materials and Methods

This chapter provides the experimental details of how the original work presented in chapters 4-7 was performed.

3.1. Materials

We procured all solvents, reagents, and catalyst precursors from Fischer Scientific or Sigma-Aldrich (≥ 98% purity, except n-hexane ≥ 95% purity) and used them as received. Raney Ni 2800 was obtained from Sigma Aldrich, the γ-AlOOH that was used as a catalyst support and a catalyst bed diluent was obtained from Morton Thiokol. γ-AlOOH was converted to γ-Al_2O_3 during the calcination and reduction of the catalysts (shown later), therefore, we refer to all such catalysts as Al_2O_3-supported. ZrO_2 was obtained from Alpha Aesar and deionized water was prepared in house. We obtained microalga, *Nannochloropsis* sp., in a slurry from Reed Mariculture, Inc. (Nannochloropsis 3600).

3.2. Catalyst synthesis

Table 3.1 lists the catalysts used in this dissertation, the chapter in which they were used, the catalyst supplier, and the reactor type that was used to test the catalysts.

Table 3.1. Catalysts, active metal loading, and reactor types used to test catalysts.

Catalyst	wt% active metal or dopant	Supplier or synthesized	Chapter	Reactor type
Pt/C	5	Sigma Aldrich	5,6	4.1 mL batch
$Ni/Al_2O_3SiO_2$	65	Sigma Aldrich	6	Single feed flow
Raney Ni 2800	---	Sigma Aldrich	6	Single feed flow
Raney NiCu	10	Synthesized	6	Single feed flow
Raney NiCu	1 to 40	Synthesized	7	4.1 mL batch
Calcined Raney Ni	---	Synthesized	7	4.1 mL batch, multi feed flow
Calcined Raney NiCu	5	Synthesized	7	Multi feed flow
$NiCu/Al_2O_3$	10 (Ni), 0.5 (Cu)	Synthesized	7	Multi feed flow

We synthesized the Cu doped Raney Ni catalysts, referred to as Raney NiCu catalysts in keeping with previous literature [1], by dissolving $Cu(NO_3)_2•2.5H_2O$ in 5 mL of ethanol, adding this solution to reduced Raney Ni, heating the resulting mixture to 100 °C in a sealed vial for 1 hr, and then reducing the catalyst in flowing H_2 at 400 °C for 3 hr with a 5°C/min ramp rate. For example, to synthesize the 5% Raney NiCu catalyst we added, by puncturing the parafilm covering the vial, a solution containing 0.137 g of $Cu(NO_3)_2•2.5H_2O$ and 5 mL of ethanol to an Ar filled vial containing 0.713 g of reduced Raney Ni before carrying out the heating and reduction procedures above.

The Al_2O_3- and ZrO_2-supported catalysts were synthesized by impregnating the support with a $Ni(NO_3)_2•6H_2O$ or a $Ni(NO_3)_2•6H_2O$ and $Cu(NO_3)_2•2.5H_2O$ solution in DI H_2O. In general, to achieve the desired metal loadings we performed two impregnations of the γ-AlOOH for the Al_2O_3-supported catalysts, and three impregnations for the ZrO_2-supported catalyst. For example, to synthesize the 10%, 0.5% $NiCu/Al_2O_3$ catalyst we performed two impregnations of 4.5 g of γ-AlOOH with a solution that contained 6.6 g of $Ni(NO_3)_2•6H_2O$ and 0.25 g of $Cu(NO_3)_2•2.5H_2O$ in 13.2 mL of DI H_2O. Following each impregnation, we

dried the catalysts at 110 °C for 12 hr and then calcined them in air by increasing the temperature at 10 °C/min to 400 °C where the temperature was held for 4 hr. The calcined catalysts were crushed and sieved (150 μm), and then reduced in flowing H_2 by increasing the temperature at 5 °C/min to 400 °C where the temperature was held for 3 hr.

Last, to produce the calcined Raney Ni and calcined Raney NiCu catalysts, we heated the Raney Ni in DI water to 80 °C for 3 hr, followed by drying and calcining the catalysts using the procedure outlined above. The calcined 5% Raney NiCu catalyst was synthesized by adding 0.590 g of $Cu(NO_3)_2 \bullet 2.5H_2O$ in 5 mL of ethanol to 3.047 g of calcined Raney Ni. The resulting mixture was heated and reduced using the procedure discussed for producing the Raney NiCu catalysts.

3.3. Catalyst characterization

We performed X-ray Diffraction (XRD), transmission electron microscopy (TEM), and CO temperature programmed desorption (TPD) using catalysts passivated overnight at 70 °C in 1% O_2 in He. XRD characterization was performed on a Rigaku Miniflex 600 with a scan rate of 1.25 °/min. TEM/STEM was performed on a Jeol 2010f, and CO TPD was performed on a Micrometrics Autochem 2910. The passivated catalysts were reduced in situ at 430 °C for 180 min, prior to the TPD experiments. CO was added to the catalyst surface at 25 °C and the catalyst was heated at 10 °C/min to 550 °C.

We determined the weight fraction of catalytic metals in chapter 6 by dissolving four different samples (5 to 15 mg) of the fresh and spent catalyst in 3 ml of aqua regia, diluting the samples with deionized water, and analyzing the samples and known

standards with a Perkin Elmer Optima 2000 DV inductively coupled plasma optical emission spectrometer (ICP-OES).

3.4. Reactor descriptions

A variety of reactors were constructed and used to obtain the experimental results discussed in chapters 4-7. Below we describe each reactor.

3.4.1. Batch reactors

The 31 mL batch reactors, used only in the HTL experiments in chapter 4, consisted of an 8 in. length of 316 stainless steel tubing (¾ in. OD, 0.065 in. wall thickness) fitted with a Swagelok cap at each end. For reactions in which gases were analyzed, we attached a High Pressure Equipment Company high-pressure (30,000 psi) valve to the reactor via 8.8 in. of 1/8 in. OD stainless steel tubing (0.028 in. wall thickness). The difference in volume between a reactor with a cap and one with a valve was calculated to be only 0.54 mL.

The 4.1 mL batch reactors, used in chapters 5 and 7 and shown in fig. 3.1, were constructed from a ½ in. Swagelok port connector, cap, and ½ to 1/8 in. reducing union fitted with 9 in. of 1/8 o.d. stainless steel tubing and a 30,000 psi High Pressure Equipment Company valve. The assembled reactors had a nominal volume of 4.1 ml. Prior to use in reactions, all reactors were loaded with deionized water and heated to 350 °C for 60 min to expose the reactor walls to a hydrothermal environment.

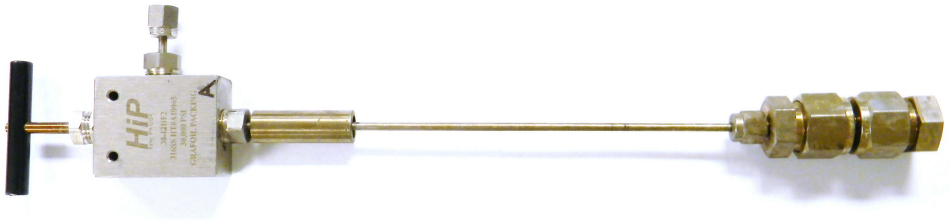

Fig. 3.1. Batch reactor (4.1 mL). Courtesy of Peter Valdez.

3.4.2. Single feed flow reactor

We constructed a flow reactor with two inlets, as shown in fig. 3.2, from 316 stainless steel tubing. The first inlet, used for all liquid reagents, consisted of an 8 ft preheating section of 1/8 in. o.d. tubing connecting to 22 in. of 1/4 in. o.d. tubing. The total volume of the inlet lines leading from the feed solution to the catalyst bed was 13.8 mL. The second inlet, used only for in-situ catalyst reduction prior to reaction, consisted of 9 ft of 1/16 in. o.d. tubing. The two inlets merged at a cross fitting prior to reaching the catalyst bed. The temperature at this location was measured by a thermocouple placed within the cross, and was maintained to the desired reactor temperature. We constructed the catalyst bed from 4.5 in. of 1/4 in. o.d. tubing and placed porous Hastelloy frits with 5 μm pores at each end of the catalyst bed to hold the catalyst in place. Prior to reaction the entire reactor assembly was leak tested with H_2 at 70 bar, as this was the highest pressure available from the H_2 regulator.

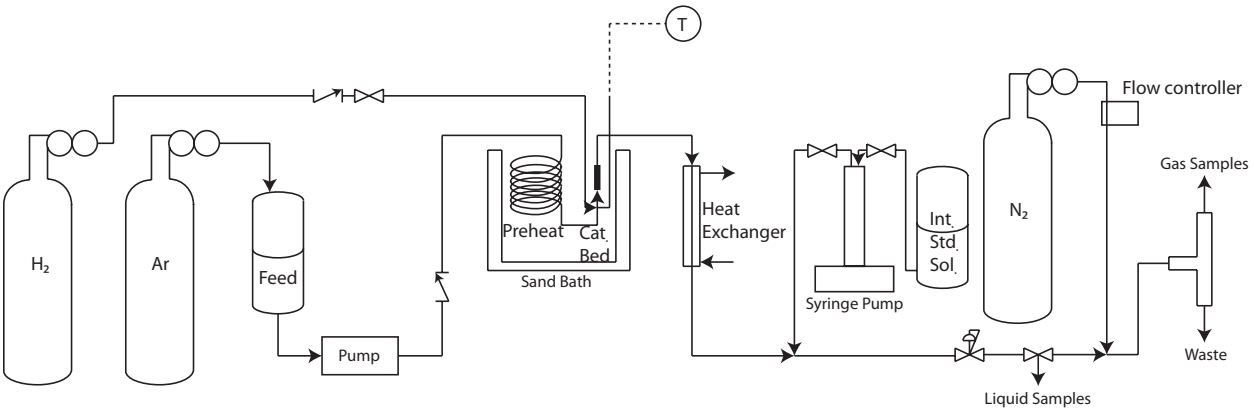

Fig. 3.2: Single feed flow reactor process flow diagram.

As shown in figure 3.2, the preheating sections and catalyst bed resided in a Techne SBL 2D fluidized sand bath that maintained the desired reactor temperature. A tube-in-tube heat exchanger cooled the reactor effluent with tap water, and a backpressure regulator maintained reactor pressure. After depressurization, a three-way valve allowed for the collection of liquid samples and a flash column separated gas samples.

A 2 L Parr vessel filled with the feed solution containing 24.8 g/L of o-cresol, 147 mL/L of formic acid, and the balance with DI water was purged and pressured with 2-3 bar of Ar or N_2. This feed solution and reactor carried out all of the reactions in chapter 6. An internal standard solution of isopropanol with 5 g/L of phenol (Pt/C reaction) or 4 g/L of isopropylphenol (all other reactions) was loaded into an Isco 260D syringe pump and injected to the cooled reactor effluent to form a single homogeneous liquid phase.

3.4.3. Multiple feed flow reactor

A second flow reactor configuration, used in section 7.2 and shown in fig. 3.3, is similar to the previous setup, but with a few major improvements. First, H_2 was delivered

to the flow reactor with a mass flow controller, instead of using the in situ decomposition of formic acid as the H_2 source. Second, separate pumps for DI water and o-cresol allowed for varying concentrations of o-cresol to be fed to the reactor. Last, we used a tube furnace as the heating source of the reactor to allow for faster heat up and cool down times.

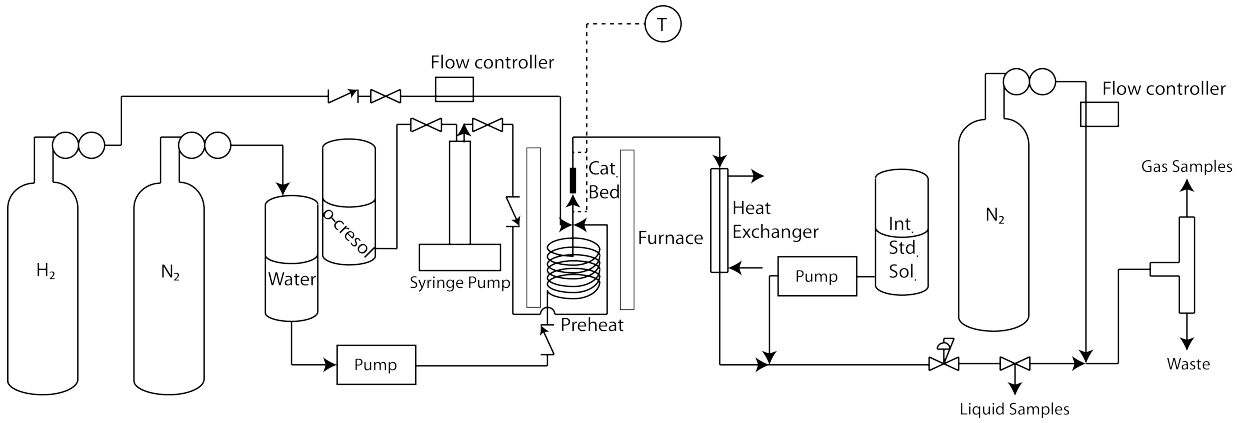

Fig. 3.3. Modified flow reactor with multiple feeds process flow diagram.

The modified flow reactor, shown in fig. 3.3, has three 316 stainless steel inlet lines. Chrom Tech Series III pumps fed DI water and the internal standard solution (4 g/L 4-isopropylphenol in isopropanol) to the reactor and cooled reactor effluent, respectively. o-Cresol, heated to 35 to 40 °C by heat tape, was fed by an ISCO 260D syringe pump, and H_2 was fed through a Brooks 5850 TR mass flow controller from a 6000 psig H_2 cylinder. The preheating tubing within the Applied Test Systems furnace, which was controlled by an Omega PID controller, was 1/16 in. o.d. tubing. The water, H_2, and o-cresol preheating lines were 80, 60, and 15 in. in length, respectively, and mixed in a cross fitting prior to entering the catalyst bed. The temperature within this cross fitting was monitored by a thermocouple and data logger. The 3.5 in. catalyst bed was constructed from 1/4 in. o.d. tubing with 5 μm Hastelloy frits placed at both ends. The catalyst bed was loaded with

catalyst and γ-AlOOH, a diluent, in the Ar glove box. We covered the ends of the catalyst bed with parafilm in the glove box to minimize the exposure of the catalyst to air when the catalyst bed was transferred to the flow reactor. A second thermocouple, positioned in a T fitting, measured the temperature of the product stream exiting the catalyst bed. A tube-in-tube heat exchanger cooled the reactor effluent to room temperature, and a backpressure regulator maintained the desired reaction pressure. 15 to 20 mL/min of N_2 was added to the reaction stream through an Omega 5400/5500 mass flow controller after the backpressure regulator to provide a reference gas. A Gilson 223 fraction collector with an automated switching valve collected liquid samples in test tubes containing ~3 mL of 2-propanol. When the fraction collector was not collecting liquid samples, the reactor effluent was diverted to a 250 mL flash column that separated the liquid and gas products.

3.5. Reaction procedures and chemical analyses

The details of the reaction procedures and chemical analyses are presented below. The procedures are organized around the type of reactor used.

3.5.1. Algae liquefaction experiments - 31 mL batch reactors

For the liquefaction experiments performed in chapter 4, each reactor was loaded with 19.4 g of wet algae paste that was 20 – 25 wt % solids. We chose this amount because the liquid water in the algae paste would expand to occupy about 90% of the reactor volume at the reaction temperature of 350 °C. Previous research indicated that 350 °C provided the highest bio-oil yield when using a 60 min reaction time [2]. For reactions in which gases were not analyzed, each loaded reactor was securely fitted with a second cap

on the open end, leaving air in the reactor headspace. Experimentation and stoichiometric calculations showed that oxygen in the reactor headspace does not significantly affect the product yields. If gas analysis was desired, the reactors were fitted with a cap connected to a high-pressure valve, and the air within the reactor was replaced with helium by three repeated cycles of evacuation (1.5 psia) and pressurization (10 psig) with helium.

A preheated Techne Fluidized Sand Bath (model SBL-2) with a Techne TC-8D temperature controller heated the reactors to 350 ± 2 °C within 3 min. After 60 min, the reactors were removed from the sand bath, quenched in water at room temperature, and allowed to equilibrate at room temperature for at least 60 min. Gas analysis, when desired, was performed at this point using an Agilent 6890N gas chromatograph with a thermal conductivity detector (GC/TCD). A 15 ft Carboxen 1000 packed column separated the product gasses using Ar as the carrier gas. The GC oven was initially held at 35 °C for 5 min, and then ramped to 225 °C at a rate of 20 °C/min. The 225 °C final temperature was maintained for 15 min.

Post reaction and gas analysis, we opened the reactors and added 10 mL of the desired solvent, pre-weighed, to each reactor. The reactors were then resealed and slowly rotated end over end (10 rpm) at room temperature for 120 min. We performed this step to provide extensive contact between the solvent and reactor wall, where much of the bio-oil resided. After rotation, the reactors were placed into an oven at 70 °C for 180 min to break an emulsion that formed when using decane and hexadecane as solvents. Post heating, we cooled the reactors for 60 min at room temperature. The reactors were opened, and their contents poured into a centrifuge tube. We attempted to improve the recovery of any viscous materials by resealing and reheating the reactors to 70 °C, and then reopening

them while still hot. The remaining contents, if any, were poured into the same centrifuge tube. This reheating step sometimes provided recovery of additional liquid products, but only when using decane and hexadecane as solvents.

We centrifuged the tubes at 3220 relative centrifugal forces for 10 min to separate the organic, aqueous, and solid phases. The organic and aqueous layers were decanted, leaving behind the solids. The organic and aqueous layers, both in one tube, were centrifuged again, and the lower phase was removed via Pasteur pipette. The liquefaction and workup procedure was performed with 3 or 4 replicates for each solvent. The values reported in chapter 4 are the means and the uncertainties reported are the standard deviations.

An aliquot of 0.2 – 1.0 mL of aqueous phase was frozen in liquid nitrogen and lyophilized for 22 hr using a Labconco Freezone 2.5 freeze dryer set at -40 °C and 0.120 mBar. Aliquots of organic phase (500 μL) were dried under flowing N_2 for 6 hr, except for the decane sample (200 μL), which was dried for 26 hr, and the hexadecane sample, which was not dried. The appropriate drying times were determined by periodically measuring the mass until there was no measurable change. The mass of material remaining after solvent removal was determined for the aliquots of the organic and aqueous phases and then used to calculate the gravimetric yields of bio-oil and dissolved aqueous solids. The residual solids were dried by flowing N_2 over them for 6 hr. The gravimetric yield of solids was calculated directly from the mass of the solids after drying. Lastly, samples of microalgae, bio-oil, residual solids, and dissolved aqueous solids were sent to Atlantic Microlab, Inc. for elemental analysis (C, H, and N).

We measured the concentration of ammonia in the aqueous phase with a HACH Nitrogen-Ammonia Reagent Set. We diluted the aqueous phase (1:200) with deionized water, and added the diluted sample to the HACH reagents. The absorbance of the solution at 655 nm was obtained using a Thermo Scientific Genesys20 spectrophotometer, and the ammonia concentration was determined by a linear fit to standards with known concentrations.

For experiments with hexadecane as the solvent, we determined the bio-oil mass as the difference between the mass of hexadecane added to the reactor and the mass of water-free organic phase obtained after separating the product fractions. We determined the water content of the bio-oil and hexadecane mixture using a Mettler Toledo Karl Fischer titrator with Aquastar Composite 2K, pyridine free reagent, and high purity (>99.8%) toluene and methanol. A 1:1 mixture of the organic phase and isopropanol was used to break any remaining emulsion and then 200 μL of sample was injected into the titrator. Isopropanol blanks were also analyzed and the water content was found to be within the error of the measurements. The water content of the hexadecane and bio-oil phase was 5.1 ± 0.9 wt%, and the bio-oil yield has been corrected for this value.

We analyzed the solvent-free bio-oil samples with a VG 70-250-S magnetic sector mass spectrometer, using both electron impact ionization (EI) and chemical ionization (CI) techniques. For EI, the ionization source was set at 70 eV. For CI, methane was used with a source accelerating voltage of 8 kV. In both cases, the source temperature was set at 240 °C and a direct probe heated from room temperature to 300 °C, under vacuum, volatilized the samples.

We identified specific bio-oil compounds by analyzing the organic phase, prior to evaporating the solvent, on an Agilent 6890N GC with a mass spectrometric detector (GC/MSD), and an Agilent HP-5MS non-polar capillary column (50 m × 200 μm × 0.33 μm). Analyzing the bio-oil prior to the evaporation of the solvent allowed us to identify and quantify volatile compounds. We injected 2 μL of organic phase into a 300 °C inlet with a 10:1 split ratio. The column was initially held at 35 °C for 5 min, then ramped at 1 °C/min to 50 °C, 3 °C/min to 300 °C, and finally held isothermally for 15 min. Helium (0.9 mL/min) served as the carrier gas.

Quantification of bio-oil compounds was carried out on an Agilent Technologies 7890 GC with a flame ionization detector (GC/FID). For all compounds except free fatty acids, the quantification was performed with an Agilent HP-5 non-polar capillary column (50 m × 200 μm × 0.33 μm) using the same conditions as the GC/MSD, except the split ratio was increased to 15:1 and the column flow was increased to 1 mL/min. Quantification of free fatty acids proved inconsistent on the HP-5 column, so we used a Supelco Nukol capillary column (30 m × 320 μm × 0.25 μm) and a cool on-column inlet. A 0.5 μL sample of organic phase was injected onto the column at 100 °C. The temperature was then ramped at 10 °C/min to 220 °C and held for 18 min. Analyzing the solvent blanks with the GC-FID, we determined that the solvents contained no detectable impurities.

We produced calibration curves by analyzing standards containing authentic compounds in known concentrations on GC-FID. It was not practical to generate calibration curves for all of the compounds identified by GC-MSD because of their great number and cost. Thus, some compounds were quantified using the calibration determined experimentally for a different component with a similar chemical structure.

3.5.2. Batch catalytic HDO experiments - 4.1 mL batch reactors

For the reactions performed in chapter 5, unless otherwise specified, 10 mg of 5 wt% Pt/C, 100 µl (900 µmol) of benzofuran (or the molar equivalent of ethylcyclohexanol, ethylcyclohexane, ethylbenzene, or ethylphenol), and 0.67 ml deionized water were loaded into each reactor. After loading the catalyst and liquid reagents, we sealed the reactors and connected them to a gas manifold that included hydrogen and helium cylinders and a vacuum pump. Air was removed from the reactors by four cycles of helium pressurization (50 psig) followed by evacuation by the vacuum pump (1.5 psia). On the last cycle, we placed 77 psig of helium into the reactor to act as an internal standard, followed by final pressurization with hydrogen to achieve the desired nominal hydrogen to reactant molar ratio (0:1, 0.5:1, 2:1, 3:1, 4:1, and 6:1). The hydrogen to reactant ratios were chosen to be moderately substoichiometric with respect to producing ethylcyclohexane through deoxygenation and hydrogenation reactions, with the exception of the 6:1 hydrogen to benzofuran reactions, which were stoichiometric. The tables in Appendix A, located at the end of this chapter 5, provide the exact hydrogen pressures for each reaction. The reactors were checked for leaks during this pressurization by placing them in water.

For each batch hydrothermal HDO experiment performed in chapter 7, the reduced catalysts were transferred from the tube furnace, where they were reduced in H_2, to an Ar glove box in the reduction tube to minimize oxygen exposure. The reduced catalysts were loaded into 4.1 mL Swagelok batch reactors in the Ar glove box, and the open end of each reactor was sealed with parafilm. The batch reactors were filled outside of the glove box with 0.67 mL of DI H_2O and either 20 or 100 mg of o-cresol by poking holes in the parafilm

and injecting the liquids, thereby minimizing exposure of the catalyst to air. The batch reactors were then capped, purged with He, and pressurized with He and H_2.

A preheated Techne Fluidized Sand Bath (model SBL-2) with a Techne TC-8D temperature controller heated the 4.1 mL reactors to the desired temperature in approximately 2 min. We started a reaction timer when the reactors were placed in the sandbath. The reactors were continuously agitated using a wrist-action shaker set to 1° of rotation. After the desired time, the reactors were removed from the sand bath, quenched in water at room temperature, and allowed to equilibrate at room temperature for at least 120 min.

We analyzed the gas content of the reactors with GC/TCD and the method discussed in section 3.5.1, and then extracted the liquid contents of the reactors with acetone into a 10 mL volumetric flask. An Agilent 6890N GC/FID quantified the liquid contents of the reactors with a 50 m HP-5MS capillary column. In general, the injected sample, 1 μL, was heated by an inlet at 310 °C and separated by the capillary column by holding the column at 35 °C for 10 min, and then ramping the oven temperature at 2 °C/min to 50 °C, 10 °C/min to 160 °C, 30 °C/min to 300 °C, and holding for 2 min. On occasion, slight variations to this method were used to achieve complete separation of the analytes.

In some instances, multiple reactions were run at a single reaction condition to obtain estimates of the experimental uncertainty, represented by one standard deviation. We report data only from reactors with carbon balances greater than 80%, but in general, the carbon balances were greater than 90%.

3.5.3. Continuous catalytic HDO experiments - Single feed flow reactor

The single feed flow reactor and this reaction procedure are used primarily in chapter 6, and for a single catalyst, 2% Raney NiCu, in chapter 7. While the sand bath was heating to the reaction temperature, H_2, flowing at approximately 50-100 mL/min, was used to reduce all the catalysts in situ except $Ni/SiO_2Al_2O_3$ as the manufacturer indicated that this catalyst was supplied reduced and stabilized. For the $Ni/SiO_2Al_2O_3$ catalyst, the reactor was simply purged with H_2 prior to heating. When the sand bath reached the 380 °C reaction temperature, the H_2 flow was stopped. We then pumped the feed solution at an initial rate of 2 mL/min with a Chrom Tech Series lll piston pump until a pressure of 305 bar was achieved, at which point we set the flow rate to 0.218 mL/min (at ambient conditions), unless otherwise noted. Also at this time, the syringe pump containing the internal standard solution was set to 0.328 mL/min (at ambient conditions) This flow rate was maintained for at least 2 hr, providing at least three reactor volumes of fluid, prior to collecting samples to allow for reactor equilibration at steady state [3]. Time on stream (TOS) equal to zero corresponds to the time of collection of the first sample.

We collected approximately 2 mL liquid samples by flowing the liquid and gas reactor effluent through 6 mL of 0 °C isopropanol. The samples were analyzed offline by an Agilent 6890N gas chromatograph with a flame ionization detector (GC/FID) using a HP-5MS capillary column and a 2 μL injection. The inlet was held at 310 °C and a 25:1 split ratio was used. The column was initially held at 35 °C for 10 min, then ramped at 2 °C/min to 50 °C, 10 °C/min to 160 °C, and 30 °C/min to 300 °C, where it was held for 2 min. Species concentrations were calculated from their peak areas and those of the internal standard, which was present in a known concentration. Gas samples were analyzed online using a

GC/TCD and the method outlined in section 3.5.1. Analysis of the liquid reactor effluent for formic acid was carried out on a Hewlett Packard 1100 high performance liquid chromatograph (HPLC) with a refractive index detector. 5 µl of sample was injected into 0.005 N H_2SO_4 flowing at 0.5 mL/min through Rezex ROA column at 60 °C.

3.5.4. Continuous catalytic HDO experiments - Multiple feed flow reactor

The multiple feed flow reactor and procedure were used exclusively in chapter 7. To start up the flow reactor shown in fig. 3.3, we first attached the catalyst bed to the reactor, then pressurized the system with 70 bar H_2 to check for leaks. After confirming the absence of leaks, we released the reactor pressure, and began flowing H_2 at 50 – 100 mL/min while heating the reactor to 550 °C for at least one hour for the in situ catalyst reduction. We then cooled the reactor to approximately 400 °C and started flowing water, H_2, and o-cresol. For the calcined Raney Ni and calcined 5% Raney NiCu catalysts we set the H_2O, o-cresol, and H_2 flow rates to 1 mL/min, 0.030 mL/min, and 0.006 mol/min, respectively, to build the reaction pressure. Upon the reactor reaching ~240 bar, we lowered the H_2O flow rate to the desired steady state value of 0.270 mL/min, while maintaining the other flow rates. At this point, we also started the internal standard solution flowing at 0.400 mL/min and the N_2 reference gas at 20 mL/min. The startup procedure for the 10%, 0.5% $NiCu/Al_2O_3$ catalyst differed only in the H_2O flow rate, which was set at 0.270 mL/min during the entire startup period. Upon reaching the desired temperature of 365 °C at the mixing point thermocouple and the desired reactor pressure of 280 bar, we began collecting samples. We found that the reactor took approximately 225 min to achieve steady carbon balances and we report this time as zero min on stream.

The liquid products not collected for analysis were sent to a waste container while the gas products were sent to the GC/TCD and analyzed using the method described earlier. The liquid samples were analyzed on a GC/FID with a 50m HP-5MS capillary column. The injected sample, 1 μL, was heated by an inlet at 310 °C and separated by the capillary column by holding the column at 35 °C for 10 min, and then ramping the oven temperature at 2 °C/min to 50 °C, 10 °C/min to 160 °C, 30 °C/min to 300 °C, and holding for 2 min. A GC/MS used this same method and column to determine the identities of some molecules.

3.6. Data Analysis

We calculated conversion, yield, selectivity, and carbon recovery as follows:

$$Conversion = 1 - \frac{C_{OR,e}}{C_{OR,O}} \quad Eq. 3.1$$

$$Yield = \frac{C_i}{C_{OR,O}} \quad Eq. 3.2$$

$$Selectivity = \frac{C_i}{\sum C_i} \quad Eq. 3.3$$

$$Carbon\ recovery = \frac{\sum C_i}{C_{OR,O}} \quad Eq. 3.4$$

where $C_{OR,e}$, $C_{OR,o}$, and C_i refer to the concentrations, in mol C/L, of organic reagent (OR) exiting the reactor, of organic reagent entering the reactor, and of any product, respectively. We also will refer to the liquid hydrocarbon yield (terminology used in chapter 7), or synonymously the deoxygenated product yield (terminology used in chapters 5 and 6), which is the sum of the yields of all hydrocarbons in the liquid phase reactor effluent. On occasion, the flow reactor would release a large volume of gas, resulting in a slight pressure

drop in the reactor. This increased gas flow resulted in high yields of the carbon containing gasses (i.e., methane and CO_2) and high carbon recoveries (≥ 120%) if sampling occurred simultaneously with a gas release. When such anomalous data were collected, we removed them from the data set.

References

1. G. W. Huber, J. W. Shabaker, J. A. Dumesic, Science 300, (2003) 2075.
2. T. M. Brown, P. Duan, P. E. Savage, Energy Fuels 24, (2010) 3639-3646.
3. J. N. Jensen, Journal of environmental engineering 127, (2001) 13-18.

Chapter 4

Characterization of Product Fractions from Hydrothermal Liquefaction of *Nannochloropsis* sp. and the Influence of Solvents

The work in the chapter was performed with an equal contribution from Peter Valdez.

The use of different solvents to extract bio-oils from microalgae HTL in previous studies makes it difficult to compare results from different studies, even with the same feedstock, because it is unclear how or whether the different solvents affect the yields and compositions of the bio-oil, and by extension, the dissolved aqueous solids and insoluble solid residue. It is likely that some of the hydrothermal liquefaction products partition differently among the solid, aqueous, and organic phases when different solvents are used to recover the bio-oil. Thus, the solvent might have an effect on the yield and composition of the crude bio-oil and other fractions produced from hydrothermal liquefaction. To our knowledge, this potential effect has not been the subject of any previous published research.

The research reported herein elucidates how the yields and compositions of the product fractions from hydrothermal liquefaction of a marine alga (*Nannochloropsis* sp.) depend on the solvent used to recover the crude bio-oil. We chose to study dichloromethane, chloroform, hexane, and cyclohexane because they have been used in

previous liquefaction studies [1-6]. We included decane and hexadecane because these straight-chain-alkanes mimic the main compounds expected to exist in a potential recycle stream of upgraded algae bio-oil that has undergone deoxygenation and some cracking reactions. These solvents could also allow identification and quantification of volatile compounds in the bio-oil that would co-elute with the light solvents that are more commonly used. Methoxycyclopentane was included as a greener alternative to chlorinated solvents [7]. We classify hexadecane, decane, hexane, and cyclohexane as non-polar solvents and methoxycyclopentane, chloroform, and dichloromethane as polar solvents.

In addition to elucidating the influence of different solvents, the work reported herein is noteworthy because we collected and analyzed all of the product fractions from hydrothermal liquefaction. Previous studies have focused primarily on the bio-oil and perhaps the gas fraction, but no previous article on algae liquefaction has analyzed and quantified directly the amount of material in all four of the product fractions, including the aqueous phase products and residual solids. Our analyses include gravimetric yields measured directly (not inferred by assuming mass balance closure), elemental analysis, and, where possible, quantitative molecular characterization of the product fractions. These results are essential to understanding the composition of the bio-oil produced from the HTL of microalgae, and determining the product classes that need to be examined for HDO in chapters 5-7.

4.1. Control experiment

To determine the effectiveness of the post-reaction procedures and to quantify systematic mass losses from sample transfers and solvent evaporation, we performed control experiments with a simple three-component synthetic crude algal bio-oil. The synthetic crude bio-oil consisted of 100 mg of palmitic acid, 50 mg of cholesterol, and 10 mg of tetracosane dissolved in 1 mL of chloroform. These components represent those identified in the crude bio-oil from previous work with this alga [3, 6]. This solution was deposited into the reactors, and the solvent was evaporated by flowing N_2 into the open reactors for 1 hr. We chose this method to mimic the post liquefaction conditions in the reactor in which the bio-oil adheres to the reactor walls. We next added 19.4 mL of deionized water and 10 mL of solvent to each reactor. Duplicate experiments were performed for each solvent. We sealed the reactors and followed the workup procedure described above. The recovery of palmitic acid, cholesterol, and tetracosane was determined using GC-FID.

Table 4.1 shows the percentage of each compound recovered with each of the solvents in this study. With the exception of hexadecane, each solvent recovered at least 84% of each compound. The recoveries of palmitic acid and cholesterol were highest when using the chlorinated solvents and methoxycyclopentane (i.e., the polar solvents). The recovery of tetracosane was around 85% in all of the solvents except for hexadecane. The losses can be attributed to the failure of the solvent to completely remove the compounds from the reactor walls or to dissolve all of the material present in the reactor. Low recovery with hexadecane is likely due to its high molecular weight and reduced molar volume

inhibiting it from fully dissolving the synthetic bio-oil components [8]. Since the methods used here to recover the components in the synthetic bio-oil are identical to those used to recover the bio-oil from algae liquefaction, we anticipate hexadecane being the poorest solvent for these components in the bio-oil and the polar solvents being the best.

Table 4.1. Recovery (%) with different solvents of components in synthetic bio-oil.

	Hexadecane	Decane	Hexane	Cyclohexane	Methoxy cyclopentane	Chloroform	Dichloromethane
Palmitic Acid	74±3	88±1	85±1	89±0	92±1	91±2	95±4
Tetracosane	63±0	84±1	86±4	84±1	88±3	88±1	85±4
Cholesterol	76±3	90±9	89±8	87±1	93±5	93±1	93±6

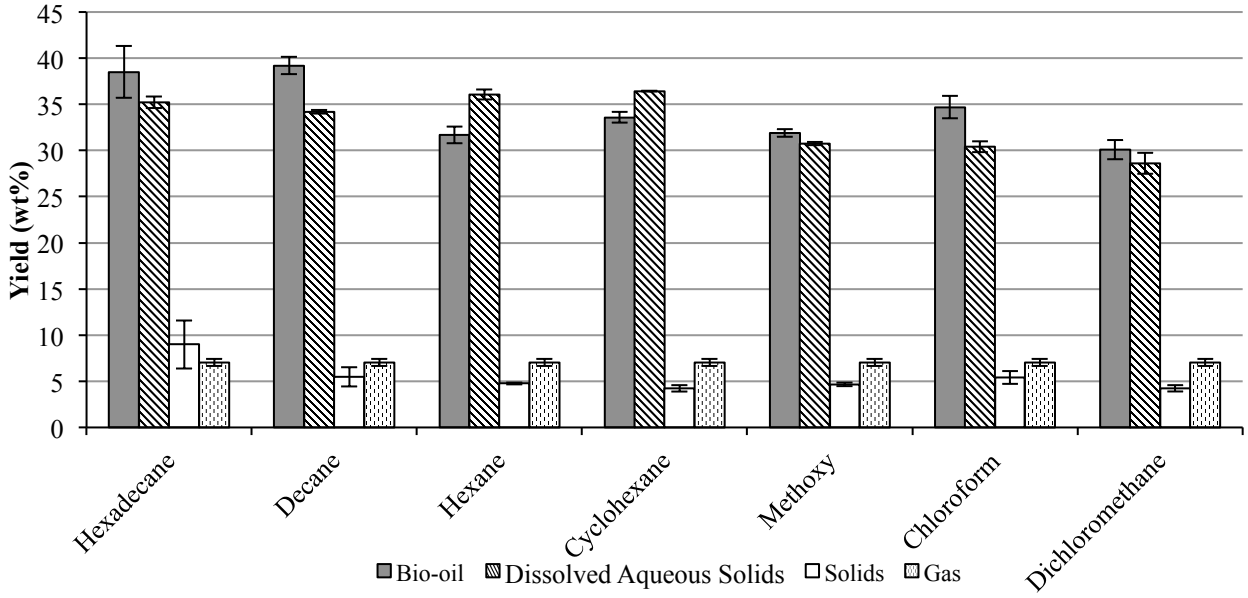

Figure 4.1. Yields of liquefaction product fractions with different solvents.

4.2. Gravimetric yields of liquefaction product fractions

Fig. 4.1 shows the yields of the four liquefaction product fractions obtained using different solvents. Each yield was calculated as the mass of each dry product phase relative

to the mass of the algae solids (dry basis) added to each reactor. The bio-oil, which ranged from 30 – 39 wt% yield, and the dissolved aqueous solids, which ranged from 29 – 36 wt% yield, were always the most abundant products. Residual solids (4 – 9 wt% yield) and gases (7 wt% yield) were less abundant. Biller and Ross[8] reported yields within these ranges for bio-oil, residual solids, and gases from *Nannochloropsis* sp. liquefaction with dichloromethane as solvent. Fig. 4.1 verifies that the yield of a given product fraction varies from solvent to solvent, but this variation is within bounds of only a few wt%. Of course, the gas yield is independent of the solvent.

The yield of residual solids was higher with the straight-chain alkane solvents, and it increases as the carbon number of the solvent increases. The high solids yield does not appear to be accompanied by lower yields of bio-oil or dissolved aqueous solids.

The yield of dissolved aqueous solids was always comparable to the yield of bio-oil. These aqueous-phase products include the water-soluble compounds that formed during liquefaction, salts that were present in the algae slurry media, and any water-soluble metals or minerals present in the algae. The use of a non-polar solvent increased aqueous product yields when compared to the polar solvents. In fact, using hexane and cyclohexane resulted in more mass being partitioned to the aqueous solids than to the bio-oil. Hexadecane and decane show the same high yields of dissolved aqueous solids as did hexane and cyclohexane, but there is not the same concomitant decrease in the yield of bio-oil. The yield of bio-oil from hexadecane might be high because a different method was used to quantify it. The yield from decane would be high if some residual decane remained

in the bio-oil, even after the extensive efforts to remove all of the solvent. Given the low vapor pressure of decane, this is possible.

Table 4.2. NH_3 content in aqueous phase after liquefaction

	NH_3 conc (mg/mL)	NH_3 Yield (mg / g Dry Algae)	% N % N in Dry Algae
Hexadecane	12.1±1.1	46.2±4.5	54.7±5.3
Decane	11.3±0.1	41.5±0.4	49.1±0.4
Hexane	11.5±0.7	42.6±2.5	50.4±2.9
Cyclohexane	10.4±1.0	40.5±0.9	48.0±1.0
Methoxycyclopentane	12.1±0.7	43.6±2.5	51.6±2.9
Chloroform	11.9±0.1	43.6±0.4	51.6±0.4
Dichloromethane	12.1±0.6	44.1±2.2	52.2±2.6

In addition to the solids that survive the lyophilization procedure, the aqueous phase also contained ammonia. It had an ammonia scent, along with a foul smell from other compounds. That the aqueous phase had a strong odor indicates that some of the aqueous-phase products had a high volatility and escaped into the vapor phase. Thus, the ammonia concentration that would be measured in the aqueous phase would necessarily represent a lower bound. The actual amount of ammonia initially present immediately after liquefaction would have been even higher. We determined the ammonia content of the aqueous phase recovered from the liquefaction experiments, and table 4.2 shows the results. Nearly half of the N in the algal biomass is converted into ammonia that partitions into the aqueous phase. The ammonia concentration in the aqueous phase is independent of the solvent selected to extract the bio-oil.

Previous studies of hydrothermal liquefaction of *Nannochloropsis* sp. at 350 °C for 60 min reported that the yields of bio-oil, recovered with dichloromethane, were 43 wt% and 35 wt% [3, 6]. The present bio-oil yield using dichloromethane was 30 wt%. The different methods used in these studies to recover the bio-oil probably play a role in obtaining these different yields. For example, Brown et al.[10] used three separate 15 mL aliquots of dichloromethane (45 mL total) to recover the bio-oil from 0.9 g algae (dry weight). The present study used just a single 10 mL aliquot of solvent to recover bio-oil from ~ 4 g of algal biomass (dry weight). Additionally, some of the differences in the bio-oil yields are likely due to the batch-to-batch variation of the purchased algae.

The overall recovery of total mass (algae paste and solvent) in the present liquefaction experiments is 95 ± 1%. Only about 15% of this total mass is dry algal biomass, however, and 74 – 94 wt% of the initial algal mass appears in the products that we recovered. Some mass loss is unavoidable in the multiple transfers that take place during product workup. Other material losses likely occur during the lyophilization procedure used to isolate the dissolved aqueous solids. Some ammonia is likely lost due to volatilization during sample handling and product recovery. Char that was insoluble in both organic solvent and water or some crude bio-oil may have remained within the reactor (likely adhering to the reactor wall) as yet another source of mass loss. That some material remained within the reactor was evident during reactor cleaning after an experiment. Solvents and brushes used to clean the reactor walls always returned discolored by a dark material. Finally, we know that some CO_2 was dissolved in the aqueous phase and hence not detected by the gas analysis. On the basis of Henry's Law, we calculate

that the mass of dissolved CO_2 was at least 6 wt% of the initial mass of the algae (dry basis) loaded into the reactor. The actual amount of dissolved CO_2 could be even higher, because the aqueous phase also contained ammonia, which can react with CO_2 and thereby increase the amount of CO_2 absorbed into the aqueous phase.

4.3 Gas analysis

Table 4.3 shows the composition (mol %) and mass yield of H_2, CH_4, CO_2, C_2H_4, and C_2H_6 from hydrothermal liquefaction. No O_2, N_2, CO, or C_3 gases were detected. The gas composition is similar to that obtained previously using the same feedstock and reaction conditions. Duan and Savage [6] report a composition of 80 mol % CO_2 and 15 mol % H_2. Likewise, Brown et al. [3] report a composition of 66 mol % CO_2 and 30 mol % H_2. Overall, 88 ± 15 mol % of the gas phase was accounted for with this analysis, and it consisted of a large proportion of CO_2. NH_3, N_2O, NO_2, and HCN are not detectable when using the methods described previously. Water is expected to be present, but only in its saturation composition of about 2.5 mol %.

Table 4.3. Composition and Yields (mg/g dry algae) of Gas Phase Products

Gas	mol %	Yield
Hydrogen	10±3	0.4±0.1
Methane	1.8±0.4	0.6±0.1
Carbon Dioxide	74±14	68±4
Ethene	0.4±0.2	0.2±0.1
Ethane	0.7±0.2	0.4±0.1

4.4. Elemental analysis.

The dried *Nannochloropsis* sp. microalgae was 41.89, 5.64 and 6.95 wt% carbon, hydrogen, and nitrogen respectively. This elemental composition is very similar to that reported in other studies with *Nannochloropsis* sp., both in our lab [3, 6] and that of others [9]. We did not measure S or O, but they have been reported previously as 0.5 and 25.1 wt%, respectively [3]. The H/C and N/C atomic ratios are 1.60 and 0.14, respectively.

Table 4.4 summarizes the elemental compositions and the H/C and N/C ratios for each of the product fractions. The bio-oil always had a higher wt% of carbon, hydrogen, and nitrogen than did the dissolved aqueous solids and the residual solids. The bio-oils were enriched in carbon and hydrogen, but depleted in nitrogen relative to the original alga feedstock. This preferential partitioning of C and H into and N away from the bio-oil is both desirable and consistent with previous reports of hydrothermal liquefaction of microalgae at similar conditions [3, 5, 6, 9-11] The bio-oil H/C ratios are modestly higher than those in the dry algae, and the N/C ratio is reduced to nearly one third of its value in the dry feedstock. The polar solvents produced bio-oils with the highest carbon content and dissolved aqueous solids with the lowest carbon content. This outcome for the bio-oil can be rationalized on the basis of past research that showed that chloroform recovered bio-oil contained large, carbon rich molecules similar to resins and asphaltenes [12]. Such compounds would be insoluble in non-polar solvents. The elemental composition of the bio-oil recovered with dichloromethane was nearly the same as that reported in our earlier work [3, 6] with the same alga processed at the same liquefaction conditions. In these

earlier studies, the C, H, and N content of the bio-oils were 75.3, 10.2, and 4.18 wt% [6] and 76.0, 10.3, and 3.9 wt% [3].

The residual solids typically have a higher H/C and N/C ratio than do the dissolved aqueous solids. To the best of our knowledge, only one other lab has provided information about the elemental composition of both of these product fractions from algae liquefaction [12] The H/C ratio of around 2.0 for the dissolved aqueous solids is consistent with these materials containing some organic acids, which have been reported as aqueous-phase byproducts from hydrothermal treatment of algal biomass [13].

Table 4.4. Elemental composition (wt% and atomic ratio) of product fractions.

Solvent	Bio-oil					Dissolved Aqueous Solids					Residual Solids				
	C	H	N	H/C	N/C	C	H	N	H/C	N/C	C	H	N	H/C	N/C
Hexadecane	N/A*	N/A	N/A	N/A	N/A	16.32	2.53	1.32	1.8	0.07	29.73	6.55	2.12	2.6	0.06
Decane	68.80	9.37	4.44	1.6	0.06	15.74	2.67	1.31	2.0	0.07	13.42	3.30	1.73	2.9	0.11
Hexane	70.45	9.80	4.04	1.7	0.05	15.76	2.58	1.18	2.0	0.06	18.32	4.25	2.79	2.8	0.13
Cyclohexane	64.87	9.76	3.87	1.8	0.05	14.59	2.40	1.26	2.0	0.07	13.04	4.42	3.17	4.0	0.21
Methoxycyclopentane	72.27	9.70	4.06	1.6	0.05	13.71	3.24	0.93	2.8	0.06	11.82	3.79	2.69	3.8	0.20
Chloroform	73.68	9.85	4.62	1.6	0.05	13.87	2.60	0.95	2.2	0.06	20.39	5.43	2.4	3.2	0.10
Dichloromethane	75.76	10.57	4.52	1.7	0.05	13.75	2.54	1.02	2.2	0.06	21.10	4.47	2.70	2.5	0.11

*Bio-oil in hexadecane could not be dried for elemental analysis

The elemental compositions of the algae feedstock and the product fractions were used to calculate the distribution of elements in the various product fractions. The

distribution of each element in each fraction is calculated as its mass in that product fraction relative to its mass in the algae feedstock. Figures 4.2 – 4.4 display the results.

Fig. 4.2 shows that the bio-oil typically contained 50 – 65% of the amount of C and H and about 20% of the N originally present in the algae feedstock. In fact, the majority of the C and H that we recovered resided in the bio-oil fraction. The C and H yields in the bio-oils were nearly identical for a given solvent, and there was not much variation from solvent to solvent. Fig. 4.3 shows that the C, H, and N yields in the dissolved aqueous solids were typically around 12, 15, and 5%, respectively. These values are only about one fourth as large as the yields in the bio-oil. The polar solvents had lower C and N yields than did the hydrocarbon solvents. Fig. 5 shows that the yields of C, H, and N in the residual solids are even lower. Inspecting Figs. 4.3 and 4.4 further shows that the H yields in the dissolved aqueous solids and in the residual solids always exceed the carbon yields. The N yields were always the lowest of the three in the dissolved aqueous solids, whereas they were comparable to the C yields in the residual solids.

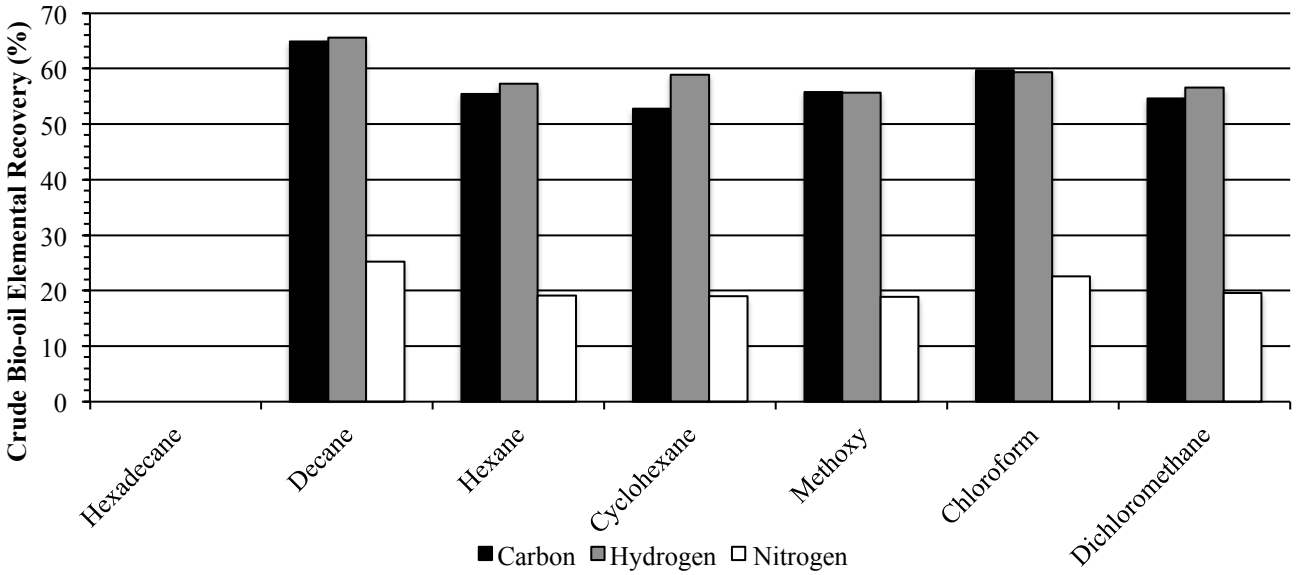

Figure 4.2. Percentage of C, H, and N in algae transferred to crude bio-oil.

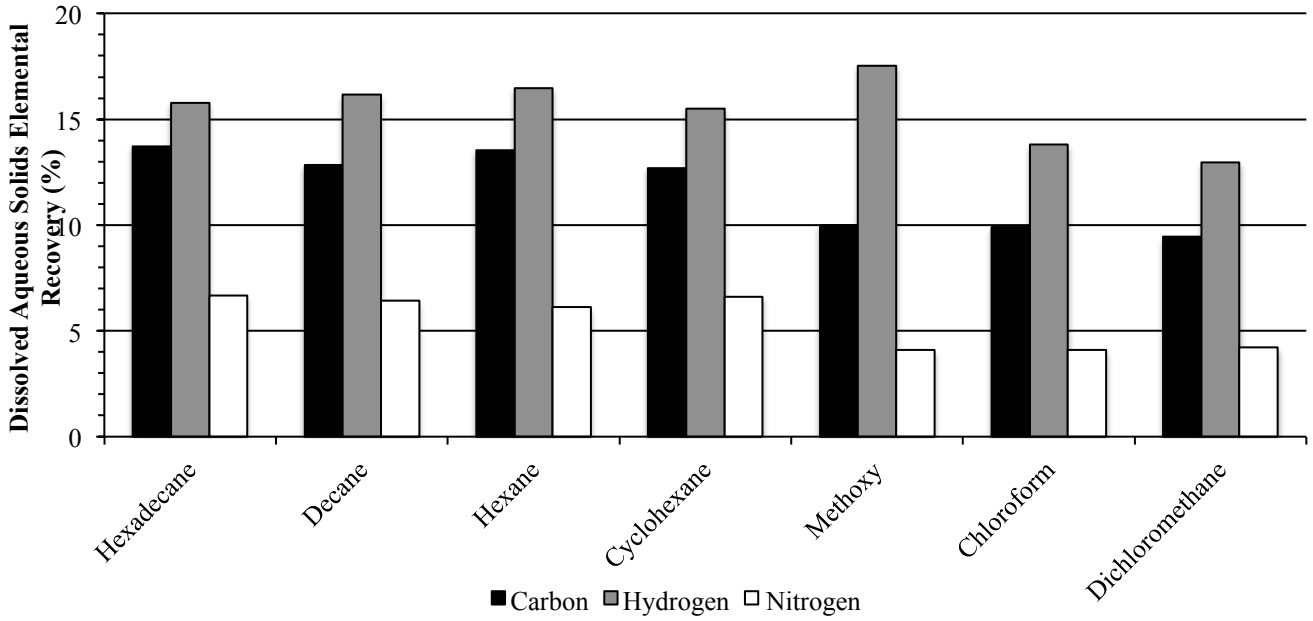

Figure 4.3. Percentage of C, H, N in algae transferred to dissolved aqueous solids.

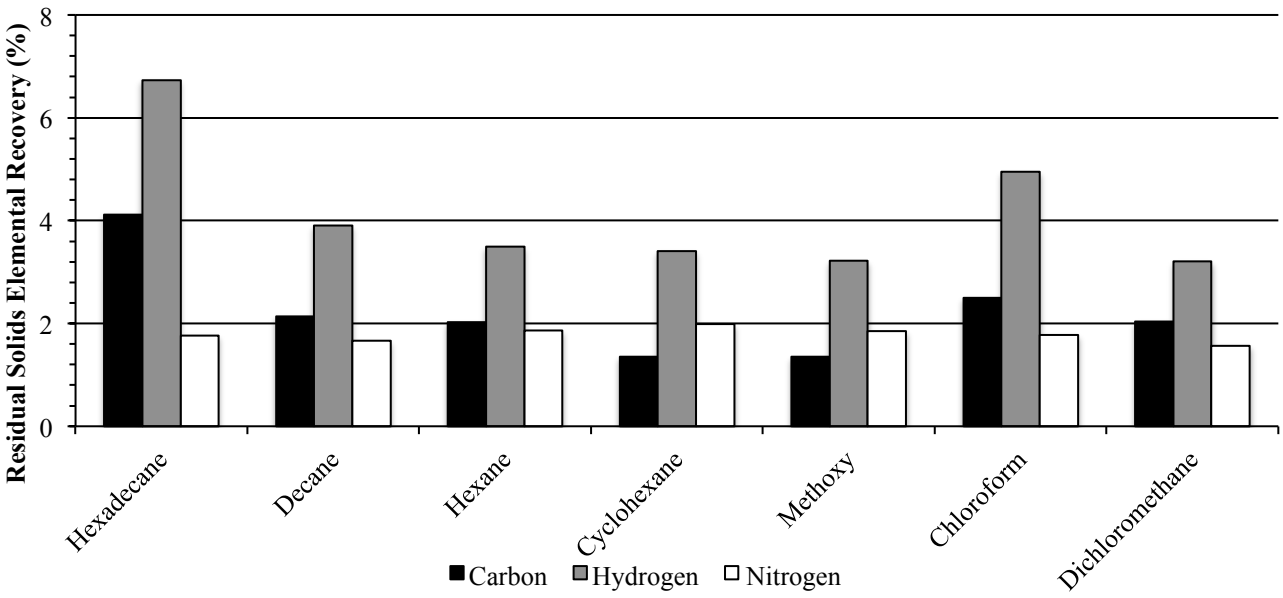

Figure 4.4. Percentage of C, H, and N in algae transferred to residual solids

Knowing the yields of C, H, and N within each of the four product fractions (bio-oil, dissolved aqueous solids, solids, gas) and the ammonia concentration in the aqueous phase permits calculation of the overall recovery of each element. We could not do this calculation for the experiment with hexadecane as we had no elemental analysis for the bio-oil in this case. Table 4.5 shows that the atom recovery always exceeded 66% for C, 87% for H, and 76% for N. The recoveries were about the same for all of the solvents save decane, which led to the highest recovery of C, H, and N. Table 4.5 also shows the overall mass balance in terms of mass of material recovered in the four product fractions plus ammonia relative to the dry weight of algae loaded into the reactor. The mass balance is higher with the non-polar solvents (e.g., 90 wt% with decane and 94 wt% with hexadecane) than it is with the polar solvents (e.g., 74 wt% with dichloromethane).

Table 4.5. C, H, N, and mass balance for liquefaction products

Solvent*	% Recovery			Mass Balance (wt%)	Modified % Recovery			Modified Mass Balance (wt%)
	C	H	N		C	H	N	
Decane	80	99	82	90	100	104	100	104
Hexane	71	91	78	84	100	97	100	102
Cyclohexane	67	91	76	85	100	97	100	106
Methoxy-cyclopentane	67	90	76	79	100	97	100	99
Chloroform	72	92	80	82	100	97	100	100
Dichloromethane	66	87	78	74	100	93	100	95

*Bio-oil in hexadecane could not be dried for elemental analysis, but mass balance was 94 wt%.

The data in Table 4.5 permit a rough test of hypotheses mentioned earlier in this chapter for the mass balances being less than 100 wt%. We assume that the losses from carbon can be accounted for by dissolved CO_2 in the aqueous phase and carbonaceous char that remains unrecovered in the reactors. We calculated the amount of dissolved CO_2 from Henry's Law and the known CO_2 yield. We then closed the C balance by assuming that all of the remaining unrecovered C atoms were resident in char, which was assumed to contain only carbon. We assume that the nitrogen losses are exclusively NH_3 vapors lost during the experimental protocol. Making these assumptions about the missing C and N atoms leads to the modified element and mass balances shown in the right half of Table 4.5. The modified H recovery and mass balance both close to within a few percent for all of the solvents. Thus, the hypothesis that the missing C is primarily dissolved CO_2 and char and

that the missing N (and H) is primarily lost NH_3 is consistent with the data we obtained. The modified H recovery and modified mass balance being lower for dichloromethane indicate that char and NH_3 alone might not account for all of the missing material. We suspect that this solvent did not remove all of the crude bio-oil from the reactor and that this missing bio-oil perhaps accounts for the remainder of the material. Recall that dichloromethane gave the lowest bio-oil yield of any of the solvents and that the yield was lower than those we had obtained in the past when working with the same algae strain.

4.5 Bio-oil composition

All of the bio-oils were analyzed chromatographically to gain information about their molecular composition. Figs. 4.5 and 4.6 show chromatograms of two crude bio-oils analyzed with two different GC columns. We have quantified 19 molecular components in the crude algal bio-oil for the first time. We apportioned the identified compounds into three different classes: light ends, aliphatics, and fatty acyls. We classify compounds that have boiling points less than 150 °C as the light ends. Examples include 1-methylpyrrole, dimethyl disulfide, 2-methyl-1-butanol, methyl benzene, 1-ethyl pyrrole, ethyl benzene, 1,2-dimethyl benzene, and 1,5-dimethyl pyrrole as shown in fig. 4.5. The bio-oil also contained aliphatic compounds such as heptadecane, phytane (3,7,11,15-tetramethyl hexadecane), phytene (2,6,4,10-tetramethyl 2-hexadecene and 3,7,11,15-tetramethyl 2-hexadecene), docosane, cholestane, and cholestene. The fatty acyls in the bio-oil are palmitic (hexadecanoic), palmitoleic (hexadecenoic), stearic (octadecanoic), and oleic (octadecenoic) acids as well as palmitic amide (hexadecanamide).

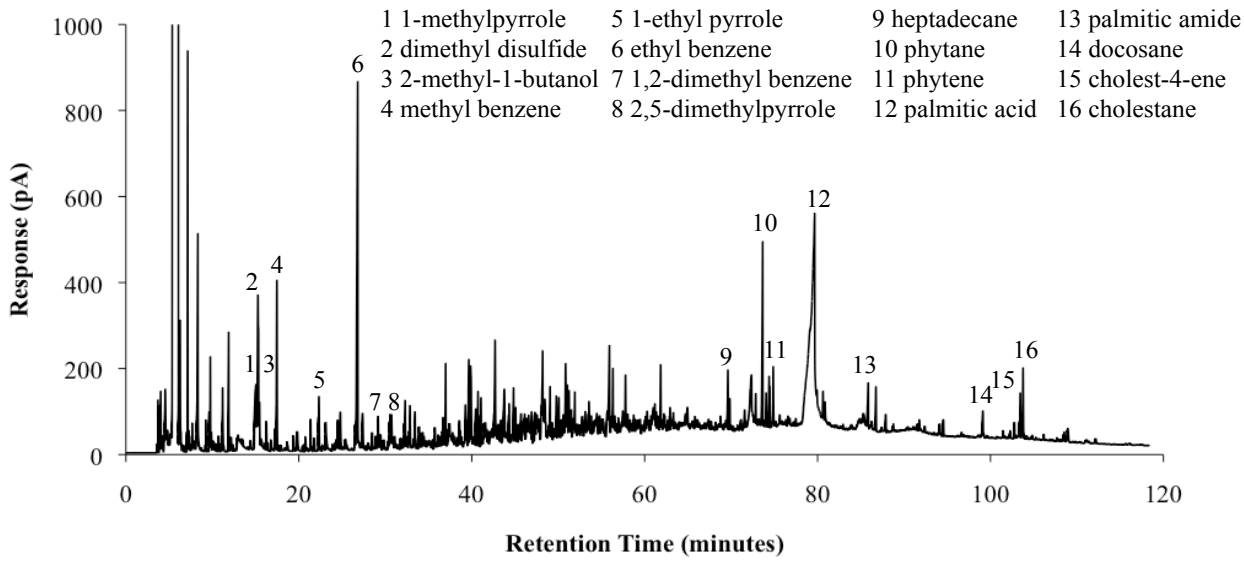

Figure 4.5. Chromatogram of crude bio-oil (dichloromethane solvent, HP-5 capillary column).

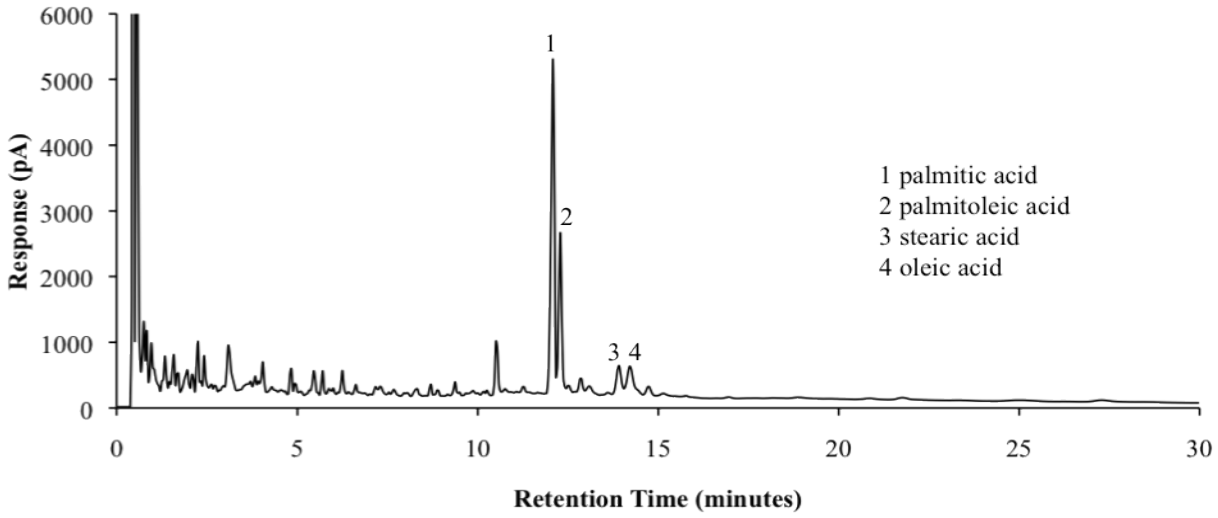

Figure 4.6. Chromatogram of crude bio-oil for fatty acid analysis (chloroform solvent, Nukol capillary column).

Table 4.6 displays the yields of each compound we identified as well as the total yields of each class of compounds in the bio-oil. To the best of our knowledge, these data are the first to give quantitative information about the absolute yields of individual molecules in algal bio-oil from hydrothermal liquefaction. Previous work provided only information about the relative abundance of different components [3, 5, 6, 12]. The compounds in the bio-oil that have been quantified in this work account for roughly 62% of the total peak areas found in the chromatograms, but less than 22 ± 8 wt% (on average) of the bio-oil mass. Adding in the 38% of the total peak area that was not identified would increase the GC-elutable portion of the bio-oil to roughly 35% of the total. Thus, it seems that the bio-oil contained a significant proportion (~ 65%) of high molecular weight compounds that are not amenable to analysis by capillary column GC.

The molecules categorized as light ends include N-, O-, and S-containing compounds in addition to aromatic hydrocarbons. Dimethyl disulfide and ethylbenzene are the most abundant of the light ends. Dichloromethane and chloroform, two of the polar solvents, extracted the highest amount of light ends in the bio-oil. The yields of light ends vary by about a factor of two over the range of solvents studied. Most of this variation is due to the low yields of light ends in decane and methoxycyclopentane. Most light end compounds were not detectable in methoxycyclopentane because the solvent peak eluted at the same time as the compounds of interest. The yields were low in decane because the use of the least volatile solvents considered in this work (hexadecane and decane) led to poor chromatographic resolution of compounds that eluted just before the solvent peak. Most of the light end compounds eluted shortly before the decane solvent peak, and they were not

chromatographically resolved and hence not quantified. Solvent effects did not influence the light end peaks in hexadecane because the elution time between light ends and solvent was long enough to allow for chromatographic development of the solute in the column.

The total yields of aliphatic compounds shown in Table 4.6 do not vary significantly from solvent to solvent, but the three polar solvents produced modestly higher recoveries of aliphatic compounds than did the non-polar solvents. The most abundant aliphatic compounds are phytyl chains and cholesterol derivatives. Straight chain alkanes were also present but only at 10 – 20% of the concentration of the other aliphatic compounds. The branched alkanes and the cholesterol derivatives had a higher yield in hexadecane than in the other solvents.

Table 4.6. Yields (mg/g dry algae) of Bio-oil Compounds Recovered with Different Solvents.

		Hexadecane	Decane	Hexane	Cyclohexane	Methoxy cyclopentane	Chloroform	Dichloromethane
Light Ends	1-Methyl Pyrrole	0.66±0.16	0.95±0.01	1.01±0.02	1.23±0.04	NQ	1.28±0.02	1.24±0.12
	Dimethyl Disulfide	2.65±0.76	2.75±0.04	4.50±0.20	1.99±0.10	NQ	7.49±0.36	6.88±1.52
	2-Methyl-1-Butanol	0.79±0.09	0.70±0.03	1.08±0.52	0.87±0.10	NQ	0.88±0.09	0.69±0.04
	Toluene	0.88±0.23	0.239±0.001	1.23±0.04	1.24±0.02	NQ	1.50±0.01	1.48±0.11
	1-Ethylpyrrole	0.53±0.06	NQ	0.66±0.06	0.63±0.01	0.48±0.01	0.67±0.01	0.68±0.05
	Ethyl Benzene	3.79±0.45	3.40±0.12	4.33±0.19	4.33±0.05	4.54±0.03	4.96±0.04	4.80±0.47
	o-Xylene	0.98±1.21	NQ	0.32±0.01	0.36±0.01	0.358±0.002	0.27±0.01	0.32±0.04
	2,5 Dimethyl Pyrrole	0.54±0.06	NQ	0.52±0.01	0.567±0.002	0.77±0.01	0.56±0.11	0.57±0.11
	Total	10.8±1.5	8.05±0.13	13.6±0.6	11.2±0.2	6.15±0.03	17.6±0.4	16.7±1.6
Aliphatics	Phytane	1.69±0.16	0.88±0.72	1.31±0.02	1.29±0.03	1.40±0.05	1.37±0.05	1.38±0.16
	Phytene	2.02±0.08	1.30±0.48	1.51±0.22	1.54±0.11	1.69±0.01	1.68±0.08	1.85±0.65
	Heptadecane	0.15±0.26	0.25±0.18	0.31±0.00	0.36±0.01	0.39±0.02	0.34±0.02	0.31±0.05
	Docosane	0.11±0.10	0.139±0.001	NQ	NQ	0.14	0.153±0.004	0.10±0.09
	Cholest-4-ene	0.48±0.07	0.28±0.17	0.36±0.01	0.40±0.01	0.37±0.02	0.323±0.001	0.34±0.01
	Cholestane	0.75±0.08	0.41±0.28	0.56±0.01	0.59±0.02	0.65±0.01	0.58±0.01	0.61±0.03
	Total	5.19±0.34	3.27±0.94	4.05±0.22	4.18±0.12	4.64±0.06	4.45±0.09	4.59±0.68
Fatty Acyls	Palmitic Amide	2.69±1.98	0.58±0.09	0.50±0.14	0.67±0.25	0.44±0.01	1.22±0.27	0.70±0.03
	Palmitic Acid	4.96±0.57	8.88±3.96	17.3± 4.2	11.2±2.9	13.3±1.4	30.9±2.2	26.4±1.8
	Palmitoleic Acid	4.72±0.48	10.6±6.2	14.3±2.8	15.0±1.5	16.0±1.1	15.2±1.2	13.6±0.5
	Stearic Acid	8.56±0.20	9.76±1.01	12.7±3.4	10.0±1.5	11.4±1.4	25.2±1.1	22.4±1.4
	Oleic Acid	12.3±0.2	12.6±1.0	14.3±1.6	13.1±1.2	14.1±0.4	17.5±0.4	15.8±0.4
	Total	33.2±2.1	42.7±7.5	59.4±6.3	50.4±3.8	55.7±2.2	90.0±2.8	79.9±2.4

NQ: Not quantifiable

We identified and quantified four free fatty acids (palmitic, palmitoleic, stearic, oleic) in the algae liquefaction bio-oil. There are also some free fatty amides present, but in

lower concentration. The free fatty acyls make up the majority (~ 80%) of the material quantified by GC-FID. Solvent selection significantly affects the yields of free fatty acyls, with the chlorinated solvents producing the highest yields of free fatty acyls in the bio-oil. In contrast, hexadecane and decane provided the lowest yields. This outcome is likely due to these solvents being unable to dissolve fully all of the free fatty acyls.

4.6. High molecular weight compounds

As noted in the previous section, GC analysis quantified at most 22 wt% of the compounds in the crude bio-oil. It is likely that much of the remaining material consists of high molecular weight compounds that do not elute from a GC column. We used field desorption mass spectrometry to test this hypothesis that higher molecular weight compounds are present in the bio-oil. Fig. 4.7 shows the mass spectrum obtained using electron impact ionization for the bio-oil sample that was recovered using dichloromethane. The sample shows peaks, albeit at low abundance, at mass/charge (m/z) ratios exceeding 500. Electron impact methods lead to fragmentation of the compound(s) of interest, so the peaks in fig. 4.7 probably do not correspond to molecular ions. Thus, we next used chemical ionization MS, which generates ions without fragmenting the molecule. This technique led to peaks that were in the same mass range as determined by the EI analysis. Inspection of the insertion probe after taking the mass spectrum revealed that much of the material remained on the probe, indicating that the compounds were not volatilized and thus not detected by the MS. This result nevertheless confirms the hypothesis that the crude bio-oil contained a large proportion of high-molecular weight compounds. If these

compounds could not be liberated from the MS probe by heating to 300 °C, under vacuum, they clearly would not be able to enter and/or elute from a capillary GC column.

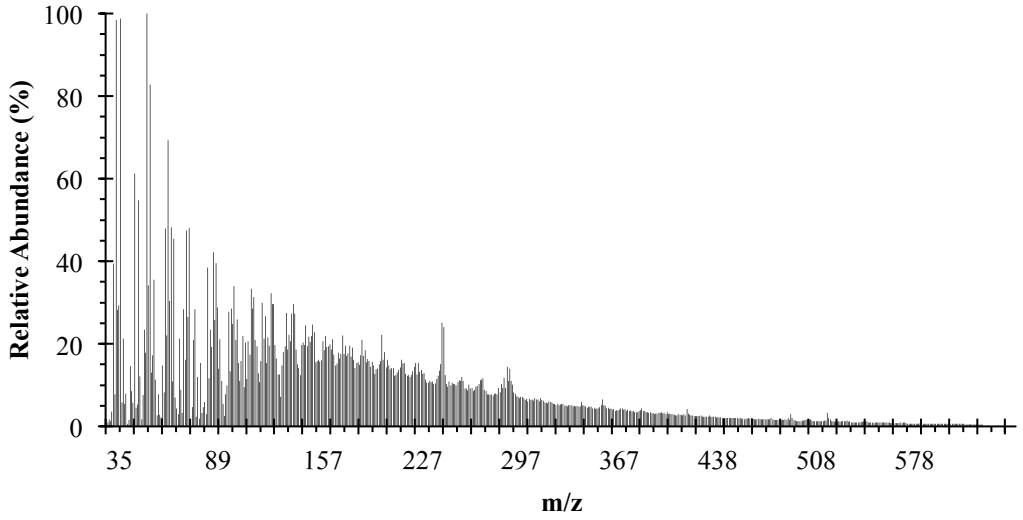

Figure 4.7. EI Mass spectrum of bio-oil recovered using dichloromethane.

4.7. Conclusions

This work is the first to quantify directly the amount and composition of material in each of the four product fractions formed by hydrothermal liquefaction of microalgae. Doing so accounted for up to 94 wt% of the initial mass of the dry algae loaded into the reactor (with hexadecane as solvent). Accounting for products observed but not quantified (dissolved CO_2, char, NH_3 losses) led to mass balances ranging from 95 – 106 wt% for the different solvents employed. Solids dissolved in the aqueous phase and solids insoluble in both water and the organic solvent contained largely inorganic material, but the H/C atomic ratios typically exceeded two, which suggests the presence of some organic

compounds in these product fractions. This work also confirms the presence of high-molecular weight compounds in the crude bio-oil fraction.

With the experimental protocol used herein, the choice of solvent used to recover crude bio-oil from hydrothermal liquefaction of microalgae affects the bio-oil yield and composition. Non-polar solvents gave modestly higher gravimetric yields but bio-oils with lower carbon content and thus lower energy density. Polar solvents gave lower yields but a much higher fatty acid content. Solvent choice also had an effect on the carbon content of the dissolved aqueous solids. The polar solvents produced solids that were lower in both C and N relative to those recovered with nonpolar solvents.

For a given solvent and given microalgae strain, the yield of bio-oil that is recovered can depend on the specific lot of algae used and the specific conditions used to recover the crude bio-oil. A lower oil yield was obtained when using a lower ratio of solvent to algae.

Acknowledgements

This work was completed with an equal contribution from Peter Valdez. We thank Mike Nelson for assistance with the ammonia measurements and Jim Windak for performing the electron and chemical ionization mass spectrometry.

References

1. Y. Dote, S. Sawayama, S. Inoue, T. Minowa, S. Yokoyama, Fuel 73, (1994) 1855-1857.
2. T. Minowa, S. Yokoyama, M. Kishimoto, T. Okakura, Fuel 74, (1995) 1735-1738.
3. T. M. Brown, P. Duan, P. E. Savage, Energy Fuels 24, (2010) 3639-3646.
4. T. Matsui, A. Nishihara, C. Ueda, M. Ohtsuki, N. Ikenaga, T. Suzuki, Fuel 76, (1997) 1043-1048.
5. A. B. Ross, P. Biller, M. L. Kubacki, H. Li, A. Lea-Langton, J. M. Jones, Fuel 89, (2010) 2234-2243.
6. P. Duan, P. E. Savage, Ind. Eng. Chem. Res. 50, (2011) 52-61.
7. K. Watanabe, N. Yamagiwa, Y. Torisawa, Organic process research & development 11, (2007) 251-258.
8. G. Wypych, Handbook of Solvents, ChemTec Publishing, Toronto, Canada, 2001.
9. P. Biller, A. B. Ross, Bioresour. Technol. 102, (2010) 215-225.
10. P. Duan, P. E. Savage, Energy Environ. Sci. 4, (2011) 1447-1456.
11. P. Duan, P. E. Savage, Bioresour. Technol. 102, (2011) 1899-1906.
12. Y. F. Yang, C. P. Feng, Y. Inamori, T. Maekawa, Resources, conservation and recycling 43, (2004) 21-33.
13. D. Zhou, L. Zhang, S. Zhang, H. Fu, J. Chen, Energy Fuels 24, (2010) 4054-4061.

Chapter 5

Hydrothermal HDO of Benzofuran Over a Platinum Catalyst

Chapter 2 showed that there have been limited studies on hydrothermal HDO and work discussed in chapter 4 identified oxygenated molecules present in HTL bio-oils from microalgae. This chapter uses the knowledge gained from these previous two chapters to examine the hydrothermal HDO of benzofuran.

Duan and Savage found that using supercritical water as a reaction medium changed the reaction pathways for the hydrodenitrogenation of pyridine over a Pt/C catalyst, indicating that studies performed in a conventional hydrotreating environment may not be applicable to those carried out in a hydrothermal environment [1]. Fu *et al.* found that Pt/C was an effective catalyst for the decarboxylation of free fatty acids in sub- and supercritical water and suffered no significant change in activity through three consecutive 3 hr reactions at 370 °C [2, 3]. Interestingly, the decarboxylation occurred without the addition of hydrogen to the reaction. This result led to speculation that under these conditions, water may donate hydrogen to the reactions. To the best of our knowledge, there has not been a detailed study of reaction kinetics or the influence of process variables on the catalytic HDO of furans or phenols in sub- or supercritical water.

To fill this knowledge gap, we chose the hydrothermal HDO of 2,3-benzofuran as a model oxygenated compound. Previous studies in non-aqueous environments suggest that benzofuran deoxygenates through a pathway that includes phenols and alcohols, which, as

we will show, led us to insights about the effects of having these various species all present in the reaction [4-7]. We report, herein, a reaction network and the kinetics of deoxygenation, both of which are essential to the design of future catalytic processes. Experiments and kinetic modeling were accomplished over a wide range of conversions and yields of deoxygenated products to provide industrially relevant information. We also report on the process variables that affect reaction rate and selectivity. Selectively producing aromatic deoxygenated products instead of hydrogenated deoxygenated products was desired to minimize hydrogen consumption.

This chapter provides information about control experiments (5.1), reaction products (5.2), the reaction network (5.3), and reaction kinetics (5.4) for the hydrothermal HDO of benzofuran. We first discuss the experiments performed to ensure that the chemical transformations observed were due to the presence of the 5 wt% Pt/C catalyst and to quantify the mass losses from the laboratory procedures. The second section reports the identities and yields of the reaction products and the effect of process variables. We performed replicate experiments and report the mean values along with the standard deviation as an estimate of the uncertainty. The third section provides a reaction network deduced from the results from reacting benzofuran, reaction intermediates, and reaction products. Finally, we use the network and experimental data to develop a kinetic model.

5.1. Control experiments

To determine the amount of organic material lost during air evacuation, sample workup, and adsorption to the Pt/C, three reactors were loaded, purged, pressurized, agitated for one hour at room temperature, and extracted using the procedure outlined in

the Materials and Methods section. Quantification of the recovered benzofuran using GC-FID indicated that 849 ± 36 μmol of the original 900 μmol benzofuran was recovered. Similarly, control experiments with reactors loaded with ethylphenol and ethylcyclohexanol had recoveries of 802 ± 22 and 865 ± 18 μmol, respectively, of the original 900 μmol. The high viscosity of ethylphenol made fully loading the reactors difficult, and this led to the lower carbon recovery. These values were used to determine that the average recovery of carbon from the reactors was greater than 94 % for all reactions where the starting reagents were benzofuran, ethylphenol, or ethylcyclohexanol. The recovered amounts of benzofuran, ethylphenol, and ethylcyclohexanol were used to compute the initial concentrations of the starting reagents.

We performed a set of uncatalyzed reactions to be certain that the chemical transformations were due to the presence of the Pt/C catalyst. A benzofuran reaction at 450 °C for 60 min with a 5:1 hydrogen to benzofuran molar ratio showed the presence of no deoxygenated products and a conversion of less than 10 %.

5.2 Reaction products

GC-MSD and GC-TCD analysis identified numerous liquid- and gas-phase products from reacting benzofuran over the 5 wt % Pt/C catalyst at 380 °C. These included liquid-phase oxygenated products (2-ethylphenol, 2-ethylcyclohexanone, 2-ethylcyclohexanol, 2-methylphenol, and phenol), liquid-phase deoxygenated products (ethylbenzene, ethylcyclohexane, toluene, benzene, and heptane), and gas phase products (ethane, methane, hydrogen, and carbon dioxide). This section shows how process variables such as batch holding time, water density, hydrogen loading, and catalyst loading affect the

concentrations of the products. With the knowledge obtained from these experiments, we later develop a reaction network and kinetic model.

5.2.1 Influence of batch holding time

Figs. 5.1 and 5.2 show the effect of reaction time on the concentration of the major products from the hydrothermal catalytic deoxygenation of benzofuran at two different hydrogen to benzofuran molar ratios. The large symbols on the figures represent the experimental data and the curves, with the corresponding smaller symbols, represent model results. The kinetic model will be discussed in section 5.4. In this section we confine the discussion to the trends evident in the experimental data.

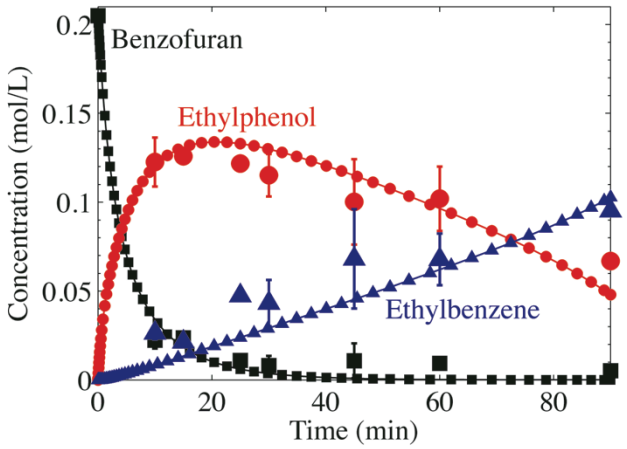

Figure 5.1. Major products from benzofuran at 380 °C with a 4:1 hydrogen to benzofuran molar ratio.

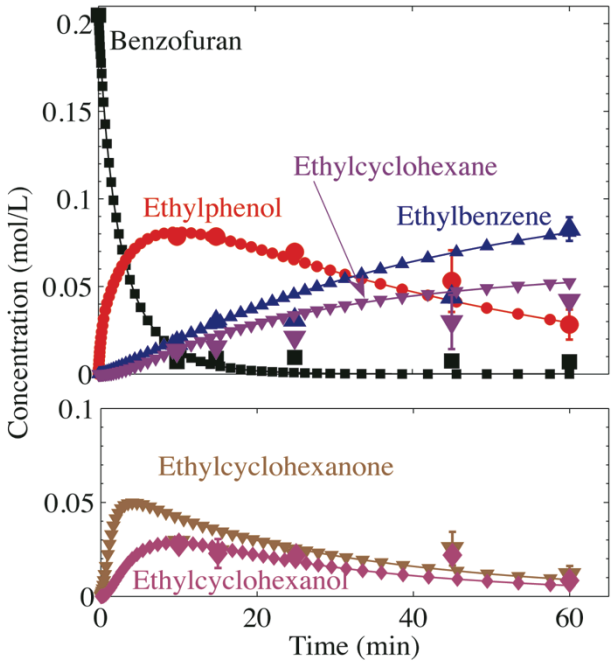

Figure 5.2. Major products from benzofuran at 380 °C with a 6:1 hydrogen to benzofuran molar ratio.

Figs. 5.1 and 5.2 show that the benzofuran concentration rapidly decreases with time. Conversions of 89 ± 2 % and 95 ± 3 % were obtained in 10 min with the 4:1 and 6:1 ratios, respectively. The concentration of ethylphenol increased rapidly as benzofuran was consumed, reaching a maximum of approximately 0.13 and 0.08 M for the 4:1 and 6:1 reactions, respectively. The reasons for the differences in concentrations of the reaction products at the two different hydrogen loadings will be discussed in section 5.2.3. After reaching a maximum value between 10 and 15 min, the concentration of ethylphenol decreases approximately linearly. The experimental data in Fig. 5.2 indicate that at a 6:1 hydrogen to benzofuran molar ratio, the concentrations of ethylcyclohexanone and ethylcyclohexanol reach a maximum (0.03 M) at 10 min before decreasing. Only low (< 0.008 M) concentrations of ethylcyclohexanone and ethylcyclohexanol were observed at

the lower hydrogen loading (Table A.1, appendix), therefore these products were considered minor for this reaction. The reason for the distinction between minor and major products and the causes of this distinction will be discussed later.

Figs. 5.1 and 5.2 indicate that ethylbenzene was the major deoxygenated product at both reaction conditions. Both figures show that the concentration of ethylbenzene increases approximately linearly with time. The concentration of ethylbenzene at 60 min is nearly identical for both reactions with values of 0.07 ± 0.01 and 0.083 ± 0.007 M for the 4:1 and 6:1 reactions, respectively. In addition to ethylbenzene, ethylcyclohexane was observed at the higher hydrogen loading. Similar to ethylbenzene, the concentration of ethylcyclohexane increased nearly linearly for the reaction times studied.

These observations provide significant insight into the reaction network of benzofuran. The high concentration of ethylphenol in Figs. 5.1 and 5.2, and this concentration passing through a maximum before declining, indicates that ethylphenol is a major reaction intermediate for benzofuran deoxygenation. Fig. 5.2 indicated that ethylcyclohexanone and ethylcyclohexanol also passed through maximum concentrations, again suggesting that these products were intermediates in the deoxygenation of benzofuran. Figs. 5.1 and 5.2 also showed that the concentrations of ethylbenzene and ethylcyclohexane continuously increased under the conditions studied. This behavior suggests that these are the terminal products of the reaction. The full reaction network will be discussed in detail in section 5.3.

5.2.2. Influence of water density

Previous work on hydrothermal catalytic denitrogenation indicates that catalytic reaction pathways and selectivities can be altered when the reactions are conducted in water [1]. Fig. 5.3 shows the effect of water loading on the product yields. It should be noted that for all of these reactions the amounts of Pt/C (10 mg), benzofuran (900 μmol), helium (77 psig at 25 °C), and hydrogen (350 to 400 psia at 25 °C) were fixed so all the reactors had the same concentrations of hydrogen, benzofuran, and catalyst. The reactors had different pressures, however, due to the different water loadings. We estimate the pressures to be 870, 4000, 4100, and 4200 psig, respectively.

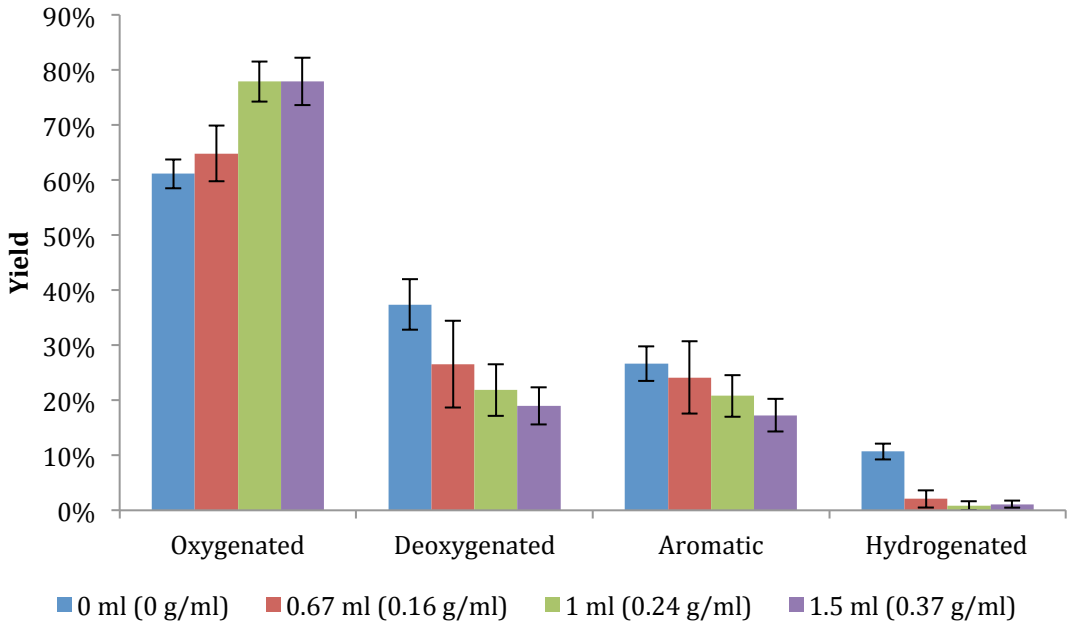

Figure 5.3. Effect of water loading on the product distribution from benzofuran at 380 °C for 30 min with a 4:1 hydrogen to benzofuran ratio. The water densities at the reaction conditions are listed in parentheses. The aromatic and hydrogenated products are the two classes of deoxygenated products.

Fig. 5.3 and Table A.2 indicate that as the water density increases, the yield of deoxygenated products decreases whereas the yield of oxygenated products increases.

Furthermore, the distribution of deoxygenated products, designated as aromatic and hydrogenated, changes significantly as more water is added. With no water present, the yields of hydrogenated and aromatic products were 11 ± 1 % and 27 ± 3 %, respectively. At a water density of 0.16 g/ml, the yield of hydrogenated products decreases dramatically to 2 ± 2 %, whereas the yield of aromatic products, 24 ± 7 %, shows little change. Increasing the water density further has little effect on the yield of hydrogenated products, but the yield of aromatic products decreases. These results indicate that water density can be used to alter the selectivity to deoxygenated products and their extent of hydrogenation.

The reason for the decrease in deoxygenated product yield (undesired) and in selectivity toward hydrogenated products (desired) with increasing water concentration is not clear at present. We suspect that competitive binding of water to the platinum surface might play a role. The presence of water on the catalyst surface would reduce the number of sites available for benzofuran and hydrogen, thereby reducing the rates for both deoxygenation and hydrogenation of the oxygenated products. Fig. 5.3 showed that the presence of water has a larger influence on hydrogenation than deoxygenation. This result is likely related to multiple surface bound hydrogen atoms being needed to fully hydrogenate the molecule. The presence of water may decrease the likelihood of bound hydrogen atoms interacting with the bound aromatic molecule to hydrogenate it. From a rate law perspective, this suggests that the rate of hydrogenation is more dependent on the hydrogen concentration than is the rate of deoxygenation.

5.2.3 Influence of hydrogen loading

Fig. 5.4 shows that the initial amount of hydrogen loaded into each reactor had a large effect on product yields from benzofuran. Increasing the hydrogen loading from 4:1 to 6:1 increased the yield of hydrogenated products at 60 min from 2.2 ± 0.4 to 23 ± 2 %, decreased the yield of oxygenated products from 54 ± 13 to 24 ± 7 %, but had no significant effect on the yield of aromatic products (38 ± 7 and 44 ± 3 %, respectively). The absolute increase in yield of hydrogenated products with the 6:1 hydrogen to benzofuran molar ratio is about the same as the increase in the yield of deoxygenated products and decrease in yield of oxygenated products. The ten-fold relative increase in yield of hydrogenated products, which greatly exceeds the 70 % relative increase in yield of deoxygenated products, suggests that the rate of the hydrogenation pathway has a higher hydrogen reaction order than does the direct deoxygenation pathway, which produces aromatic products. Recall that the experimental data in the previous section also suggested a higher hydrogen order for the hydrogenation pathway. The increase in the yield of hydrogenated products was also accompanied by an increase in the amount of hydrogen consumed per molecule of benzofuran at 60 min (2.4 ± 0.3 to 2.8 ± 0.1, respectively).

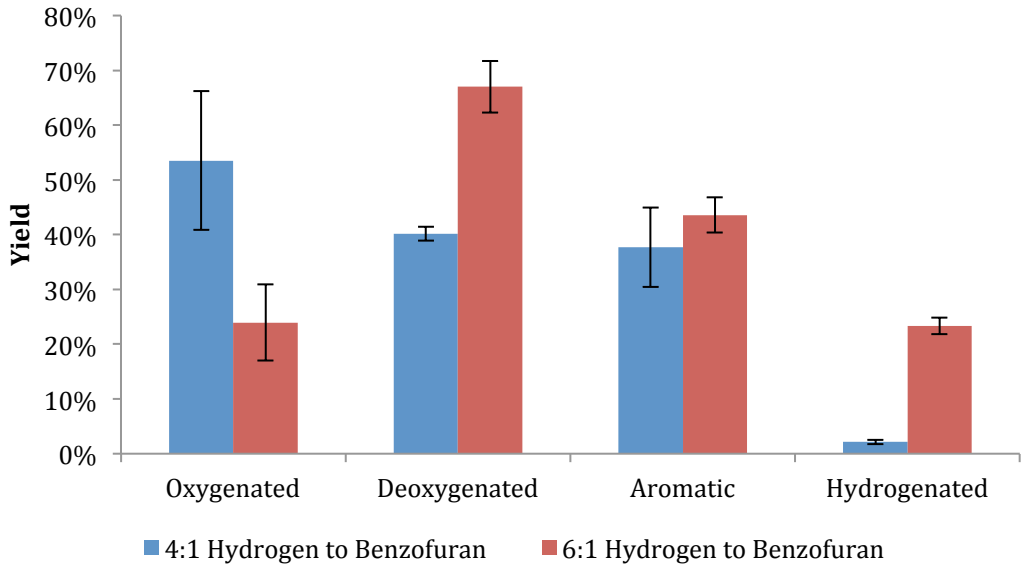

Figure 5.4. Product yields from reacting benzofuran with hydrogen at 4:1 and 6:1 molar ratios at 380 °C, 60 min.

The influence of hydrogen on the reaction is also apparent in Figs. 5.1 and 5.2. Both conditions resulted in the rapid conversion of benzofuran, but the 4:1 reaction produced a higher concentration of ethylphenol (0.12 ± 0.01 M) than the 6:1 reaction (0.08 M). The higher concentration of ethylphenol in the 4:1 reaction is likely a result of slower hydrogenation of the ethylphenol at the lower hydrogen loading. This hypothesis is supported by ethylcyclohexanone and ethylcyclohexanol being present in lower concentrations at the 4:1 hydrogen to benzofuran ratio (0.008 M, maximum for each) than at the 6:1 ratio (0.03 M, maximum for each) as shown in Table A.1 and Fig. 5.2. The combined concentrations of ethylphenol, ethylcyclohexanone, and ethylcyclohexanol are similar for both reaction conditions at 10 min (Table A.1).

Table 5.1. Gases produced 380 °C, 60 min.

	CO_2 (μmol)	CH_4 (μmol)	C_2H_6 (μmol)	Total yield (%)
4:1 Hydrogen:Benzofuran	96 ± 6	14 ± 6	7.3	1.6 ± 0.1
6:1 Hydrogen:Benzofuran	87 ± 4	5.5 ± 0.3	0	1.36 ± 0.07

Gas analysis, shown in Table 5.1, indicated that the reaction produced primarily carbon dioxide. Methane and ethane were also present, but in approximately 10 - 20 % of the quantity of carbon dioxide. Overall, the yield of carbon-containing gases was approximately 1.5 % for both the 4:1 and 6:1 hydrogen to benzofuran ratios. Table 5.1 indicates that the amount of carbon dioxide produced is similar for both conditions, but the amounts of methane and ethane decrease with increasing hydrogen concentration. The increase in methane and ethane production at lower hydrogen concentrations suggests that hydrogen suppresses cracking reactions. The similar concentrations of carbon dioxide are likely because carbon dioxide can be produced upon oxidation of the catalyst support [8].

5.2.4. Influence of catalyst loading

Fig. 5.5 and Table A.3 show the results from the hydrothermal catalytic deoxygenation of benzofuran with 5 and 10 mg loadings of Pt/C. The yield of deoxygenated products was much lower at the lower catalyst loading. This decrease in deoxygenated products was accompanied by only a modest decrease in the conversion of benzofuran (89 ± 2 % with 10 mg of Pt/C, 83 % with 5 mg of Pt/C). This result confirms that benzofuran conversion is faster than deoxygenation. The deoxygenated products at both catalyst

loadings consisted almost entirely of aromatic products, and both catalyst loadings produced about the same yield of hydrogenated products. These results show that adding more catalyst increases the selectivity of deoxygenated products and decreases the selectivity of oxygenated products. This change in selectivity provides further evidence that the oxygenated products are reaction intermediates and the deoxygenated products are terminal products, because increasing the catalyst loading increases the reaction rate causing the reaction to move more toward completion.

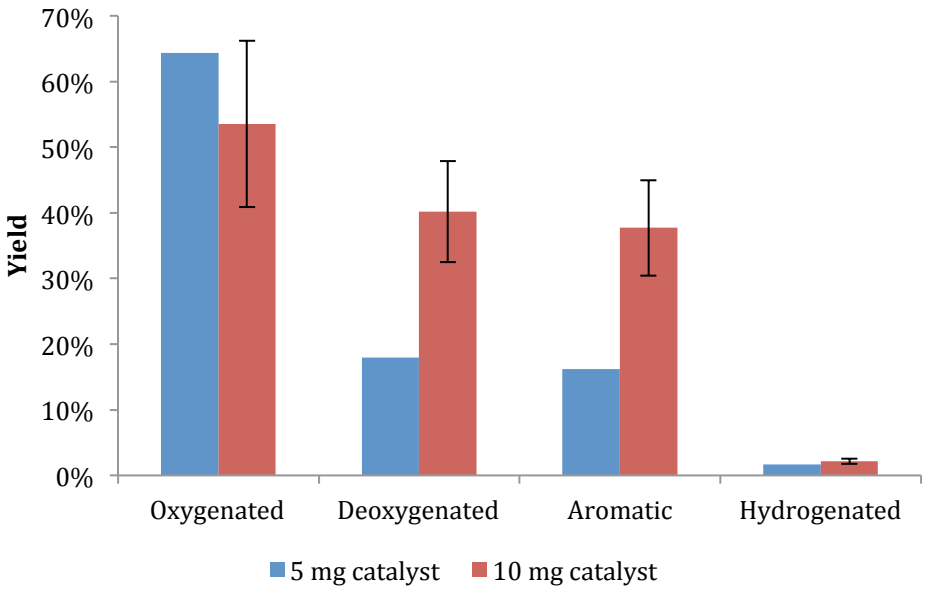

Figure 5.5. Product yields from benzofuran with hydrogen at a 4:1 molar ratio at 380 °C, 60 min with 5 or 10 mg of 5 wt % Pt/C.

5.3 Reaction network

The results presented in the previous sections provided numerous insights into the reaction network for benzofuran deoxygenation. Recall that ethylbenzene and ethylcyclohexane were terminal reaction products because their concentrations

continuously increased with time. Ethylphenol, ethylcyclohexanone, and ethylcyclohexanol were intermediate products because their concentrations passed through a maximum as time increased. This section provides results from experiments with each of these products as the starting material. These results ultimately lead to the construction of a complete reaction network for the hydrothermal catalytic deoxygenation of benzofuran.

Reacting hydrogen and ethylbenzene in supercritical water in a 2:1 molar ratio produced only ethylcyclohexane. The hydrogenation of ethylbenzene occurred rapidly and reached equilibrium in less than 10 min at 380 °C (Table A.1). At equilibrium, the yield of ethylcyclohexane was 43 ± 4 %. Reacting ethylcyclohexane without hydrogen for 15 min produced a 43 % yield of ethylbenzene (Table A.1). These results indicate that ethylbenzene and ethylcyclohexane are linked by a reversible hydrogenation/dehydrogenation reaction. Also, the absence of phenols, alcohols, and ketones in these experiments provided evidence that any hydrogenolysis reactions that remove oxygen atoms as water, to produce ethylbenzene or ethylcyclohexane, are irreversible.

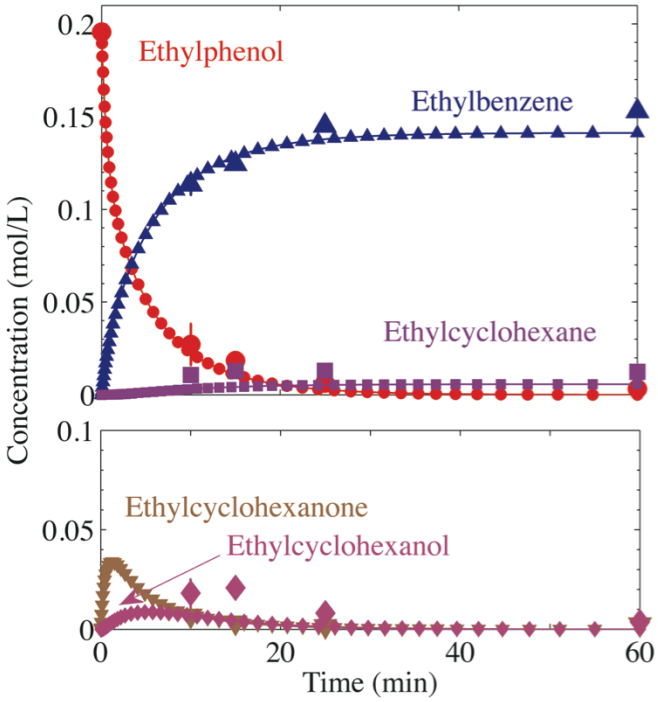

Figure 5.6. Major products from ethylphenol at 380 °C with a 3:1 hydrogen to ethylphenol molar ratio.

Fig. 5.6 shows the results from experiments starting with ethylphenol and a 3:1 hydrogen to ethylphenol molar ratio. The first data point, taken at 10 min, shows ethylbenzene and ethylcyclohexane concentrations that correspond to a 64 ± 2 % yield of deoxygenated products. This result represents a significant increase in the rate of deoxygenation when compared to either benzofuran reaction (Figs. 5.1 and 5.2), where the maximum yield of deoxygenated products was just 17 % at 10 min. Of the deoxygenated products, 86 % are aromatic, while 14 % are hydrogenated. Ethylbenzene was the major reaction product. This result indicates that ethylbenzene is likely formed directly from ethylphenol. Smaller amounts of ethylcyclohexane, ethylcyclohexanone, and ethylcyclohexanol also formed. Hydrogenation of ethylphenol must be responsible for the presence of ethylcyclohexanone and ethylcyclohexanol. We hypothesize that

ethylcyclohexanone was first produced from ethylphenol, followed by a rapid hydrogenation to ethylcyclohexanol. We determined that the hydrogenation reactions for ethylphenol and ethylcyclohexanone are reversible by finding that ethylcyclohexanol produced ethylcyclohexanone and ethylphenol, as shown in Fig. 5.7. We also propose that ethylcyclohexane is produced by the irreversible elimination of the hydroxyl group in ethylcyclohexanol.

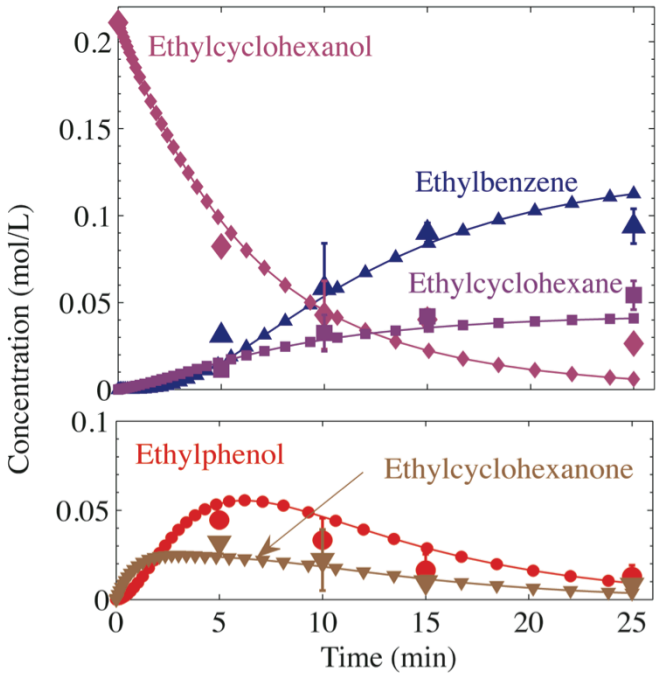

Figure 5.7. Major products from ethylcyclohexanol at 380 °C with a 0.5:1 hydrogen to ethylcyclohexanol molar ratio.

The ratio of the concentration of ethylbenzene to ethylcyclohexane at 25 min varied with the starting reagent. Starting with ethylphenol (Fig. 5.6), ethylcyclohexanol (Fig. 5.7), and benzofuran (6:1, Fig. 5.2) resulted in ethylbenzene to ethylcyclohexane ratios of 11, 1.7, and 1.5, respectively (see Table A.1 for concentration data). The much higher ratio for experiments starting with ethylphenol led us to speculate that ethylphenol inhibits the

reversible hydrogenation of ethylbenzene to ethylcyclohexane. To test this hypothesis we reacted ethylbenzene and 2-methylphenol (1:1 molar ratio, 450 μmol each) in supercritical water. We chose methylphenol as an ethylphenol analog, because it produces toluene, not ethylbenzene, upon deoxygenation, allowing us to distinguish between the products from the two starting reagents. This reaction produced significantly less ethylcyclohexane than when we started with pure ethylbenzene and hydrogen (Table A.4). At 10 min, with a 2:1 hydrogen to organic reagent molar ratio, the ethylbenzene and methylphenol reaction produced only 37 μmol of ethylcyclohexane while 377 μmol of ethylbenzene remained. From these values we calculate a yield of ethylcyclohexane from ethylbenzene of 8 %. This yield represents a significant retardation in ethylbenzene hydrogenation when compared to the 43 % yield of ethylcyclohexane formed when pure ethylbenzene was reacted. This result indicates that in the presence of ethylphenol, the hydrogenation/dehydrogenation of ethylbenzene and ethylcyclohexane are not major reactions. No previous researchers have noted such an effect.

The inhibition of ethylbenzene hydrogenation in the presence of ethylphenol may be due to ethylphenol adsorbing more strongly than ethylbenzene on the catalyst surface. Some oxygenated aromatics (i.e., acetophenone) can have significantly higher adsorption energies than benzene on Pd [9]. A higher heat of adsorption for the oxygenated species means it is likely to be more dominant on the catalyst surface.

Experiments with benzofuran as the starting reagent gave dihydrobenzofuran in small quantities (< 6 % yield) at short reaction times (< 30 min). The rapid appearance of ethylphenol and very low concentration of dihydrobenzofuran suggests that after

benzofuran is hydrogenated to dihydrobenzofuran, hydrogenolysis of the furan ring rapidly produces ethylphenol. Fig. 5.8 summarizes the major reaction pathways outlined above.

In addition to the major pathways, a set of minor pathways led to less abundant products such as phenol, 2-methylphenol, toluene, benzene, and heptane. Reactions of benzofuran produced maximum yields of each of 0.8, 2.5, 3.5, 2.0, and 2.3 %, respectively. Experiments starting with ethylphenol or ethylcyclohexanol produced maximum heptane yields of 5.5 and 3.9 %, respectively. In general, the average yield of minor products was similar when ethylphenol (5 ± 1 %), ethylcyclohexanol (3 ± 3 %), and benzofuran (6 ± 1 %, 4:1 and 4 ± 1 %, 6:1) were the starting reactants.

The low concentrations of these products permit only a speculative discussion of their reaction pathways. Heptane could be formed by a partial hydrogenation of the aromatic ring in ethylphenol, hydrogenolysis of the ring and hydroxyl group, and hydrogenation of any remaining double bonds. Methylphenol is likely produced from the hydrogenolysis of the carbon-carbon bond in the ethyl group on ethylphenol. Hydrogenolysis of the hydroxyl group on the resulting methylphenol molecule then produces toluene. Further hydrogenolysis of the methyl substituent on methylphenol could produce phenol, which then produces benzene through hydrogenolysis of the hydroxyl group. It is unlikely that the hydrogenolysis of ethylbenzene produced toluene and benzene, because these products were not observed when pure ethylbenzene was reacted. A direct reaction path between ethylphenol and phenol is supported by the presence of ethane in the gas product.

Fig. 5.8 shows the major and minor reaction pathways discussed above. This reaction network is similar to those previously proposed for non-hydrothermal conditions

with the exception of the inclusion of ethylcyclohexanone and exclusion of molecules where the aromatic ring is only partially hydrogenated [4-7, 10].

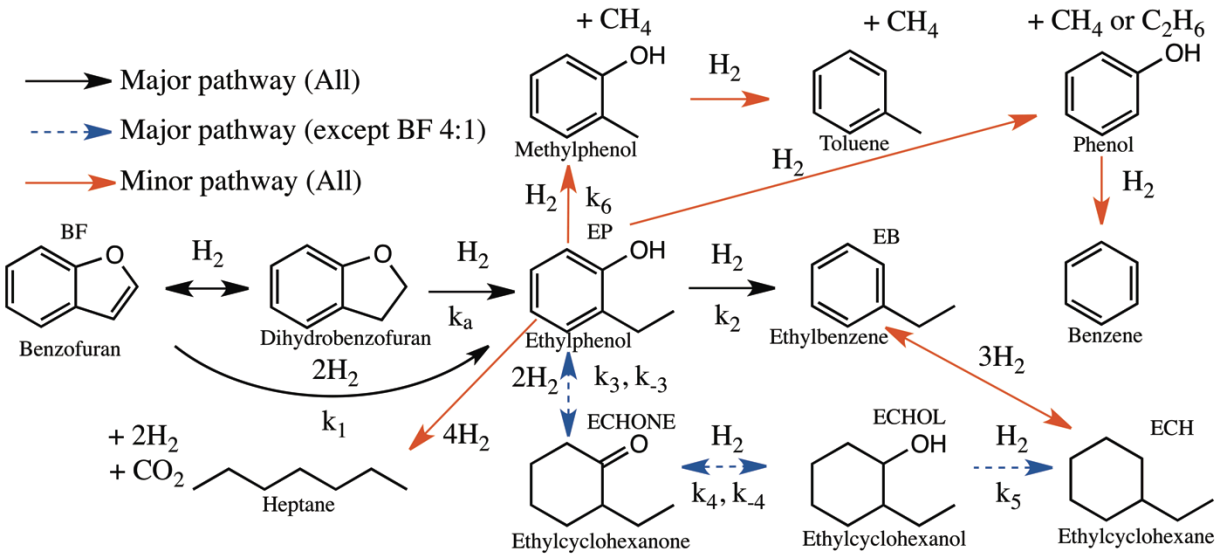

Figure 5.8. Proposed reaction network for benzofuran deoxygenation in supercritical water at 380°C.

5.4. Reaction kinetics

Having established a reaction network for benzofuran deoxygenation, we next used the major reaction pathways as the basis for a kinetics model. Fig. 5.8 defines the subscript (e.g., BF for benzofuran) for each concentration variable and the associated rate constants.

5.4.1. Model definition

The model is a set of differential equations (Table 5.2) resulting from combining the batch reactor design equation with rate equations for the major reaction paths. We performed parameter estimation and solved the differential equation kinetic model using Matlab® and the optimtool package. A variety of kinetic models were proposed and fit. The ability of the models to fit the data was compared based on the minimized error between

the model and experimental concentrations, C_i, as shown below, and the absence of systematic deviations in parity plots.

$$Error = \sum_i (C_{i,Data} - C_{i,Model})^2 \quad \text{Eq. 5.1}$$

The reaction orders for each reaction follow the reaction stoichiometry with the exception of reaction 1. Here we assume that k_a is essentially instantaneous because of the very low concentration of dihydrobenzofuran in the reaction products, and thus take k_1 to be the rate constant for both the hydrogenation of benzofuran and the hydrogenolysis of dihydrobenzofuran. Fitting the temporal variations of the species' concentrations from the experiments with each of the different starting reagents (i.e. benzofuran, ethylphenol, and ethycyclohexanol) separately revealed that each of the rate constants was of similar magnitude, regardless of the starting reagent, with the exception of k_2. As noted in section 5.3, when the starting reactant was benzofuran, reaction 2 (Fig. 5.8) was significantly slower than when starting with ethylphenol or ethylcyclohexanol. This lower value for k_2 indicates that benzofuran inhibited this reaction. This inhibition by benzofuran has also been observed with a $CoMo/Al_2O_3$ catalyst [6]. In addition to this reaction, we also noted in section 5.3 that the minor product yields were similar for all of the starting reagents even though ethylphenol was present in greater concentrations for longer times when benzofuran was the starting reagent. This observation suggests that the rate of minor product formation is faster without benzofuran present, implying that benzofuran inhibits this lumped reaction. To account for this inhibition, we included a "$1+K_{BF}C_{BF}$" term in the denominators of the rate equations for the direct deoxygenation pathway (reaction 2, Fig.

5.8) and the lumped minor products pathway (reaction 6, Fig. 5.8). Furthermore, to improve the accuracy of this model, we used a linear fit of the experimental benzofuran concentration data for times greater than zero to calculate the benzofuran concentration in the "$1+K_{BF}C_{BF}$" denominator.

Table 5.2. Kinetics model of the major benzofuran reaction pathways shown in Figure 5.8 at 380 °C and a 0.16 g/ml water density at reaction conditions. W is the catalyst mass (gcat).

$$\frac{dC_{BF}}{dt} = -k_1 C_{BF} C_{H2} \quad \text{Eq. 5.2}$$

$$\frac{dC_{EP}}{dt} = k_1 C_{BF} C_{H2} - \frac{C_{EP} C_{H2}(k_2 + k_6)}{1 + K_1 C_{BF}} - k_3 C_{EP} C_{H2}^2 + k_{-3} C_{ECHONE} \quad \text{Eq. 5.3}$$

$$\frac{dC_{EB}}{dt} = \frac{k_2 C_{EP} C_{H2}}{1 + K_1 C_1} \quad \text{Eq. 5.4}$$

$$\frac{dC_{ECHONE}}{dt} = k_3 C_{EP} C_{H2}^2 - k_{-3} C_{ECHONE} - k_4 C_{ECHONE} C_{H2} + k_{-4} C_{ECHOL} \quad \text{Eq. 5.5}$$

$$\frac{dC_{ECHOL}}{dt} = k_4 C_{EP} C_{H2} - k_{-4} C_{ECHOL} - k_5 C_{ECHOL} C_{H2} \quad \text{Eq. 5.6}$$

$$\frac{dC_6}{dt} = k_5 C_{ECHOL} C_{H2} \quad \text{Eq. 5.7}$$

$$\frac{dC_{H2}}{dt} = -2k_1 C_{BF} C_{H2} - \frac{C_{EP} C_{H2}(k_2 + k_6)}{1 + K_1 C_{BF}} - 2k_3 C_{EP} C_{H2}^2 + 2k_{-3} C_{ECHONE} \quad \text{Eq. 5.8}$$
$$-k_4 C_{EP} C_{H2} + k_{-4} C_{ECHOL} - k_5 C_{ECHOL} C_{H2}$$

We speculate that the physical basis for this inhibition is that benzofuran blocks the active site for the direct deoxygenation of ethylphenol, while leaving the active sites for other reactions unaffected. It is puzzling that a similar decrease in the rate of ethylphenol hydrogenation to ethylcyclohexanone did not occur, but its absence may be because the hydrogenation and hydrogenolysis reactions occur at different active sites.

5.4.2 Kinetic parameters

Table 5.3 shows the optimized values for the eight reaction rate constants and the benzofuran adsorption equilibrium constant (K_{BF}). To aid in the discussion of these rate constants, we also define the effective k_2, $k_{2,eff}$, as $k_2/(1+K_{BF}C_{BF})$. An optimized value of 965 L/mol for K_{BF} suggests that when benzofuran is present, it absorbs strongly to the catalyst surface, thereby occupying many of the active sites. The average concentration of benzofuran in both sets of reactions (4:1 and 6:1 hydrogen to benzofuran) was approximately 0.01 M, so the value of the denominator in the expression for $k_{2,eff}$ is approximately 10. Thus, $k_{2,eff}$ is about 10 % of the value of k_2 given in Table 5.3. This result fits well with the significant decrease observed in section 5.3 in the direct deoxygenation reaction rate when starting with benzofuran.

Table 5.3. Optimized values of the rate constants in Figure 5.8.

k_1^*	k_2^*	k_3^{**}	$k_{-3}^{\#}$	k_4^*	$k_{-4}^{\#}$	k_5^*	k_6^*	$K_{BF}^{\#\#}$
0.146	0.161	0.501	0.338	0.0934	0.0580	0.0424	0.0554	965

Units: $*L^2/(mol\ min\ g_{cat})$ $**L^3/(mol^2\ min\ g_{cat})$ #L/(min g_{cat}) ##L/(mol)

These rate constants, $k_{2,eff}$ and k_2, indicate that the hydrogenolysis of ethylphenol to form ethylbenzene is the rate-limiting step in this reaction sequence when benzofuran is present because $k_{2,eff}$ is slowed significantly by benzofuran. A comparison of k_5 and $k_{2,eff}$ shows that inhibition by benzofuran on the direct deoxygenation pathway (reaction 2) provides a basis for the difference in selectivity to deoxygenated products when starting with benzofuran and ethylphenol. Recall from section 3.3 that the ethylphenol (3:1) and

benzofuran (6:1) reactions produced very different ethylbenzene to ethylcyclohexane ratios of 11 and 1.7, respectively, at 25 min. When ethylphenol is the starting reagent, the effective direct deoxygenation rate constant ($k_{2,eff} = k_2 = 0.161$ $L^2/(mol\ min\ g_{cat})$) is about four times the rate constant for ethylcyclohexanol deoxygenation ($k_5 = 0.0424$ $L^2/(mol\ min\ g_{cat})$), thereby producing more ethylbenzene than ethylcyclohexane. When benzofuran is the starting reagent, the effective direct deoxygenation rate constant drops approximately an order of magnitude ($k_{2,eff} \approx 0.016$ $L^2/(mol\ min\ g_{cat})$) while the ethylcyclohexanol deoxygenation rate constant (k_5) remains unchanged. This results in k_5 being about 2.5 times $k_{2,eff}$.

A comparison of the hydrogenation/dehydrogenation rate constants (k_3, k_{-3}, k_4, k_{-4}) shows that dehydrogenation of ethylcyclohexanone occurs more readily than the dehydrogenation of ethylcyclohexanol (k_{-3} is about 6 times larger than k_{-4}). The rate constant for ethylcyclohexanone hydrogenation (k_4) is also the same magnitude as k_1 and k_2, indicating that ethylcyclohexanone can be readily hydrogenated under these reaction conditions.

5.4.3 Model analysis

The optimized kinetic model accurately correlates the concentration of each reaction species as shown in Figs. 5.1, 2, 6, and 7. In general, the kinetic model captures the trends in the experimental data and is within the experimental error bars (standard deviations). A more detailed comparison of the fit of the kinetic model to the experimental data is examined in section 5.4.4. The kinetic model is also useful for understanding how process variables affected the product distribution, and it provides insights into the

reaction network not observed solely from the experimental data. We elaborate on these points below.

5.4.3.1 Benzofuran

Figs. 5.1 and 5.2 show the fit of the kinetic model to the experimental data for the benzofuran reactions. The kinetic model captured the increase in ethylcyclohexanone concentration at the higher hydrogen loading by using a second order dependence on hydrogen for the ethylphenol hydrogenation reaction. A rate equation that was first order in hydrogen was not capable of fitting the data. This hydrogenation step is the only one in the kinetic model that has a reaction order higher than unity for a given reactant. This second order dependence is important for capturing the change in deoxygenated product distribution at the higher hydrogen loading because the only route to produce ethylcyclohexane begins with the hydrogenation of ethylphenol to produce ethylcyclohexanone, as shown in Fig. 5.8. The higher hydrogen loading doubles the rate of ethylphenol hydrogenation to ethylcyclohexanone from 0.012 to 0.024 mol/(min g_{cat}) at 15 min, thereby allowing for the formation of ethylcyclohexane. The second order dependence on hydrogen for this hydrogenation reaction means that very little (< 0.008 M) ethylcyclohexanone and ethylcyclohexane are produced at the 4:1 hydrogen to benzofuran molar ratio.

Further examination of Fig. 5.2 reveals that the kinetic model suggests that the concentration of ethylcyclohexanone increases rapidly before reaching a maximum at approximately 5 min, and then is partially consumed before the first experimental data point was taken at 10 min. The appearance of 0.014 M ethylcyclohexane at 10 min in the

experimental data necessitates this behavior in the kinetic model because the formation ethylcyclohexane requires that the ethylcyclohexanone and ethylcyclohexanol reactions proceed rapidly.

5.4.3.2 Ethylphenol

Fig. 5.6 shows the fit of the kinetic model to the experimental data for the ethylphenol reactions. The experimental data and model show that the concentration of ethylphenol decreases rapidly and is primarily directly deoxygenated to ethylbenzene. The limited production of ethylcyclohexane is a result of the limited hydrogenation of ethylphenol to produce ethylcyclohexanone. The model suggests that the concentration of ethylcyclohexanone increases rapidly, and then is mostly consumed within 10 min. The majority of the ethylcyclohexanone is dehydrogenated back to ethylphenol while a smaller amount is converted to ethylcyclohexanol. The majority of the ethylcyclohexanol produced is deoxygenated to ethylcyclohexane.

Comparing the calculated ethylcyclohexanone concentrations in Figs. 5.2 and 5.6 reveals that ethylcyclohexanone is consumed more rapidly when ethylphenol, rather than benzofuran, is the starting reactant. This result is evident from the rapid decrease in the calculated ethylcyclohexanone concentration from its maximum in Fig. 5.6 and comparing it to the gradual decrease from its maximum in Fig. 5.2. The slower decrease in Fig. 5.2 is a result of the direct deoxygenation pathway being inhibited by the presence of benzofuran, as discussed in section 5.4.2.

5.4.3.3 Ethylcyclohexanol

Fig. 5.7 shows the temporal variation in the concentration of the major products for reactions at 380 °C with a 0.5 to 1 hydrogen to ethylcyclohexanol ratio. The model captures the high conversion (79 ± 9 % at 10 min) and the concentration of the major reaction products. Interestingly, the major deoxygenation product was ethylbenzene even at short reaction times (10 min). An analysis of the rate constants in the previous section indicated that ethylbenzene is the major deoxygenated product because the hydrogenation/dehydrogenation reactions between ethylphenol, ethylcyclohexanone, and ethylcyclohexanol occur rapidly. Furthermore, when compared to the benzofuran reactions in Fig. 5.2, the experimental and model results for the ethylcyclohexanol reactions in Fig. 5.7 show significantly lower concentrations of ethylphenol and ethylcyclohexanone at all reaction times even though the reaction network (Fig. 5.8) shows that ethylcyclohexanone and ethylphenol must be formed before producing ethylbenzene. The reason for the lower ethylphenol and ethylcyclohexanone concentrations is that without benzofuran present, the direct deoxygenation of ethylphenol occurs quickly, thereby keeping the concentration of ethylphenol and subsequently ethylcyclohexanone low.

5.4.4 Comparison of experimental and calculated results

Table 5.4 shows the error (Eq. 5.1), normalized for the number of data points, for each data set that was fit to the kinetic model, along with the total error. The values in this table indicate that the error per data point was distributed fairly evenly across all of the data sets, suggesting that the model is not favoring one data set over another.

Table 5.4. Tabulation of normalized error between the kinetic model calculations and the experimental data for the concentration of each reaction species. The errors are normalized by the number of data points.

Model	Error (mol^2/L^2) x 10^3
4:1 Benzofuran	4.54
6:1 Benzofuran	3.50
0.5:1 Ethylcyclohexanol	4.20
3:1 Ethylphenol	1.78
Total	**14.02**

Fig. 5.9 shows a parity plot for all of the data fit with the kinetic model. This plot has scatter about the diagonal parity line, but it appears to be free of systematic deviations from the parity line. Furthermore, error bars of one standard deviation encompassed the parity line in most cases. This outcome indicates that the model adequately describes the data with the experimental error. The deviations from the parity line may be due to several factors. First, the adsorption equilibrium constants of reaction species other than benzofuran might play roles in the reaction rates, but these terms were omitted for simplicity in this model. Second, the reaction orders for hydrogen and the organic reactants may differ slightly from those used in this model. We did examine a variety of integer reaction orders, and the present model provided the best results. It may be possible, however, that a better fit could be obtained with a non-integer reaction order.

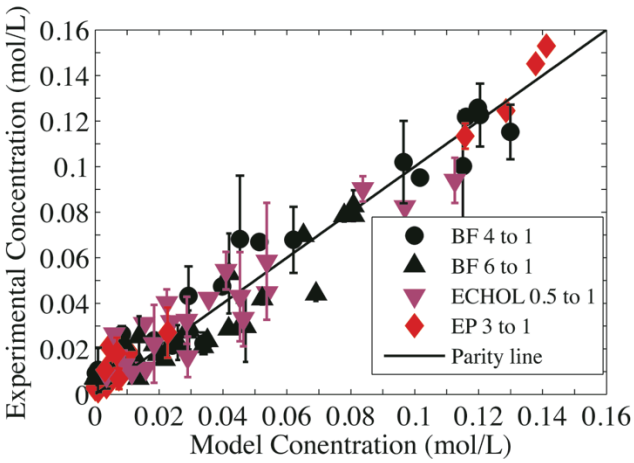

Figure 5.9. Parity plot for the kinetic model.

5.4.5 Model validation

To validate the kinetic model presented above, we predicted the temporal variation of the concentrations of major products when benzofuran was reacted at a 4:1 hydrogen to benzofuran molar ratio with only 5 mg of the Pt/C (as opposed to the 10 mg used in Fig. 5.1). Fig. 5.10, which shows these results, indicates that at this lower catalyst loading, the model accurately predicts the experimental concentration for each major product. This result provides further evidence that the model accurately captures the phenomena occurring in the reactor during the hydrothermal catalytic deoxygenation of benzofuran.

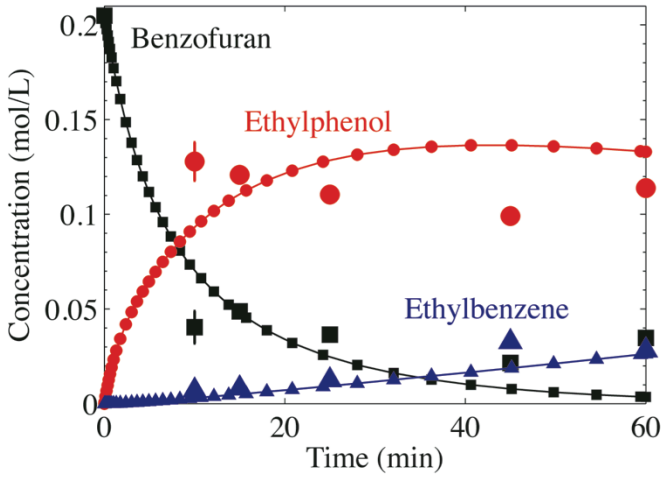

Figure 5.10. Experimental results and model predictions for the major products from benzofuran at 380 °C with a 4:1 hydrogen to benzofuran molar ratio and 5 mg of 5 wt % Pt/C.

5.4.6 Hydrogen consumption

Recent related research in our lab showed that catalytic deoxygenation reactions (of fatty acids) can occur in water without added hydrogen [2, 3]. This observation led to speculation that water may be able to donate hydrogen to perform deoxygenation. If water were a major contributor of hydrogen to the present reaction, the experimental hydrogen concentrations should be consistently higher than the concentrations present if the hydrogen gas loaded into the reactor were the sole hydrogen source. We used the kinetic model, in which all H atoms are supplied by the hydrogen gas, to calculate these hydrogen concentrations. Note that the experimental hydrogen concentrations were not used to determine the model parameters, so the model calculations for the hydrogen concentrations are predictions and not a correlation of results.

Fig. 5.11 shows that the model predicts the experimental concentration of hydrogen with reasonable accuracy, especially at the lower hydrogen loadings (benzofuran 4:1 and

ethylcyclohexanol 0.5:1). Moreover, the hydrogen concentrations clearly decrease significantly from their initial values in the benzofuran experiments. These results indicate that water is likely not a major contributor of hydrogen for these reactions. Reactions for 30 min with benzofuran under a helium atmosphere had only a 16.2 ± 0.5 % conversion and less than 1 % deoxygenation, confirming this hypothesis.

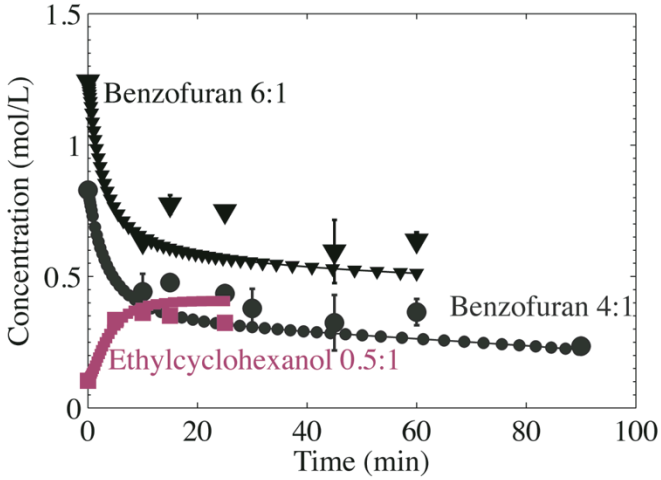

Figure 5.11. Concentration of hydrogen from experiments and the kinetic model prediction.

5.5. Diffusion limitations

Although a wrist action shaker continuously agitated the reactors during the experiments, we wanted to be certain we were measuring the intrinsic reaction kinetics. To test for the possibility of pore diffusion limitations, the Weisz-Prater parameter, C_{wp}, was calculated. C_{wp} values less than unity indicate that the reaction is under kinetic control and pore diffusion limitations are negligible [11].

$$C_{wp} = \frac{-r(obs)R^2}{D_e C_{As}} \quad \text{Eq. 5.9}$$

C_{As}, the concentration of reactant at the catalyst surface, was taken to be the initial bulk benzofuran concentration (0.21 mol/L). Fu *et al.* obtained R, the radius of the catalyst particle, from the catalyst manufacturer as 2.5 x 10^{-3} cm [2]. D_{AB}, the diffusivity of benzofuran in supercritical water at 380 °C and 4200 psig, was estimated to be 1.5 x 10^{-3} cm^2/s from the empirical equation developed by Fuller, Schettler, and Giddings [12]. This estimate accounts for the temperature and pressure at reaction conditions, and molecular structure of water and benzofuran. The effective diffusivity, D_e, was then calculated (1.6 x 10^{-4} cm^2/s) using the same scaling factor as Fu *et al.* to account for the porosity and tortuosity of the catalyst particle [2]. The initial observed rate, -r(obs) was calculated at 380 °C from the model as 0.08 mol/Ls. These values led to a C_{wp} value of 0.01, indicating this reaction is kinetically controlled under the conditions investigated.

5.6. Conclusion

Pt/C (5 wt %) was an effective catalyst for the deoxygenation of benzofuran in supercritical water. Examination of process variables revealed new methods to tune product selectivities to favor either aromatic or hydrogenated deoxygenated products. Not surprisingly, decreasing the hydrogen loading decreased the selectivity to fully hydrogenated products, but more surprisingly, so did increasing the water loading. The results from these experiments and others, as outlined above, led to the development of a reaction network for benzofuran. During the development of the reaction network, we found that phenols inhibited the hydrogenation of ethylbenzene and the dehydrogenation of ethylcyclohexane, and that the rate equation for hydrogenation of ethylphenol is highly dependent (reaction order > 1) on the concentration of hydrogen. Last, we developed and

validated a kinetic model that included benzofuran inhibiting the direct deoxygenation of ethylphenol to ethylbenzene. This model was also used to determine that water is unlikely to be a major source of hydrogen for the reactions described herein, as was previously speculated for the deoxygenation of fatty acids [2].

Appendix A. Supplementary data

Table A.1 Concentration (M) data for all the reactions at 380 °C with 0.67 ml water, 10 mg of 5 wt.% Pt/C, and 900 μmol of organic reagent. All times are in minutes. Each set of reactions is labeled by the starting reagent and the hydrogen to starting reagent molar ratio. The final pressurization with hydrogen was 425, 615, 330, 100, 240, and 77 psig in descending order.

2,3-Benzofuran 4:1							
Time	**Benzofuran**	**Ethylphenol**	**Ethylbenzene**	**Ethylcyclohexanone**	**Ethylcyclohexanol**	**Ethylcyclohexane**	**Hydrogen**
10	0.022 ± 0.005	0.12 ± 0.01	0.026 ± 0.004	0.008 ± 0.003	0.007 ± 0.006	0.001 ± 0.001	0.44 ± 0.07
15	0.024	0.126	0.021	0.004	0.005	0.001	0.477
25	0.011	0.122	0.047	0.005	0.005	0.001	0.435
30	0.008 ± 0.005	0.11 ± 0.01	0.04 ± 0.01	0.008 ± 0.006	0.004 ± 0.003	0.001 ± 0.002	0.38 ± 0.07
45	0.01 ± 0.01	0.10 ± 0.02	0.07 ± 0.03	0.007 ± 0.000	0.003 ± 0.001	0.002 ± 0.002	0.3 ± 0.1
60	0.009 ± 0.003	0.10 ± 0.02	0.07 ± 0.01	0.005 ± 0.003	0.002 ± 0.001	0.001 ±0.001	0.36 ± 0.05
90	0.005	0.067	0.095	0.007	0.004	0.007	0.235
2,3-Benzofuran 6:1							
10	0.007	0.079	0.018	0.029	0.027	0.014	0.634
15	0.009 ± 0.002	0.08 ± 0.003	0.030 ± 0.003	0.024 ± 0.002	0.023 ± 0.008	0.015 ± 0.001	0.77 ± 0.04
25	0.009	0.07	0.031	0.022	0.022	0.021	0.748
45	0.007 ± 0.003	0.05 ± 0.02	0.044 ± 0.003	0.025 ± 0.009	0.022 ±0.002	0.03 ± 0.02	0.6 ± 0.1
60	0.007 ± 0.002	0.028 ± 0.009	0.083 ± 0.007	0.012 ± 0.005	0.008 ± 0.001	0.042 ± 0.003	0.64 ± 0.03
2-Ethylphenol 3:1							
10	0	0.03 ± 0.01	0.113 ± 0.006	0.007 ± 0.004	0.018 ± 0.007	0.011 ± 0.002	-
15	0	0.018	0.125	0.003	0.021	0.013	-
25	0	0.006	0.145	0.002	0.008	0.013	-
60	0	0.003	0.153	0.002	0.004	0.012	-
2-Ethylcyclohexanol 0.5:1							
5	0	0.045	0.031	0.032	0.082	0.011	0.334
10	0	0.03 ± 0.01	0.06 ± 0.03	0.02 ± 0.02	0.04 ± 0.02	0.03 ± 0.01	0.36 ± 0.02
15	0	0.016 ± 0.009	0.090 ± 0.006	0.010 ± 0.002	0.040 ± 0.006	0.042 ± 0.001	0.351 ± 0.003
25	0	0.013	0.094	0.008	0.026	0.054	0.324
Ethylbenzene 2:1							
10	0	0	0.105 ± 0.0004	0.080 ± 0.008	0	0	0.168 ±0.003
15	0	0	0.11 ± 0.06	0.09 ± 0.04	0	0	0.16 ± 0.13
20	0	0	0.12	0.08	0	0	0.14
25	0	0	0.09	0.11	0	0	0.09
Ethylcyclohexane 0:1							
10	0	0	0.063	0.128	0	0	0.307
15	0	0	0.087	0.117	0	0	0.333

Table A.2 Concentration (M) data for the reactions at 380 °C with 0, 1, 1.5 ml of water and 10 mg of 5 wt.% Pt/C. The batch holding time was 30 min for all reactions. A 4:1 hydrogen to benzofuran molar ratio was achieved by pressuring the reactors with 330, 390, and 470 psia of hydrogen, respectively.

2,3-Benzofuran 4:1							
Water	**Benzofuran**	**Ethylphenol**	**Ethylbenzene**	**Ethylcyclohexanone**	**Ethylcyclohexanol**	**Ethylcyclohexane**	**Hydrogen**
0	0.001 ± 0.000	0.084 ± 0.007	0.052 ± 0.006	0.031 ± 0.002	0.012 ± 0.000	0.019 ± 0.003	0.281 ± 0.006
1	0.007 ± 0.002	0.141 ± 0.008	0.036 ± 0.007	0.005 ± 0.001	0.005 ± 0.001	0.001 ± 0.001	0.38 ± 0.02
1.5	0.005 ± 0.000	0.14 ± 0.01	0.029 ± 0.007	0.004 ± 0.002	0.003 ± 0.003	0.001 ± 0.002	0.35 ± 0.07

Table A.3 Concentration (M) data for the reactions at 380 °C with 0.67 ml water, 5 mg of 5 wt.% Pt/C, 900 µmol of benzofuran, and a 4:1 hydrogen to benzofuran molar ratio. All times are in minutes.

2,3-Benzofuran 4:1							
Time	**Benzofuran**	**Ethylphenol**	**Ethylbenzene**	**Ethylcyclohexanone**	**Ethylcyclohexanol**	**Ethylcyclohexane**	**Hydrogen**
10	0.040 ± 0.008	0.13 ± 0.01	0.007 ± 0.002	0.005 ± 0.000	0.004 ± 0.002	0	0.017 ± 0.007
15	0.049	0.121	0.008	0.004	0	0	0.018
25	0.036	0.11	0.012	0.009	0.003	0.002	0.017
45	0.022	0.099	0.033	0.012	0.003	0.01	0.016
60	0.035	0.114	0.028	0.009	0	0.003	0.007

Table A.4 Concentration (M) data for the reactions at 380 °C with 0.67 ml of water and 10 mg of 5 wt.% Pt/C. 2-Methylphenol and ethylbenzene, 450 µmol of each, were loaded into each reactor with a 2:1 hydrogen to organic ratio. All times are in minutes. (MCHONE = methylcyclohexanone, MCHOL = methylcyclohexanol, and MCH = methylcyclohexane)

2-Methylphenol + Ethylbenzene 2:1								
Time	**Methylphenol**	**Ethylbenzene**	**Toluene**	**Ethylcyclohexane**	**MCHONE**	**MCHOL**	**MCH**	**Hydrogen**
10	0.02	0.092	0.061	0.009	0.004	0.005	0.006	0.268
15	0.025	0.09	0.045	0.017	0.009	0.011	0.008	0.178
20	0.014	0.091	0.063	0.01	0.004	0.005	0.007	0.246

References

1. P. Duan, P. E. Savage, Appl. Catal. B: Environ. 108-109, (2011) 54-60.
2. J. Fu, X. Lu, P. E. Savage, Energy Environ. Sci. 3, (2010) 311-317.
3. J. Fu, X. Lu, P. E. Savage, ChemSusChem 4, (2011) 481-486.
4. A. Y. Bunch, U. S. Ozkan, J. Catal. 206, (2002) 177-187.
5. A. Y. Bunch, X. Wang, U. S. Ozkan, J. Mol. Catal. A: Chem. 270, (2007) 264-272.
6. C. L. Lee, D. F. Ollis, J. Catal. 87, (1984) 325-331.
7. Y. Romero, F. Richard, Y. Renème, S. Brunet, Appl. Catal. A: Gen. 353, (2009) 46-53.
8. D. C. Elliott, L. J. Sealock Jr, E. G. Baker, Ind. Eng. Chem. Res. 32, (1993) 1542-1548.
9. A. Vargas, T. Burgi, A. Baiker, J. Catal. 222, (2004) 439-449.
10. M. C. Edelman, M. K. Maholland, R. M. Baldwin, S. W. Cowley, J. Catal. 111, (1988) 243-253.
11. H. S. Fogler, Elements of Chemical Reaction Engineering, Prentice Hall, Westford, 2008.
12. E. N. Fuller, P. D. Schettler, J. C. Giddings, Ind. Eng. Chem. Res. 58, (1966) 18-27.

Chapter 6

Stability and Activity of Pt and Ni Catalysts for Hydrothermal HDO

Chapter 5 examined the effect of process variables and the kinetics of the hydrothermal HDO of benzofuran over Pt/C. In this chapter, we seek to move away from noble metal catalysts, because, as discussed in chapter 2, of their high cost and susceptibility to poisoning, and develop cheaper non-noble metal catalysts that are both active and stable for hydrothermal HDO. We also selected a new model compound, o-cresol, which is common in bio-oils and is reasonably water soluble (25 g/L) to ease the delivery of the reactant to the flow reactor.

In this chapter, we examine the activity and stability of nominal 5 wt% Pt/C, 65 wt% $Ni/SiO_2Al_2O_3$, Raney Ni 2800, and a Raney Ni catalyst doped with 10 wt% Cu (i.e., 10 wt% Raney NiCu) for the hydrothermal HDO of o-cresol in a flow reactor at 380 °C and 305 bar. We examined Pt/C as a benchmark catalyst to determine the catalyst stability in a flow system. Next, we examined a $Ni/SiO_2Al_2O_3$ catalyst, as this catalyst removed oxygen from the bio-oil when used in the catalytic hydrothermal liquefaction of microalgae [1]. Subsequently, we examined a skeletal Ni catalyst, Raney Ni 2800, to remove the possibility of reactions on the catalyst support and degradation of the support. Finally, we modified the base Raney Ni catalyst by adding approximately 10 wt% Cu to the surface. We will show that this modified Raney NiCu catalyst provides increased selectivity for liquid HDO products by reducing C-C bond scission.

This chapter is divided into five parts. We first discuss the control experiments performed to assess the carbon balances and to ensure accurate quantification of products. The next four sections examine HDO with each catalyst. Within each of these sections we first present the reaction results and then discuss the catalyst characterization results.

6.1. Control experiments

We performed a variety of control experiments to ensure that the results presented are accurate. To verify that the reactor effluent sampling and analytical methods led to accurate species concentrations, we verified that the o-cresol concentration in the effluent in the absence of any reaction matched that at the reactor inlet ($C_{oc,o}$). We pumped the feed and internal standard solutions through the flow reactor without catalyst at room temperature and 305 bar, and collected samples for 2 hr. The experimentally determined value, $C_{oc,o}$ = 0.163 mol C/L, was 95.3 ± 3.5 % of the value expected from a mass balance assuming ideal solutions. We also performed non-catalytic reactions at temperatures from 200 to 380 °C with feed flow rates between 0.218 and 1 mL/min. We determined that complete conversion of the formic acid occurred at all feed flow rates examined when the temperature was 340 °C or higher.

At 380 °C and 305 bar with no catalyst, a 0.218 mL/min feed flow rate, and total reactor residence time of 12.4 min, the carbon recovery, based on analysis of the liquid phase, was 87 ± 5%. The missing carbon was probably resident in higher molecular weight products that form in a mechanism similar to the polymerization of formaldehyde and phenol in water [2]. The yield of these high molecular weight products at 250 °C was 8.3 ± 1.2 % of the carbon from the o-cresol in the feed stream. We observed no higher molecular

weight products in the reactions at 380 °C, but their absence may simply be due to their growth to a size that would not permit elution from the GC column. Table 6.1 shows the gas compositions from the non-catalytic reaction and indicates that H_2 and CO_2 are the major components, along with lesser amounts of CO and CH_4. Throughout this chapter, the uncertainties, when given, represent the standard deviation calculated from multiple samples.

We were also concerned that activated carbon, the support of the Pt/C catalyst and the material used to dilute the Raney Ni and Raney NiCu catalyst beds, may adsorb reagent, as we found this to occur previously [3]. We performed an experiment at 380 °C where the catalyst bed was loaded with only activated carbon. We observed no decrease in the carbon balance and no reaction products over 5 hr on stream, indicating that adsorption of reactant is not a major complication in these experiments.

6.2. Pt/C

We first determined the activity and stability for hydrothermal HDO of Pt/C, as this catalyst was used previously in similar reactions and serves as a benchmark with which we can compare other catalysts.

6.2.1. Pt/C reaction results

The major reaction products from o-cresol reacting over Pt/C with a W/F (weight of the catalyst active metal (as measured by ICP-OES) over the mass flow rate of o-cresol in the feed) of 2.7 min were methylcyclohexane, toluene, methylcyclohexanone and cis/trans methylcyclohexanol (table B.1b). Cracking products such as benzene or cyclohexane were

not observed, and correspondingly, the product gases contained less than 0.2 mol% CH_4, as shown in table 6.1 (table B.1a). Fig. 6.1 shows a proposed reaction network for o-cresol, taking into account all the products observed and previous literature [3, 4].

Table 6.1. Gas compositions (mol%, dry basis) from reactions at 380 °C and 305 bar. TOS = time on stream.

Gas	Non-catalytic	Pt/C	$Ni/SiO_2Al_2O_3$ (TOS = 73 min)	$Ni/SiO_2Al_2O_3$ (TOS = 422 min)	Raney Ni (W/F = 447 min)	Raney Ni (W/F = 12 min	Raney NiCu (First 3 hrs)	Raney NiCu (Last 3 hrs)
H_2	39 ± 18	32 ± 12	27.9	31.4	2.2 ± 1.6	5.8	12 ± 2	17 ± 7
CO	2.7 ± 0.9	0.66 ± 0.15	0	0.43	0	0	0	0
CH_4	0.31 ± 0.02	0.14 ± 0.03	7.6	1.14	34.4 ± 0.3	24.2	19 ± 3	11.3 ± 0.7
CO_2	58 ± 18	67 ± 12	64.5	67.0	63 ± 2	69	69 ± 4	72 ± 8

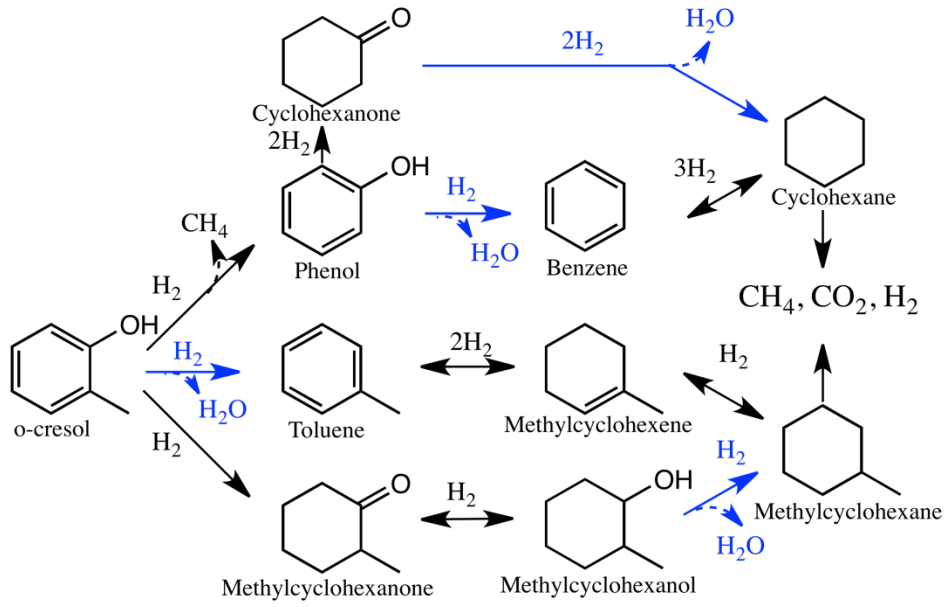

Figure 6.1. Proposed reaction network for the HDO of o-cresol. The blue arrows represent HDO reactions.

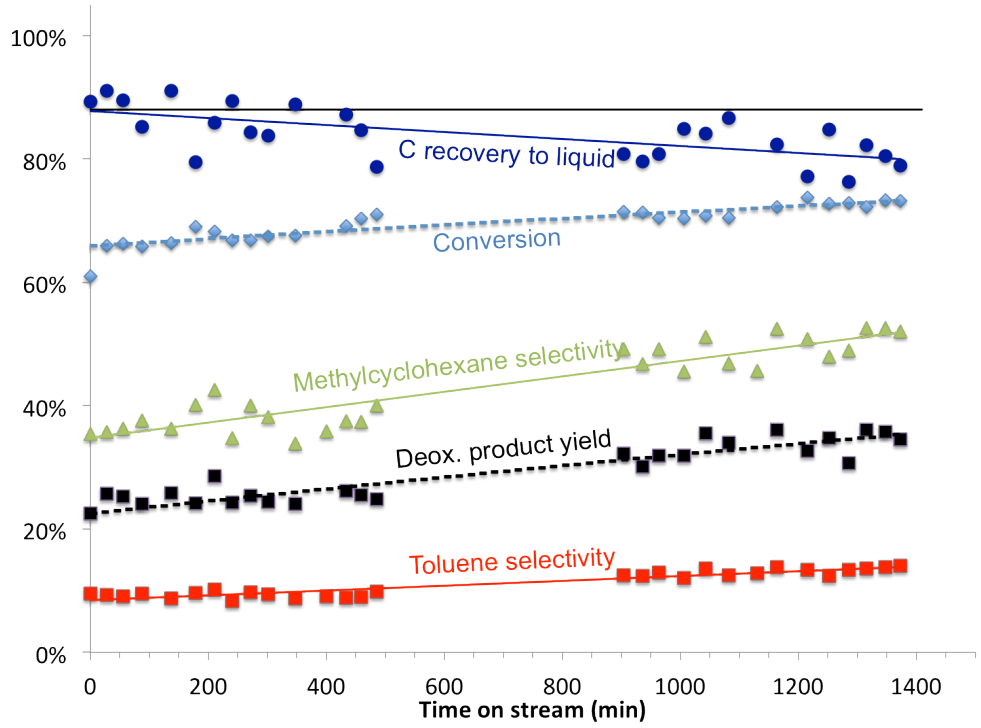

Figure 6.2. Results from reacting o-cresol in water over Pt/C (W/F = 2.7 min, T = 380 °C, P = 305 bar, feed solution (ambient conditions): 24.7 g/L o-cresol, 147 mL/L formic acid, balance DI H_2O, feed flow rate (ambient conditions) = 0.218 mL/min). The solid trend lines are from linear regressions and the hashed lines are from the deactivation model. k' (0.083 L/g_{cat} min) and k'_{HDO} (0.020 L/g_{cat} min) were determined at 28 and 0 min on stream respectively.

Fig. 6.2 shows the carbon recovery to the liquid phase, conversion, deoxygenated product yield, and selectivities for methylcyclohexane and toluene. To quantitatively assess the activity and deactivation of the all of catalysts tested, we developed a simple reaction model for the conversion of o-cresol (X) and the yield of deoxygenated products (Y_{deox}). Since the time scale for catalyst deactivation (hr) is much longer than the time scale for HDO (min), we treat the plug flow reactor as being in pseudo-steady state and, accordingly, write the design equation:

$$Eq.\,6.1.\ F_{mol\,oc,o}\frac{dX}{dw} = -r_{oc}$$

Where $F_{mol\,oc,o}$ is the molar flow rate of o-cresol in the feed stream, w is the catalysts mass, and $-r_{oc}$ is the rate of disappearance of o-cresol. We assumed that the reaction rate was first order in o-cresol and that the activity of the catalyst (a) was dependent on the time on stream (t_{os}).

$$Eq.\,6.2.\ -r_{oc} = k'\ C_{oc}a(t_{os})$$

with

$$Eq.\,6.3.\ C_{oc} = C_{oc,o}(1-X)$$

where C_{oc} is the concentration of o-cresol at reaction conditions (estimated to be 0.045 mol/L in the feed stream). Combining equations 6.1, 2 and 3 and solving gives:

$$Eq.\,6.4.\ -F_{mol\,oc,o}ln(1-X) = k'^{C_{oc,o}}wa(t_{os})$$

To model catalyst deactivation, we examined zero, first, and second order deactivation kinetics as shown in equation 6.5:

$$Eq.\,6.5a.\ \frac{da}{dt_{os}} = k_d$$

$$Eq.\,6.5b.\ \frac{da}{dt_{os}} = k_d a$$

$$Eq.\,6.5c.\ \frac{da}{dt_{os}} = k_d a^2$$

with k_d being the deactivation rate constant. Solving these differential equations with the condition that a=1 at t_{os}= 0, yields:

$$Eq\ 6.6a.\ a(t_{os}) = 1 - k_d t_{os}$$

$$Eq\ 6.6b.\ a(t_{os}) = e^{-k_d t_{os}}$$

$$Eq\ 6.6c.\ \ a(t_{os}) = \frac{1}{1 + k_d t_{os}}$$

We then combined equations 6.4 and 6.6, linearized the resulting equations, and determined the value of k_d from linear regression. In general, we selected the deactivation model with the highest correlation coefficient, R^2, to plot in figs. 6.2, 6.4, and 6.8, but the conclusions presented are independent of the model chosen. The same procedure was used to fit the data for the yield of deoxygenated products, by simply substituting Y_{deox} for X and k'_{HDO} for k'. k'_{HDO} is a composite rate constant for the initial rate of hydrodeoxygenation, represented by the blue arrows in fig. 6.1.

Table 6.2: Zero, first, and second order deactivation rate constants for conversion and deoxygenated product yield and the associated correlation coefficients.

		Deactivation Models					
		0 order		**1st order**		**2nd order**	
Catalyst	**Fit Variable**	**Slope (k_d) x10^4**	**R^2**	**Slope (k_d) x10^4**	**R^2**	**Slope (k_d) x10^4**	**R^2**
Pt/C	Conversion	-1.63 ± 0.45*	0.93	-1.50 ± 0.45	0.92	-1.38 ± 0.45	0.91
	Deox. prod. yield	-5.14 ± 1.22	0.95	-4.03 ± 0.93*	0.95	-3.23 ± 0.77	0.95
$Ni/SiO_2Al_2O_3$	Conversion	9.69 ± 20.1	0.21	16.4 ± 21.3	0.40	27.5 ± 28.3*	0.52
	Deox. prod. yield	30.5 ± 17.4	0.78	72.8 ± 27.5	0.89	301 ± 121*	0.89
Raney NiCu	Conversion	3.64 ± 1.86	0.80	4.44 ± 2.25*	0.80	5.50 ± 2.80	0.80
	Deox. prod. yield	-1.56 ± 2.70*	0.26	-1.34 ± 2.64	0.22	-1.15 ± 2.80	0.15

* Indicates the chosen model plotted in figures 6.2, 6.4, and 6.8. k_d has units of 1/min.

Fig. 6.2 shows that the conversion and deoxygenated product yield increase with time on stream (TOS). Table 6.2 shows the zero, first, and second order deactivation rate constants, k_d's, for both conversion and deoxygenated product yield are negative, quantitatively indicating that both variables are increasing with TOS because the obtained rate constants are less than zero for the confidence interval chosen. We have not selected a

specific deactivation model to discuss because all the models had a similar quality of fit, R^2, and all of the models indicated that the catalyst activity increased with TOS. We note that a negative k_d indicates that activity is increasing the TOS, a positive k_d indicates that catalyst is deactivating with TOS, and a k_d encompassing zero indicates no change in activity with TOS.

The horizontal black line on fig. 6.2, and figs. 6.4 and 6.8, indicates the 87 ± 5% carbon recovery obtained in the non-catalytic control experiment. This value represents the highest carbon recovery we expect in the catalytic experiments since parallel thermal reactions seem to produce oligomers that could not be quantified by our methods. Fig. 6.2 shows that near the beginning of the reaction, the carbon recovery to the liquid phase is near this expected recovery, but appears to decrease with TOS. Similarly, the toluene selectivity appears to remain steady with TOS, while the methylcyclohexane selectivity appears to increase.

The increasing methylcyclohexane selectivity and the toluene selectivity remaining unchanged indicates that the Pt/C catalyst appears to become more active for hydrogenation with increasing TOS, but not at the expense of HDO. We hypothesize that these trends can be attributed to the catalyst surface becoming partially oxidized by CO during the reactor startup, and then becoming more reduced with increasing TOS as the surface is reduced by the H_2 formed *in situ* from the formic acid in the feed. The non-catalytic control experiments indicated that at a feed flow rate of 1 mL/min, 7.5 ± 3.5 mol% CO was produced from the decomposition of formic acid. Therefore, at the higher feed flow rate used during reactor startup, 2 mL/min, we expect at least this this concentration of CO to contact the catalyst bed. Grabow *et al.* showed that CO covered the majority of the Pt

surface (~2/3 of a monolayer) in the low temperature (250 – 300 °C) water gas shift reaction, effectively acting as a catalyst poison [5]. This hypothesis is also consistent with the observed increase in deoxygenated product yield and conversion with increasing TOS, as a more reduced catalyst surface would have more available active sites, and therefore, a greater activity. The reason for the decrease in the carbon recovery to the liquid phase is unknown, but we suspect that as the Pt becomes more active with TOS, it is likely producing more CO_2 from the o-cresol, as we observed CO_2 previously in a similar reaction [3]. This extra CO_2 produced would be difficult to detect because of the large amount of CO_2 produced from the decomposition of formic acid.

6.2.2. Pt/C Characterization

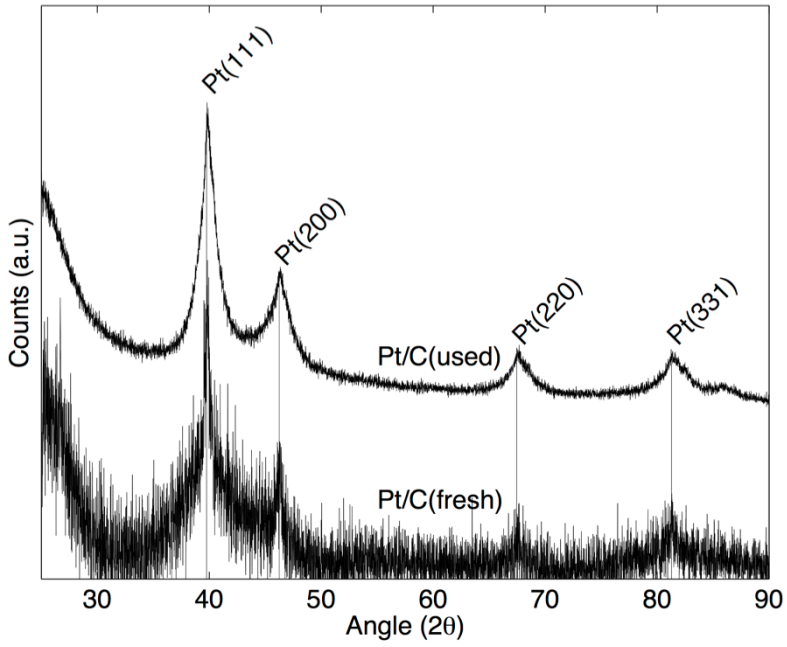

Figure 6.3. X-ray diffraction patterns of the fresh and used Pt/C catalysts.

Fig. 6.3 shows that the XRD patterns of the fresh and used Pt/C catalysts include peaks from both the Pt nanoparticles and a broad hump (< 30°) from the amorphous carbon support. We note the absence of platinum oxide peaks, indicating that the Pt is reduced within the bulk structure (n.b. a surface oxide might have nevertheless been present). Examination of fig. 6.3 reveals that the fresh catalyst had a much lower signal to noise ratio than the used catalyst, and we suspect that this is because after reaction the Pt nanoparticles are more exposed on the surface of the carbon support, rather than contained within the support. Evidence to support this claim comes from Fu *et al.* found that this same Pt/C catalyst contained only 1/3 of the original micropore volume after a reaction in a hydrothermal environment [6].

Table 6.3 lists the particle size and wt% of metals for all the catalysts tested. The ICP analysis indicates that the fresh and used catalysts contained 3.0 ± 0.2 and 2.6 ± 0.1 wt% Pt, respectively. These values differ from the loading given by the manufacturer of 4-5.2 wt%, but were verified by four separate ICP-OES analyses. The slight drop in Pt wt% with use is probably not statistically significant, especially if a 95% confidence interval (two standard deviations) is used. Table 6.3 also indicates that the Pt particle sizes for the fresh and used catalyst were both 4.4 nm.

Table 6.3: Catalyst particle sizes (from XRD and Scherrer eq.) and composition (ICP-OES).

Catalyst	Particle Size (nm)	Composition (wt%) Pt	Ni	Al	Cu
Pt/C (fresh)	4.4	3.0 ± 0.2	0	0	0
Pt/C (used)	4.4	2.6 ± 0.1	0	0	0
$Ni/SiO_2Al_2O_3$ (fresh)	3.8	0	56 ± 2	4.6 ±0.2	0
$Ni/SiO_2Al_2O_3$ (used)	36	0	43 ± 2	0.1 ± 0.2	0
Raney Ni (fresh)*	21	0	95 ± 0.5	5.2 ± 0.2	0
Raney Ni (used)*	38	0	100 ± 0.2	0.2 ± 0.2	0
Raney NiCu (fresh)*	25	0	89 ± 3	3.8 ± 1.3	7.4 ± 1.6
Raney NiCu (used)*	22	0	92 ± 1	0.2 ± 0.3	7.9 ± 0.5

*Normalized total wt% to 100%.

The reaction and characterization results presented above strongly support the conclusion that Pt/C is active and stable for at least 24 hr on stream in supercritical water for the HDO of o-cresol at 380 °C and 305 bar.

6.3. $Ni/SiO_2Al_2O_3$

The previous section showed that the benchmark catalyst, Pt/C, is both active and stable for hydrothermal HDO. Pt is a very expensive metal, however, so we sought to identify and develop less costly Ni catalysts that might also exhibit acceptable activity and stability. The first such catalyst we tested is $Ni/SiO_2Al_2O_3$, as it was used previously for hydrothermal processing of biomass [1].

6.3.1. $Ni/SiO_2Al_2O_3$ reaction results

The major products from the reaction of o-cresol over the $Ni/SiO_2Al_2O_3$ catalyst at a W/F of 74 min were methylcyclohexane, toluene, and methylcyclohexanol. Smaller

amounts of benzene, cyclohexane, and ethylcyclopentane also formed (see table B.2). In contrast to the Pt/C catalyst, this Ni catalyst produced a significant amount of CH_4. Table 6.1 shows that the gas was 7.6 mol% CH_4 after 73 min on stream.

Fig. 6.4 shows the conversion, deoxygenated product yield, carbon recovery to the liquid phase, and the toluene and methylcyclohexane selectivities as functions of time on stream. As shown in table 6.2, the second order deactivation constants, k_d, for the $Ni/SiO_2Al_2O_3$ catalyst are 2.75 ± 2.83 $x10^{-3}$ and 3.01 ± 1.21 $x10^{-2}$ min^{-1} for conversion and yield of deoxygenated products, respectively. The R^2 for the first and second order deactivation models for the deoxygenated product yield where the same (0.89), but a visual inspection of the fit of each model to the data revealed that the second order deactivation model captured the trends in the data more accurately. The k_d's obtained indicate that the catalyst is deactivating in terms the deoxygenated product yield, the variable of greatest interest. Further evidence of deactivation is that the reaction was continued for almost 1000 min (not shown in fig. 6.4) and the deoxygenated product yield remained below 1.5% (table B.2b). The second order deactivation models, which provided the best fit to the experiment data, are consistent with deactivation by sintering [7].

Fig. 6.4 shows that the toluene selectivity also decreases to near zero within 150 min on stream. The methylcyclohexane selectivity appears to trend downward with TOS, although the data presented contain significant scatter making discerning a long-term trend difficult. The scatter in the data likely occurred because the $SiO_2Al_2O_3$ support was degrading, as will be shown in the next section, and obstructing the flow through the catalyst bed. Evidence to support this claim comes from the observation that the pressure varied widely at the HPLC pump (up to 14 bar) between samples with the $Ni/SiO_2Al_2O_3$

catalyst, while we observed much smaller pressure variations (~3 bar) between samples with all the other catalysts.

Since acidic materials, such as zeolites, which are similar to the $SiO_2Al_2O_3$ used here, are known to be active for C-C bond scission and aromatic product formation [8], and Ni is an active hydrogenation catalyst, we propose that the production of toluene in this reaction is due primarily to the $SiO_2Al_2O_3$ support and that the production of methylcyclohexane is due primarily to the Ni. This two-reaction site hypothesis is consistent with the decrease in toluene selectivity with TOS and the decrease in CH_4 mol% (see table 6.1 and table B.2a). In addition, Elliot *et al.* indicated that Ni remains active under hydrothermal conditions [9], which is consistent with the decrease in methylcyclohexane selectivity being less significant than that for toluene.

The carbon recovery to liquid phase products appears to be relatively stable if not increasing slightly with TOS. After 400 min on stream the carbon recovery approaches the baseline value of 87 ± 5% expected from the non-catalytic control experiment. With this catalyst, we also flowed N_2 at 15 mL/min (room temperature and pressure) through an Omega 5400/5500 mass flow controller (see fig. 3.2) to quantify the gas products. The liquid and gas products together accounted for 88 ± 12 % of the carbon in the o-cresol in the feed. This value for the total carbon recovery encompasses the maximum expected C recovery of 87 ± 5%.

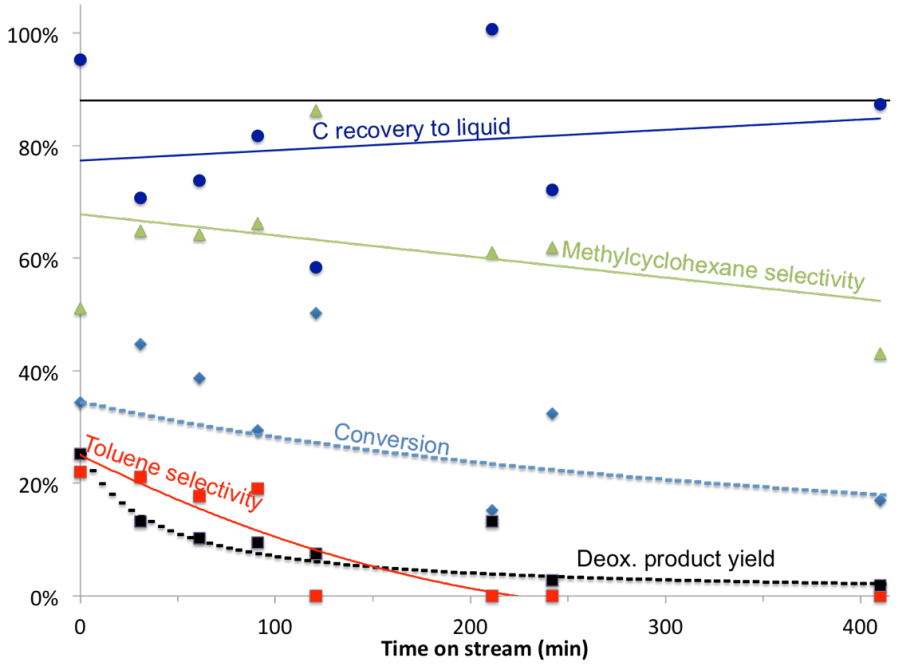

Figure 6.4. Results from reacting o-cresol in water over $Ni/SiO_2Al_2O_3$ (W/F = 74 min, T = 380 °C, P = 305 bar, feed solution (ambient conditions): 24.7 g/L o-cresol, 147 mL/L formic acid, balance DI H_2O, feed flow rate (ambient conditions) = 0.218 mL/min). The solid trend lines are from linear regressions or a second order polynomial regression (toluene selectivity) and the hashed lines are from the deactivation model. k' (1.2×10^{-3} L/g_{cat} min) and k'_{HDO} (8.1×10^{-4} L/g_{cat} min) were determined at 0 min on stream.

6.3.2. $Ni/SiO_2Al_2O_3$ characterization

Fig. 6.5 shows the XRD pattern of the fresh and used $Ni/SiO_2Al_2O_3$. The fresh $Ni/SiO_2Al_2O_3$ has characteristic peaks for Ni and NiO. The fresh catalyst pattern also contains a broad peak likely from amorphous $SiO_2Al_2O_3$ around 23°. The used $Ni/SiO_2Al_2O_3$ diffraction pattern shows primarily Ni, but also contains several peaks not present in the fresh catalyst that likely correspond to $Ni_xAl_ySi_zO$. These new peaks were difficult to identify more specifically, as they could not be readily matched in Jade®. A variety of nickel aluminum silicon oxide phases examined in the XRD database, however, had peak locations corresponding to the peaks in the used pattern. Regardless of the specific identity of these

new peaks in the used material, the XRD patterns in fig. 6.5 clearly show that a significant transformation of the catalyst support occurred during the reaction.

Prior to these results, it was unclear if the $SiO_2Al_2O_3$ support was stable under hydrothermal conditions since there are reports of hydrothermally stable aluminosilicates [10] and a report indicating that a high metal loading significantly retarded the transition of Al_2O_3 [11]. Clearly, though, this aluminosilicate is not stable. These results are consistent with several studies showing that SiO_2 and most forms of Al_2O_3 are unstable in a hydrothermal environment [11-13] and that zeolites (aluminosilicates) can convert into amorphous materials through hydrolysis of siloxane bonds (Si-O-Si) under hydrothermal conditions [14].

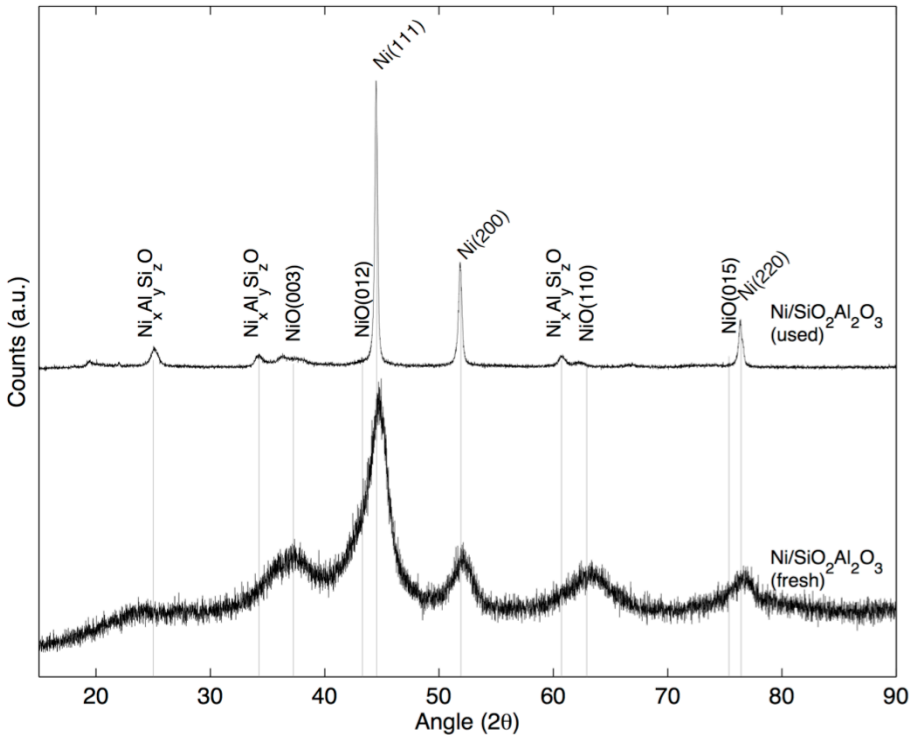

Figure 6.5. X-ray diffraction patterns of the fresh and used $Ni/SiO_2Al_2O_3$ catalysts.

Fig. 6.5 also shows a narrowing of the Ni(111) peak in the used catalyst, and table 6.3 indicates that this change is consistent with the growth of the Ni particles from 3.8 nm in the fresh catalyst to 36 nm in the used catalyst. This particle sintering is likely caused by the degradation of the $SiO_2Al_2O_3$ support. Previous researchers have also observed sintering of Ni particles supported on Al_2O_3 and SiO_2 during aqueous phase reforming [15] and supercritical water gasification, resulting in overall catalytic activity loss [12]. Table 6.3 also indicates that the used catalyst contains less Ni and Al. The decrease in Ni and Al compositions of the used catalyst are likely from the metals leaching into the reaction stream [16]. The loss of Al from the catalyst support is consistent with the two reaction site hypothesis presented above. As the support lost Al during the reaction it lost acidity, thereby losing toluene selectivity and deoxygenated product yield, as we observed.

The characterization and reaction results both show that the $Ni/SiO_2Al_2O_3$ is not stable under the reaction conditions tested. The primary cause of the catalyst instability is support degradation and sintering of the Ni particles. These results do not rule out other causes of catalyst deactivation, such as coking, nor do they examine the exact molecular mechanism that causes the $SiO_2Al_2O_3$ support to degrade, as these questions are beyond the scope of this work. Further examination of these issues may be warranted as the catalyst had a relatively high initial activity.

6.4. Raney Ni

With the working hypothesis that support degradation was causing the decrease in HDO activity for the $Ni/SiO_2Al_2O_3$, we decided to examine an unsupported Raney Ni catalyst, allowing for the examination of the activity of Ni alone.

6.4.1. Raney Ni reaction results

Fig. 6.6 shows the conversion and yield of deoxygenated products when o-cresol was reacted over Raney Ni at various W/F. At a W/F of 447 min, no liquid products or o-cresol were in the reactor effluent. Gas analysis, shown in table 6.1 (table B.3a), indicates that 34.4 ± 0.3 mol% CH_4 was produced and nearly all of the H_2 was consumed during the reaction. This CH_4 composition and H_2 consumption both represent a significant increase when compared with the $Ni/SiO_2Al_2O_3$ catalyst, indicating that the Raney Ni catalyst, under conditions used, is more active for gasification than was the $Ni/SiO_2Al_2O_3$ catalyst. After 22 hr on stream at W/F of 447 min, we increased the feed flow rate to 1 mL/min, resulting in a W/F of 98 min. Upon further reaction for 2 hr, no reaction products or o-cresol were detected in the liquid reactor effluent. This result provides strong evidence that the carbon in the feed was completely gasified. It is unlikely that coking is a major source of carbon disappearance from the liquid phase because 4.2 g o-cresol/g catalyst flowed over the catalyst by the end of this reaction, and this amount of carbon, had it been present as coke, would have plugged the reactor.

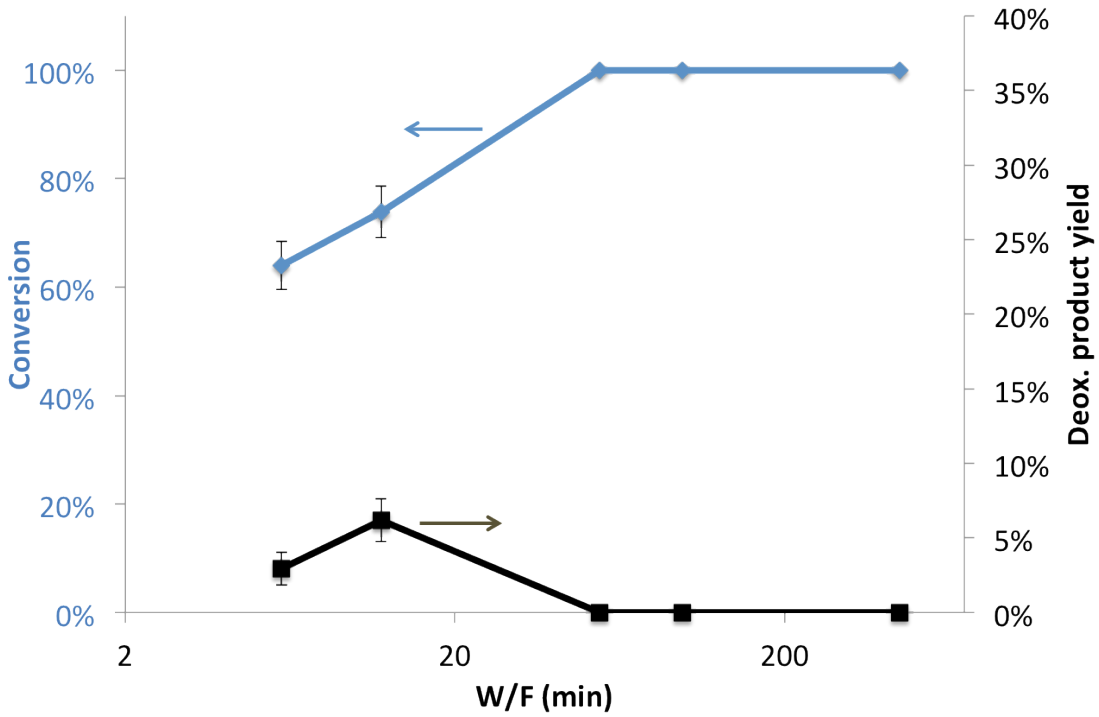

Figure 6.6. Results from reacting o-cresol in water over Raney Ni 2800 (T = 380 °C, P = 305 bar, feed solution (ambient conditions): 24.7 g/L o-cresol, 147 mL/L formic acid, balance DI H_2O, TOS (from right to left on plot) = 1320, 120, 1207, 84, and 50 min).

Complete gasification also occurred at a W/F of 55 min, but liquid deoxygenated products were observed at W/F of 12 and 6 min. The maximum yield of deoxygenated products observed with the Raney Ni catalyst was 6.2 ± 1.4% at a W/F of 12 min. Further decreasing the W/F to 6 min resulted in a decrease in the yield of deoxygenated products. Conversion also decreased from 74 ± 5% to 64 ± 4% when W/F was decreased from 12 to 6 min.

The major liquid products at a W/F of 12 and 6 min were benzene, toluene, cyclohexanone, phenol, and methylcyclohexanone (see table B.3c). For a W/F of 12 min, the most abundant product was phenol with a 29 ± 4% yield and the most abundant deoxygenated product was benzene, with a 4.6 ± 1.1% yield. Gas analysis, shown in table

6.1 (table B.3b), indicates that a significant amount of CH_4 is formed under these conditions. The carbon recovery to the liquid phase for this reaction condition was 68 ± 5%.

These results provide several insights into the Raney Ni catalyst under the conditions tested. First, at high W/F Raney Ni is an active gasification catalyst and produced mostly CH_4, as has been noted previously [15]. Second, at lower W/F, Raney Ni can produce HDO products, but in low yields. Furthermore, even at low W/F, significant C-C bond scission occurred as evidenced by the presence of CH_4, phenol, and benzene in the reaction products. Third, with Raney Ni as the catalyst, the desired deoxygenated products are intermediates in a reaction network that concludes with C-C bond scission to form gas products, as shown in fig. 6.1. This outcome is in contrast to Pt/C, which was not active for gasification under the hydrothermal reaction conditions tested, and, therefore, desired deoxygenated products were terminal products in the reaction network. Fourth, because of the high gasification activity of Raney Ni, further optimization of W/F will not significantly increase deoxygenated product yields.

Based on these observations, we decided to modify the Raney Ni catalyst in an attempt to decrease the rate of gasification.

6.4.2. Raney Ni characterization

Fig. 6.7 shows the XRD patterns of the fresh and used Raney Ni and Raney NiCu catalysts. The Raney NiCu results will be discussed in section 6.5. Examination of the fresh and used Raney Ni patterns shows that the used catalyst contains several peaks corresponding to the formation of bulk Al_2O_3 from the Al in the Raney Ni catalyst. The formation of Al_2O_3 is likely from the Al hydrates that cover most of the porous Ni

frameworks that form the bulk of Raney Ni catalysts [15, 17]. The used Raney Ni also has a narrowed Ni(111) peak, and, as table 6.3 indicates, the Ni particle size has increased from 21 to 38 nm. In general, these changes are small when compared to the dramatic changes observed in $Ni/SiO_2Al_2O_3$ XRD diffraction pattern, indicating that this catalyst is more stable under the reaction conditions tested.

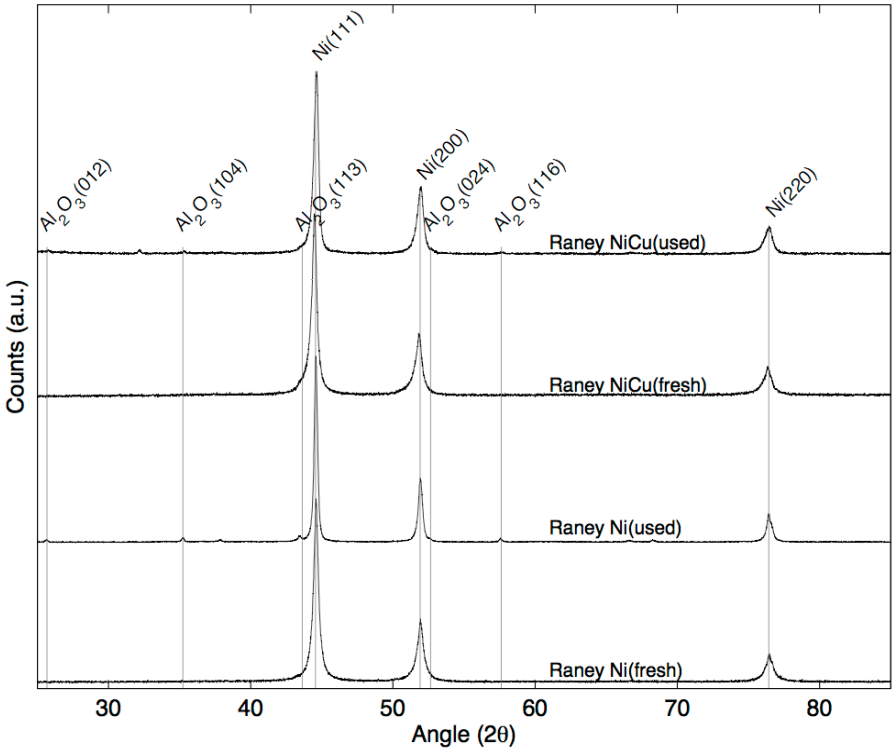

Figure 6.7. X-ray diffraction patterns of the fresh and used Raney Ni and Raney NiCu catalysts.

Table 6.3 also indicates that the fresh Raney Ni catalyst contains Ni and Al. After reaction, the Al wt% dropped significantly from 5.2 ± 0.2 to 0.2 ± 0.2 wt%. These results, and previous reports [16], indicate that Al has leached from the catalyst. Despite the minor differences between the fresh and used catalyst, the Raney Ni activity appears to be stable

under the reaction conditions due to the 100% conversion observed over all 24 hours on stream.

6.5. Raney NiCu

Literature indicated that the addition of metals such as copper [18] reduces the adsorption energy of organic molecules to the surface of active metals. Furthermore, copper is stable in a hydrothermal environment and is not active for gasification [12]. Therefore, we hypothesized that adding copper to the surface of the Raney Ni would reduce the gasification activity and increase the yield of deoxygenated products. We chose to add ~10 wt% copper to the Raney Ni base catalyst based on an optimized value for tin loading on Raney Ni used previously for the aqueous phase reforming of sugars [19].

6.5.1. Raney NiCu reaction results

The major products from the reaction of o-cresol over the Raney NiCu catalyst at a W/F of 58 min were benzene, cyclohexane, toluene, methylcyclohexane, methylcyclohexene, methylcyclohexanol, methylcyclohexanone, and phenol (table B.4b). Gas analysis, shown in table 6.1 (table B.4a), indicates that CH_4 was produced during the reaction. The CH_4 composition drops significantly from the first three hours of the reaction to the last three hours of the reaction, but these compositions of CH_4 are significantly lower than the compositions of CH_4 generated by the unmodified Raney Ni catalyst. Nonetheless, these CH_4 compositions are still significantly higher than the CH_4 composition reported for the Pt/C catalyst, and indicate that C-C cracking reactions are occurring.

Fig. 6.8 shows conversion, carbon recovery to liquid products, deoxygenated product yield, selectivities to toluene and methylcyclohexane when o-cresol was reacted over the Raney NiCu catalyst. Table 6.2 shows that the deactivation rate constants, k_d, for conversion all had the same quality of fit, R^2, and were all positive (i.e. zero was not contained within the confidence interval) indicating that the catalyst is deactivating with respect to conversion. The zero order deactivation model for the deoxygenated product yield had the highest R^2 (0.26) and had a k_d of $-1.6 \pm 2.7 \times 10^{-4}$ min^{-1}, indicating that the catalyst is stable with respect to deoxygenated product yield because zero is within the confidence interval for k_d. Again, though, this conclusion is independent of the model chosen. This stable yield of deoxygenated products over the approximately 24 hr reaction suggests that this catalyst may be active for hydrothermal HDO at a much longer TOS than was studied. This suggestion finds support in a report indicating that a Raney NiCu catalyst used in aqueous ethanol reforming at 300 °C, but near atmospheric pressure, was stable for at least 400 hr [20].

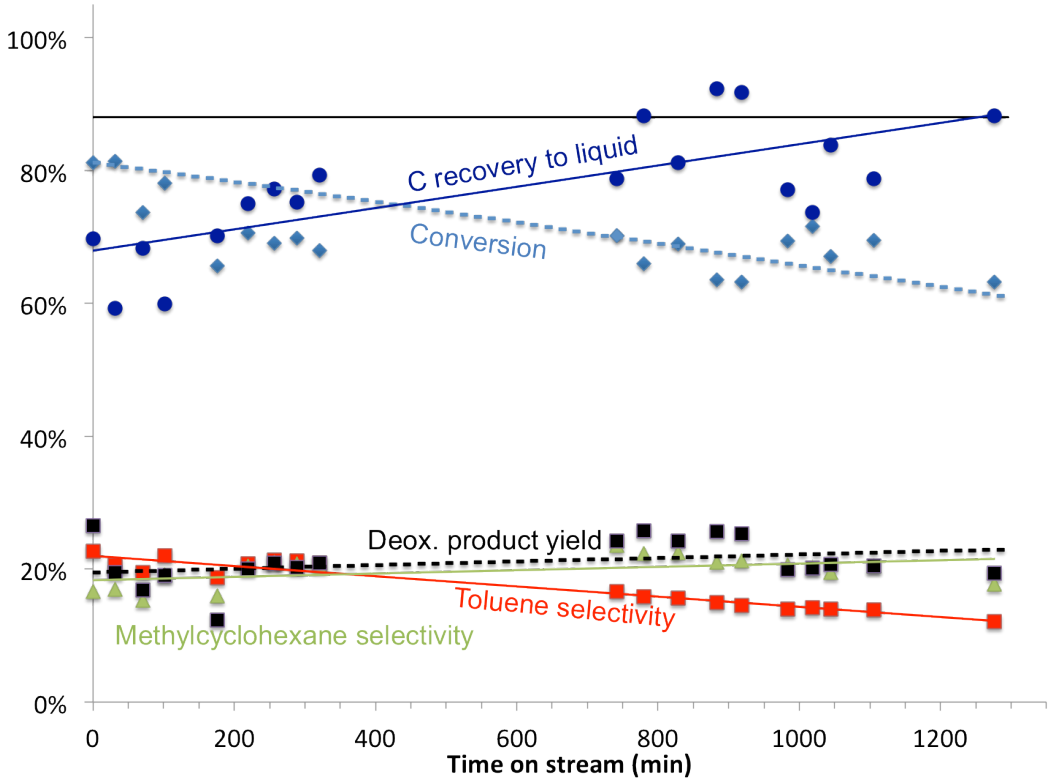

Figure 6.8. Results from reacting o-cresol in water over Raney NiCu (W/F = 58 min, T = 380 °C, P = 305 bar, feed solution (ambient conditions): 24.7 g/L o-cresol, 147 mL/L, balance DI H_2O, feed flow rate (ambient conditions) = 0.218 mL/min). The solid trend lines are from linear regressions and the hashed lines are from the deactivation model. k' (5.9 x 10^{-3} L/g_{cat} min) and k'_{HDO} (7.7 x 10^{-4} L/g_{cat} min) were determined at 0 and 31 min on stream respectively.

Fig. 6.8 also appears to show that the carbon recovery to the liquid phase increases with TOS. This trend, together with the decreasing CH_4 composition with TOS, indicates that the Raney NiCu catalyst is less active for gasification, a desired change, with increasing TOS. It is also likely that the apparent decrease in conversion with TOS is caused by the lower activity for C-C hydrogenolysis reactions. Furthermore, the toluene selectivity appears to decrease without a change in either the deoxygenated product yield or the methylcyclohexane selectivity. Examination of the product yield in table B.4 shows that the

decrease in toluene selectivity is due to the production of methylcyclohexene at longer TOS, which indicates that the catalyst became more active for hydrogenation with increasing TOS.

These changes in activity may be caused by a further reduction of the catalyst surface, as we suspect also occurred for the Pt/C catalyst, or it may come from coking of under-coordinated sites essential for gasification and reforming reactions [21]. Once the under-coordinated sites have deactivated, the carbon recovery to the liquid phase and the amount of H_2, which is need for hydrogenating toluene to methylcyclohexene, in the reactor would increase.

The results presented in fig. 6.8 represent a significant improvement over those attained with the $Ni/SiO_2Al_2O_3$ and Raney Ni catalysts tested. The Raney NiCu catalyst achieved a higher carbon recovery to the liquid phase and higher yield of deoxygenated products than the unmodified Raney Ni catalyst. In fact, the 21 ± 4 % deoxygenated product yield is a 3.4 fold increase over the best yield of deoxygenated products from the Raney Ni catalyst. We suspect that even higher yields are available by optimizing the Cu loading on the catalyst and manipulating W/F. The superior stability of the Raney NiCu catalyst also represents a significant improvement over the $Ni/SiO_2Al_2O_3$.

It is likely that the addition of Cu to the Raney Ni catalyst improves HDO selectivity by decreasing the binding energy of o-cresol and other organic reagents to the catalyst surface by disrupting the Ni ensembles. Evidence to support this speculation is that addition of Cu to a Pd catalyst decreased the binding energy of furfural to the catalyst surface [18]. These authors suspected that the decrease in binding energy was caused by a shift in the d-band center of the PdCu alloy toward the Fermi level when compared with Pd,

as explained by Lopez and Norskov [22]. A complementary alternate explanation for the addition of Cu reducing the gasification activity is that the Cu might preferentially bind to the under-coordinated Ni sites where the adsorption energy is the greatest. Thus addition of Cu would remove these active sites and lower the gasification activity of the catalyst [23].

6.5.2. Raney NiCu characterization

The XRD patterns of the fresh and used Raney NiCu are shown in fig. 6.7. Much like the Raney Ni catalyst, the Raney NiCu catalyst shows little change in the diffraction pattern between the fresh and used samples. The one major change is the appearance of Al_2O_3 peaks in the used sample for the same reasons mentioned in section 6.4.2. Also, it is important to note that there are no peaks for metallic copper or nickel copper alloys. The absence of these peaks indicates that the copper added to the Raney Ni has not been incorporated into the bulk of the catalyst. These findings are consistent with the formation of a near surface alloy of Ni and Cu, as was observed with Raney NiSn catalysts prepared in a similar manner [16].

Table 6.3 indicates that the Ni particle sizes on the Raney NiCu catalyst have not increased post reaction, as was seen in the Raney Ni catalyst. This outcome suggests that the catalyst is more resistant to sintering under the conditions tested than either one of the previous Ni catalysts. The composition data, shown in Table 6.3, indicates that this catalyst loses Al, and that 7.4 ± 1.6 wt% copper was deposited on the Raney Ni during synthesis. The used catalyst contained 7.9 ± 0.5 wt% Cu, indicating no change in Cu composition, and suggests that the Cu is resistant to leaching.

6.6. Summary and Conclusions

Table 6.4: The active metal area and turnover frequency (TOF) for each catalyst tested based on the initial rate of deoxygenation.

Catalyst	k'_{HDO} (L/g_{cat} min) x 10^3	w (g_{cat})	Area (m^2)	TOF (mol/m^2 min) x 10^5
Pt/C	20	0.014	0.89	1.40
$Ni/SiO_2Al_2O_3$	0.81	0.399	71	0.02
Raney Ni*	1.1	0.296	9.5	0.15
Raney NiCu	0.77	0.314	8.5	0.13

*Based on W/F = 12 min reaction

Table 6.4 shows the turnover frequency (TOF) for all of the catalysts tested. We assumed that the metal particles were spherical with diameters equivalent to the particle sizes listed for the fresh catalysts in table 6.3. Table 6.4 shows that the Pt/C catalyst had the highest TOF of all of the catalyst tested. The TOF of the Raney Ni and Raney NiCu catalyst were approximately an order of magnitude smaller than the Pt/C. The slight drop in TOF from the Raney Ni to the Raney NiCu catalyst was expected, as the purpose of Cu was to selectively suppress gasification activity of the catalyst, which, unsurprisingly, also decreased the overall HDO activity.

The yield of deoxygenated products and conversion with respect to W/F for each of the catalysts tested herein are shown in fig. 6.9. In general, catalysts with high yields of deoxygenated products and high conversion at a low W/F are desired. This figure shows that of the catalysts tested, Pt/C provides the highest yield of deoxygenated products and a high conversion at the lowest W/F tested. We suspect that increasing W/F for the Pt/C-catalyzed reaction with o-cresol would increase the yield of deoxygenated products and conversion to near 100%, as batch studies have reported higher yields and conversion [3, 24, 25]. The $Ni/SiO_2Al_2O_3$ catalyst had a moderate yield of deoxygenated products and a

moderate conversion initially, but both of these values dropped significantly over the course of the reaction due to support degradation and sintering. The Raney Ni catalyst, which was tested at various W/F, was active for gasification but unable to produce a high yield of deoxygenated products. The addition of Cu to the Raney Ni catalyst decreased the gasification activity and increased the yield of liquid phase deoxygenated products to 3.4 times the value achieved with Raney Ni. The Raney NiCu catalyst represents a significant improvement over the other Ni catalysts tested because it produced a stable yield of deoxygenated products and had limited gasification activity. This finding is significant because it provides an avenue for reducing the cost of stable and active HDO catalysts for hydrothermal deoxygenation of bio-oils, as Ni is ~3000 times less expensive than Pt.

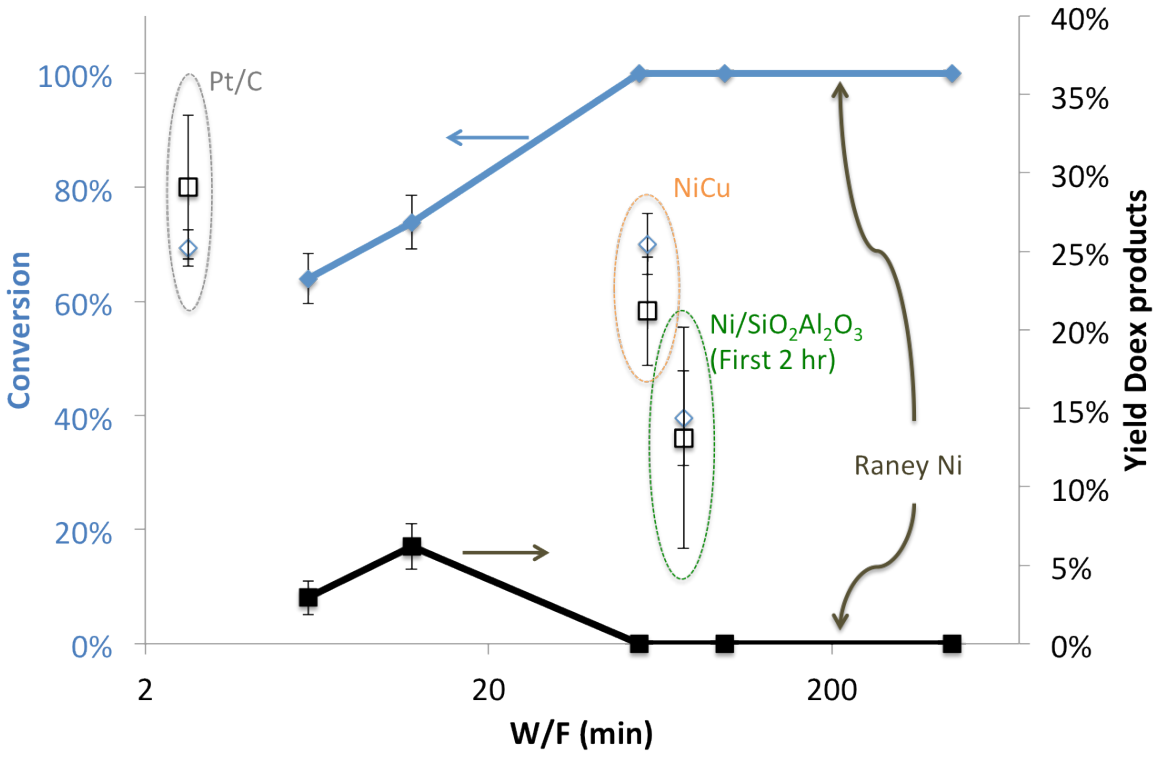

Figure 6.9. Comparison of conversions and yields of deoxygenated products from all catalysts tested. (T = 380 °C, P = 305 bar, feed solution (ambient conditions): 24.7 g/L o-cresol, 147 mL/L formic acid, balance DI H_2O).

Appendix B. Supplementary data

Table B.1a. Gas product compositions from reacting o-cresol over Pt/C.

Gas products															
Time on stream (min)	89	172	232	270	323	380	456	520	970	1022	1075	1135	1186	1340	1408
Molecule	**Mol %**	**Mol %**	**Mol %**	**Mol %**	**Mol %**	**Mol %**	**Mol %**	**Mol %**	**Mol %**	**Mol %**	**Mol %**	**Mol %**	**Mol %**	**Mol %**	**Mol %**
H_2	26.3	25.4	71.6	27.1	30.4	25.8	24.4	41.5	27.6	30.7	36.1	25.6	28.5	29.1	26.2
CO	0.6	0.6	1.1	0.6	0.6	0.6	0.6	0.8	0.6	0.7	0.7	0.6	0.6	0.6	0.6
CH_4	0.1	0.1	0.1	0.1	0.1	0.1	0.1	0.2	0.2	0.2	0.2	0.2	0.1	0.1	0.1
CO_2	73.0	73.9	27.1	72.2	68.9	73.5	74.9	57.5	71.6	68.4	63.0	73.6	70.8	70.2	73.1
C_2H_6	0.0	0.0	0.0	0.0	0.0	0.0	0.0	0.0	0.0	0.0	0.0	0.0	0.0	0.0	0.0

Table B.1b. Liquid product yields from reacting o-cresol over Pt/C.

	Liquid products																													
Time on stream (min)	0	28	56	88	137	178	211	241	272	301	347	434	459	485	904	936	964	1006	1043	1082	1164	1215	1252	1285	1315	1347	1373
Molecule	**Yield**	**Yield**	**Yield**	**Yield**	**Yield**	**Yield**	**Yield**	**Yield**	**Yield**	**Yield**	**Yield**	**Yield**	**Yield**	**Yield**	**Yield**	**Yield**	**Yield**	**Yield**	**Yield**	**Yield**	**Yield**	**Yield**	**Yield**	**Yield**	**Yield**	**Yield**	**Yield**
Benzene	0.0%	0.0%	0.0%	0.0%	0.0%	0.0%	0.0%	0.0%	0.0%	0.0%	0.0%	0.0%	0.0%	0.0%	0.0%	0.0%	0.0%	0.0%	0.0%	0.0%	0.0%	0.0%	0.0%	0.0%	0.0%	0.0%	0.0%
Methylcyclohexane	17.8%	20.4%	20.2%	19.2%	20.8%	19.5%	23.0%	19.6%	20.5%	19.6%	19.1%	21.1%	20.6%	19.9%	25.7%	23.8%	25.3%	25.2%	28.1%	26.8%	28.6%	25.9%	27.6%	24.1%	28.7%	28.3%	27.2%
Ethylcyclopentane	0.0%	0.0%	0.0%	0.0%	0.0%	0.0%	0.0%	0.0%	0.0%	0.0%	0.0%	0.0%	0.0%	0.0%	0.0%	0.0%	0.0%	0.0%	0.0%	0.0%	0.0%	0.0%	0.0%	0.0%	0.0%	0.0%	0.0%
Toluene	4.8%	5.3%	5.1%	4.9%	5.0%	4.7%	5.5%	4.7%	5.0%	4.8%	4.9%	5.0%	5.0%	4.9%	6.5%	6.3%	6.7%	6.6%	7.5%	7.2%	7.5%	6.8%	7.1%	6.6%	7.4%	7.4%	7.3%
Methylcyclohexene	0.0%	0.0%	0.0%	0.0%	0.0%	0.0%	0.0%	0.0%	0.0%	0.0%	0.0%	0.0%	0.0%	0.0%	0.0%	0.0%	0.0%	0.0%	0.0%	0.0%	0.0%	0.0%	0.0%	0.0%	0.0%	0.0%	0.0%
Cyclohexanone	0.0%	0.0%	0.0%	0.0%	0.0%	0.0%	0.0%	0.0%	0.0%	0.0%	0.0%	0.0%	0.0%	0.0%	0.0%	0.0%	0.0%	0.0%	0.0%	0.0%	0.0%	0.0%	0.0%	0.0%	0.0%	0.0%	0.0%
cis-2-methylcyclohexanol	5.5%	5.3%	5.5%	5.7%	6.2%	6.1%	6.9%	7.1%	7.0%	7.1%	7.4%	7.2%	6.9%	6.7%	5.6%	5.6%	5.6%	5.6%	5.6%	5.8%	5.4%	5.3%	5.6%	5.5%	5.6%	5.5%	5.5%
trans-2-methylcyclohexanol	2.4%	2.2%	2.3%	2.3%	2.5%	2.4%	2.7%	2.7%	2.3%	2.2%	2.6%	2.2%	2.1%	2.0%	1.4%	1.4%	1.4%	1.4%	1.5%	2.0%	1.5%	1.7%	1.9%	1.9%	2.0%	1.8%	1.8%
Methylcyclohexanone	19.8%	23.7%	22.7%	19.0%	22.9%	15.9%	16.0%	22.2%	16.4%	17.6%	22.4%	20.8%	20.5%	16.3%	13.1%	13.8%	12.4%	16.4%	12.2%	15.4%	11.5%	11.2%	15.4%	11.2%	10.8%	10.7%	10.3%
Phenol	----	----	----	----	----	----	----	----	----	----	----	----	----	----	----	----	----	----	----	----	----	----	----	----	----	----	----
o-cresol	39.0%	34.1%	33.7%	34.2%	33.6%	31.0%	31.8%	33.1%	33.2%	32.5%	32.4%	30.9%	29.6%	29.0%	28.5%	28.7%	29.5%	29.7%	29.2%	29.5%	27.8%	26.3%	27.2%	27.1%	27.8%	26.7%	26.8%

Table B.2a. Gas product compositions and yields from reacting o-cresol over $Ni/SiO_2Al_2O_3$.

Time on stream (min)	Gas Products																							
Molecule	16	73	114	150	190	242	422	791	851	937	16	73	114	150	190	242	422	791	851	937				
	Mol %	Mol %	Mol %	Mol %	Mol %	Mol %	Mol %	Mol %	Mol %	Mol %	Yield[1]	Yield[1]	Yield[1]	Yield[1]	Yield[1]	Yield[1]	Yield[1]	Yield[1]	Yield[1]	Yield[1]				
H_2	22.7	27.9	30.5	28.9	78.1	32.3	31.4	56.5	42.2	32.3	------	------	------	------	------	------	------	------	------	------				
CO	0.0	0.0	0.9	1.3	3.2	0.0	0.4	2.1	1.1	0.4	------	------	------	------	------	------	------	------	------	------				
CH_4	12.4	7.6	5.6	4.2	5.2	3.4	1.1	0.7	0.6	0.5	25.4%	17.8%	11.9%	6.6%	4.7%	7.7%	1.7%	9.6%	1.5%	1.0%				
CO_2	64.8	64.5	63.0	65.6	13.6	64.3	67.0	40.6	56.2	66.7	------	------	------	------	------	------	------	------	------	------				
C_2H_6	0	0	0	0	0	0	0	0	0	0	0	0	0	0	0	0	0	0	0	0				

[1] CH_4 and C_2H_6 are assumed to be produced from o-cresol. CO_2 and CO are assumed to be produced from formic acid.

Table B.2b. Liquid product yields from reacting o-cresol over $Ni/SiO_2Al_2O_3$.

	Liquid Products												
Time on stream (min)	0	31	61	91	121	211	242	410	781	813	850	893	937
Molecule	**Yield**	**Yield**	**Yield**	**Yield**	**Yield**	**Yield**	**Yield**	**Yield**	**Yield**	**Yield**	**Yield**	**Yield**	**Yield**
Benzene	1.9%	0.0%	0.0%	0.0%	0.0%	0.0%	0.0%	0.0%	0.0%	0.0%	0.0%	0.0%	0.0%
Methylcyclohexane	15.2%	10.0%	8.0%	7.3%	7.5%	9.7%	2.7%	1.9%	0.0%	1.4%	1.0%	0.0%	0.0%
Ethylcyclopentane	1.6%	0.0%	0.0%	0.0%	0.0%	3.6%	0.0%	0.0%	0.0%	0.0%	0.0%	0.0%	0.0%
Toluene	6.5%	3.3%	2.2%	2.1%	0.0%	0.0%	0.0%	0.0%	0.0%	0.0%	0.0%	0.0%	0.0%
Methylcyclohexene	0.0%	0.0%	0.0%	0.0%	0.0%	0.0%	0.0%	0.0%	0.0%	0.0%	0.0%	0.0%	0.0%
Cyclohexanone	0.0%	0.0%	0.0%	0.0%	0.0%	0.0%	0.0%	0.0%	0.0%	0.0%	0.0%	0.0%	0.0%
cis-2-methylcyclohexanol	0.0%	0.0%	0.0%	0.0%	0.0%	0.0%	0.0%	0.0%	0.0%	0.0%	0.0%	0.0%	0.0%
trans-2-methylcyclohexanol	3.5%	2.2%	2.3%	1.6%	1.2%	1.6%	1.7%	2.5%	1.6%	0.0%	0.5%	0.0%	0.0%
Methylcyclohexanone	0.0%	0.0%	0.0%	0.0%	0.0%	0.0%	0.0%	0.0%	0.0%	0.0%	0.0%	0.0%	0.0%
Phenol	0.9%	0.0%	0.0%	0.0%	0.0%	1.0%	0.0%	0.0%	0.0%	0.0%	0.0%	0.0%	0.0%
o-cresol	65.6%	55.3%	61.3%	70.6%	49.7%	84.8%	67.7%	83.0%	90.0%	52.3%	64.2%	83.5%	54.5%

Table B.3a. Gas product compositions from reacting o-cresol over Raney Ni at W/F = 447 min.

	Gas Analysis (Rxn 1)[1]										
Time on stream (min)	74	231	301	353	459	498	1300	626	663	1088	1133
	W/F = 447 min										
Molecule	**Mol %**	**Mol %**	**Mol %**	**Mol %**	**Mol %**	**Mol %**	**Mol %**	**Mol %**	**Mol %**	**Mol %**	**Mol %**
H_2	7.0	1.9	1.8	1.7	1.8	1.7	1.7	1.7	1.8	1.6	1.7
CO	0.0	0.0	0.0	0.0	0.0	0.0	0.0	0.0	0.0	0.0	0.0
CH_4	35.1	34.0	34.2	34.1	34.9	34.3	34.2	34.2	34.2	34.2	34.4
CO_2	57.7	64.1	64.0	64.1	63.3	64.0	64.1	64.1	64.0	64.1	64.0
C_2H_6	0.0	0.0	0.0	0.0	0.0	0.0	0.0	0.0	0.0	0.0	0.0

[1] No liquid product were detected at W/F = 447 or 98 min. Gas analysis was not taken for the W/F = 98 min. For the W/F = 447 reaction liquid samples were taken for 1400 min, but no molecules were detected.

Table B.3b. Gas product compositions from reacting o-cresol over Raney Ni at W/F = 55, 12, and 6 min.

	Gas products (Rxn 2)									
Time on stream (min)	19	78	258	296	260	312	184	976	1308	1344
	W/F = 55 min							W/F = 12 min	W/F = 6 min	
Molecule	**Mol %**	**Mol %**	**Mol %**	**Mol %**	**Mol %**	**Mol %**	**Mol %**	**Mol %**	**Mol %**	**Mol %**
H_2	8.0%	3.2%	2.1%	2.3%	2.2%	2.1%	2.0%	5.8%	7.4%	9.3%
CO	0.0%	0.0%	0.0%	0.0%	0.0%	0.0%	0.0%	0.0%	0.0%	0.0%
CH_4	27.0%	30.6%	32.5%	32.4%	32.8%	32.8%	32.7%	24.8%	24.3%	21.5%
CO_2	65.1%	66.1%	65.4%	65.3%	65.0%	65.0%	65.3%	69.5%	68.3%	69.2%
C_2H_6	0.1%	0.2%	0.1%	0.2%	0.2%	0.2%	0.2%	0.1%	0.2%	0.1%

Table B.3c. Liquid product yields from reacting o-cresol over Raney Ni at W/F = 55, 12, and 6 min.

Liquid products (Rxn 2)[2]									
Time on stream (min)	1209	1271	1304	1334	1355	1753	1764	1776	1803
	W/F = 12 min				**W/F = 6 min**				
Molecule	**Yield**	**Yield**	**Yield**	**Yield**	**Yield**	**Yield**	**Yield**	**Yield**	**Yield**
Benzene	5.4%	4.0%	5.7%	3.3%	3.8%	3.2%	2.6%	2.1%	1.8%
Methylcyclohexane	0.0%	0.0%	0.0%	0.0%	0.0%	0.0%	0.0%	0.0%	0.0%
Ethylcyclopentane	0.0%	0.0%	0.0%	0.0%	0.0%	0.0%	0.0%	0.0%	0.0%
Toluene	1.6%	1.4%	2.1%	1.3%	0.0%	1.1%	0.0%	0.0%	0.0%
Methylcyclohexene	0.0%	0.0%	0.0%	0.0%	0.0%	0.0%	0.0%	0.0%	0.0%
Cyclohexanone	3.0%	3.0%	3.1%	3.1%	3.9%	3.7%	3.4%	3.2%	3.0%
cis-2-methylcyclohexanol	0.0%	0.0%	0.0%	0.0%	0.0%	0.0%	0.0%	0.0%	0.0%
trans-2-methylcyclohexanol	0.0%	0.0%	0.0%	0.0%	0.0%	0.0%	0.0%	0.0%	0.0%
Methylcyclohexanone	2.7%	3.1%	4.3%	3.7%	3.3%	4.8%	5.0%	5.3%	5.2%
Phenol	31.6%	32.4%	23.5%	30.2%	35.5%	26.2%	22.8%	20.1%	18.7%
o-cresol	20.9%	26.7%	24.8%	32.2%	30.2%	33.3%	36.2%	39.9%	40.6%

[2] No liquid product observed at a W/F = 55 min.

Table B.4a. Gas product compositions from reacting o-cresol over Raney NiCu.

Gas Products														
Time on stream (min)	17	133	183	240	307	350	397	450	873	925	1023	1118	1225	1375
Molecule	**Mol %**	**Mol %**	**Mol %**	**Mol %**	**Mol %**	**Mol %**	**Mol %**	**Mol %**	**Mol %**	**Mol %**	**Mol %**	**Mol %**	**Mol %**	**Mol %**
H_2	18.2	12.9	11.2	13.9	8.9	10.2	11.4	11.5	19.6	20.3	22.0	23.2	22.0	12.2
CO	0.0	0.0	0.0	0.0	0.0	0.0	0.0	0.0	0.0	0.3	0.0	0.0	0.0	0.0
CH_4	16.4	21.8	19.8	19.2	15.7	18.2	17.9	17.3	12.6	12.5	12.2	11.4	11.9	10.9
CO_2	65.4	65.2	69.0	66.9	75.3	71.6	70.8	71.2	67.7	66.9	65.8	65.4	66.1	77.0
C_2H_6	0.0	0.0	0.0	0.0	0.0	0.0	0.0	0.0	0.0	0.0	0.0	0.0	0.0	0.0

Table B.4b. Liquid product yields from reacting o-cresol over Raney NiCu.

Liquid Products																							
Time on stream (min)	0	31	71	102	176	219	257	289	321	742	780	828	883	918	984	1019	1045	1106	1396
Molecule	**Yield**	**Yield**	**Yield**	**Yield**	**Yield**	**Yield**	**Yield**	**Yield**	**Yield**	**Yield**	**Yield**	**Yield**	**Yield**	**Yield**	**Yield**	**Yield**	**Yield**	**Yield**	**Yield**
Benzene	5.2%	3.2%	2.3%	2.3%	0.0%	0.0%	0.0%	0.0%	0.0%	0.0%	0.0%	0.0%	0.0%	0.0%	0.0%	0.0%	0.0%	0.0%	0.0%
Methylcyclohexane	8.5%	6.9%	6.4%	7.3%	5.7%	9.3%	9.7%	9.4%	9.7%	11.5%	12.1%	11.2%	11.7%	11.6%	9.6%	9.2%	9.9%	9.9%	9.1%
Ethylcyclopentane	1.4%	1.1%	0.0%	1.2%	0.0%	1.3%	1.3%	1.3%	1.3%	1.3%	1.4%	1.3%	1.4%	1.3%	0.0%	1.1%	0.0%	0.0%	0.0%
Toluene	11.5%	8.4%	8.2%	8.4%	6.7%	9.5%	9.9%	9.6%	9.9%	8.1%	8.6%	7.9%	8.3%	8.0%	6.5%	6.4%	7.1%	6.7%	6.2%
Methylcyclohexene	0.0%	0.0%	0.0%	0.0%	0.0%	0.0%	0.0%	0.0%	0.0%	3.3%	3.6%	3.8%	4.2%	4.4%	3.9%	3.5%	3.7%	3.9%	4.0%
Cyclohexanone	2.5%	2.1%	2.6%	2.1%	2.4%	2.0%	2.2%	2.0%	2.0%	1.0%	1.1%	1.1%	1.2%	1.2%	1.1%	1.1%	1.3%	1.1%	1.3%
cis-2-methylcyclohexanol	0.0%	0.5%	1.0%	1.0%	2.3%	2.6%	2.8%	3.0%	3.3%	4.8%	5.7%	5.0%	6.0%	5.9%	5.5%	5.2%	6.2%	5.9%	7.4%
trans-2-methylcyclohexanol	0.0%	0.0%	0.0%	0.0%	0.0%	0.7%	0.9%	0.9%	1.0%	1.0%	1.2%	0.9%	1.1%	1.0%	1.1%	1.1%	1.3%	1.3%	1.7%
Methylcyclohexanone	4.2%	3.7%	5.4%	5.9%	11.8%	13.7%	14.4%	14.4%	16.3%	17.1%	19.8%	18.3%	21.2%	20.7%	17.9%	17.0%	20.6%	18.6%	20.7%
Phenol	17.7%	14.8%	16.1%	9.9%	6.8%	6.6%	4.9%	4.5%	3.8%	0.7%	0.7%	0.7%	0.7%	0.7%	0.8%	0.7%	0.8%	0.7%	0.9%
o-cresol	18.9%	18.7%	26.3%	21.9%	34.3%	29.4%	31.0%	30.2%	32.0%	29.8%	34.0%	31.0%	36.4%	36.8%	30.7%	28.4%	32.9%	30.5%	36.7%

References

1. P. Duan, P. E. Savage, Ind. Eng. Chem. Res. 50, (2011) 52-61.
2. L. H. Baekeland, Ind. Eng. Chem. Res. 1, (1909) 149-161.
3. J. G. Dickinson, J. T. Poberezny, P. E. Savage, Appl. Catal. B: Environ. 123-124, (2012) 357-366.
4. E. O. Odebunmi, D. F. Ollis, J. Catal. 80, (1983) 56-64.
5. L. C. Grabow, A. A. Gokhale, S. T. Evans, J. A. Dumesic, M. Mavrikakis, The Journal of Physical Chemistry C 112, (2008) 4608-4617.
6. J. Fu, X. Lu, P. E. Savage, Energy Environ. Sci. 3, (2010) 311-317.
7. H. S. Fogler, Elements of Chemical Reactor Engineering, Prentice Hall, Westford, MA, 2006.
8. T. P. Vispute, H. Zhang, A. Sanna, R. Xiao, G. W. Huber, Science 330, (2010) 1222-1227.
9. D. C. Elliott, T. R. Hart, G. G. Neuenschwander, Ind. Eng. Chem. Res. 45, (2006) 3776-3781.
10. Z. Zhang, Y. Han, F.-S. Xiao, S. Qiu, L. Zhu, R. Wang, Y. Yu, Z. Zhang, B. Zou, Y. Wang, J. Am. Chem. Soc. 123, (2001) 5014-5021.
11. R. M. Ravenelle, J. R. Copeland, W.-G. Kim, J. C. Crittenden, C. Sievers, ACS Catal. 1, (2011) 552-561.
12. D. C. Elliott, L. J. Sealock Jr, E. G. Baker, Ind. Eng. Chem. Res. 32, (1993) 1542-1548.
13. J. Yu, P. E. Savage, Appl. Catal. B: Environ. 31, (2001) 123-132.
14. R. M. Ravenelle, F. Schüβler, A. D'Amico, N. Danilina, J. A. van Bokhoven, J. A. Lercher, C. W. Jones, C. Sievers, The Journal of Physical Chemistry C 114, (2010) 19582-19595.
15. J. W. Shabaker, G. W. Huber, J. A. Dumesic, J. Catal. 222, (2004) 180-191.
16. J. W. Shabaker, D. A. Simonetti, R. D. Cortright, J. A. Dumesic, J. Catal. 231, (2005) 67-76.
17. S. Robertson, J. Freel, R. B. Anderson, J. Catal. 24, (1972) 130-145.
18. S. Sitthisa, T. Pham, T. Prasomsri, T. Sooknoi, R. G. Mallinson, D. E. Resasco, J. Catal. 280, (2011) 17-27.
19. G. W. Huber, J. W. Shabaker, J. A. Dumesic, Science 300, (2003) 2075.
20. D. A. Morgenstern, J. P. Fornango, Energy Fuels 19, (2005) 1708-1716.
21. E. Nikolla, J. Schwank, S. Linic, J. Catal. 263, (2009) 220-227.
22. N. Lopez, J. K. Nørskov, Surf. Sci. 477, (2001) 59-75.
23. R. T. Vang, K. Honkala, S. Dahl, E. K. Vestergaard, J. Schnadt, E. Lægsgaard, B. S. Clausen, J. K. Nørskov, F. Besenbacher, Nature materials 4, (2005) 160-162.
24. C. Zhao, Y. Kou, A. A. Lemonidou, X. Li, J. A. Lercher, Angew. Chem. 121, (2009) 4047-4050.
25. C. Zhao, J. He, A. A. Lemonidou, X. Li, J. A. Lercher, J. Catal. 280, (2011) 8-16.

Chapter 7

Development of NiCu Catalysts for Aqueous-Phase Hydrodeoxygenation

To address the need to develop active and stable non-noble metal catalysts for hydrothermal HDO, we examined, in chapter 6, a Raney Ni catalyst doped with 10 wt% Cu and found the catalyst to be active, selective, and stable for hydrothermal HDO at 380 °C [1]. Cu was chosen as a dopant because the base Raney Ni catalyst was active for C-C bond hydrogenolysis, producing primarily methane from the o-cresol fed to the reactor, and because Elliot et al. showed that Cu was inactive for gasification [2]. We associated this increase in selectivity to liquid phase products to the fact that, in a different catalyst system, Cu reduces the adsorption energy of aromatic molecules when alloyed with Pd to make a PdCu catalyst [3]. This chapter expands on this previous work to examine the effect of Cu content on the products, selectivities, and yields from reacting o-cresol, a model oxygen-containing compound found in most bio-oils [4, 5], with H_2 over various catalysts. This work shows that increasing Cu content drastically reduces the gasification activity of the Raney NiCu catalysts, but is ineffective at increasing the yield of the desired liquid hydrocarbons. To increase the liquid hydrocarbon yield, we added Al_2O_3 to the catalysts through two parallel approaches. One approach was to synthesize a $NiCu/Al_2O_3$ catalyst and the second was to calcine the Raney Ni catalyst thereby oxidizing the Al in the Raney Ni catalyst to Al_2O_3. With these catalyst modifications, we provide, to the best of our

knowledge, the first report of a high (≥ 60 %) and stable liquid hydrocarbon yield by using only a non-noble metal catalyst for HDO in hydrothermal conditions.

This chapter is divided into two major parts. The first section examines the effect of Cu loading on product yields and selectivities for the hydrothermal HDO of o-cresol. The second section discusses improvements to the NiCu catalysts made through the addition of acid sites. Within each major section, we first discuss reaction results and then examine the findings of the catalyst characterization.

7.1 Raney NiCu catalysts and the effect of Cu loading

Previous work [1] indicates that Raney Ni 2800 promoted with 10 wt% Cu is an active and stable catalyst for hydrothermal HDO. The goal of this section is to examine the effect of Cu loading and to develop a catalyst and reaction scheme for hydrothermal HDO that produces high liquid hydrocarbon yield. To achieve this goal, the catalyst must not only be active, it must also be selective for C-O bond hydrogenolysis.

7.1.1 2% Raney NiCu

Previous work [1] showed that a 10% Raney NiCu catalyst had a lower HDO turn over frequency (TOF) than did unmodified Raney Ni. Further, the total activity (i.e., TOF for conversion) of the 10% Raney NiCu catalyst is even more suppressed when compared with the unmodified Raney Ni catalyst. We desired to learn whether reducing the Cu content would improve overall and HDO activity without diminishing the selectivity increases, and therefore the higher liquid hydrocarbon yield, observed with the 10% Raney NiCu catalyst.

Therefore, we synthesized a 2% Raney NiCu catalyst and tested this catalyst in the flow system described previously [1] at 380 °C using formic acid decomposition as the H_2 source.

Fig. 7.1 shows the variation of conversion and liquid hydrocarbon yield with time on stream (TOS). The most abundant liquid hydrocarbon products were toluene, methylcyclohexane, benzene and cyclohexane. In addition to these products, oxygenated products consisting primarily of methylcyclohexanone and phenol formed. Methane and CO_2 were the only gaseous products, but due to the presence of formic acid in the reactor feed, it is unclear whether these carbon-containing molecules originate from the formic acid or o-cresol.

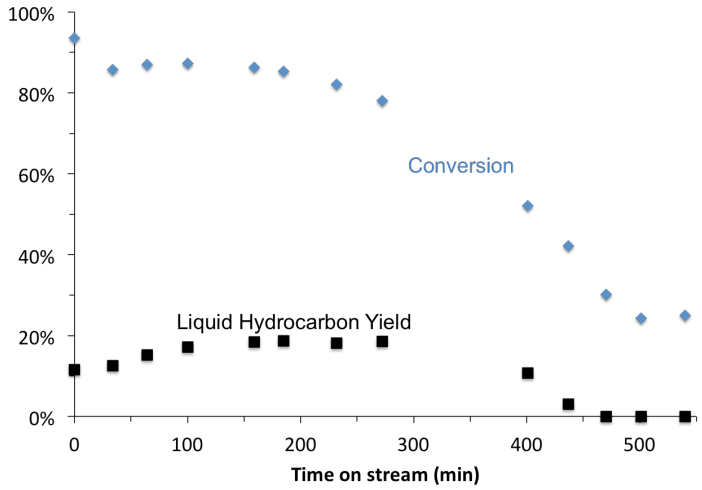

Figure 7.1. Conversion and liquid hydrocarbon yield from reacting o-cresol over 2% Raney NiCu (W/F = 56 min, 380 °C, 305 bar, feed solution (ambient conditions): 24.7 g/L o-cresol, 147 mL/L formic acid, balance DI H_2O, feed flow rate (ambient temperature) = 0.218 mL/min, 430 °C in situ H_2 catalyst reduction).

Fig. 7.1 shows that the maximum liquid hydrocarbon yield of 19% occurred around 200 min on stream. This maximum liquid hydrocarbon yield is similar to the 21 ± 4% average liquid hydrocarbon yield obtained previously from a 10% Raney NiCu catalyst using the same reaction conditions [1]. After reaching this maximum, the liquid

hydrocarbon yield quickly declined to 0% at 470 min on stream and thereafter. Likewise, conversion decreased rapidly after 200 min on stream. It is clear that the 2% Raney NiCu catalyst deactivates rapidly after about 240 min on stream.

The cause of the deactivation is unknown, and is beyond the primary focus of this work. We did perform several simple experiments, however, that permit speculation regarding the cause of deactivation. We previously reported that CO is in the reaction stream that contacts the catalyst bed. Fig. 7.2 shows the results from CO TPD of the unmodified Raney Ni catalyst and the 10% Raney NiCu catalyst used previously [1]. These results will be discussed more thoroughly in a later section. At present, we will simply remark that CO remained adsorbed to both the Raney Ni and 10% Raney NiCu catalysts at temperatures approaching 600 °C. This finding is important because it points to a possible cause of catalyst deactivation, CO poisoning, and a possible means of regenerating the catalyst, reduction of the catalyst at high temperature (e.g., 550 °C) in flowing H_2. Literature also indicates that CO_2, when reacted over a Ni catalyst, can form adsorbed CO [6]. The preferential pathway for the removal of adsorbed CO when H_2 is present is through a HCO or COH pathway that converts bound CO to methane [7].

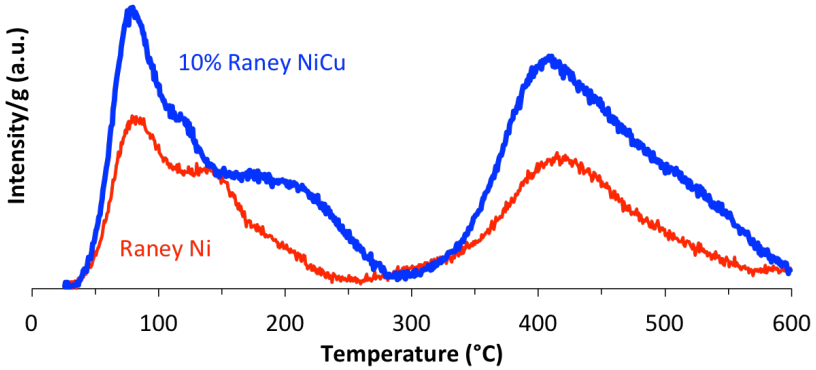

Figure 7.2. CO temperature programmed desorption spectra of Raney Ni and 10% Raney NiCu.

Fig. 7.3 shows the liquid hydrocarbon yield from three cycles of reacting o-cresol over the same 2% Raney NiCu catalyst that was used in fig. 7.1 (table C.1, supplementary information). Each cycle consisted of reducing the catalyst at 550 °C in flowing H_2, then passing the feed solution over the catalyst for 720 min. It is clear from fig. 7.3 that the liquid hydrocarbon yields for each cycle overlap, indicating that the HDO activity of the catalyst was regenerated after each cycle by simply re-reducing the catalyst. This result is consistent with CO poisoning causing the loss in catalyst activity, but it does not preclude other methods of deactivation. The catalyst could be losing activity from oxidation of the Ni metal by supercritical water, or from some other unknown catalyst poison. Other common deactivation causes such as sintering or coking are unlikely, because these conditions are irreversible by reduction.

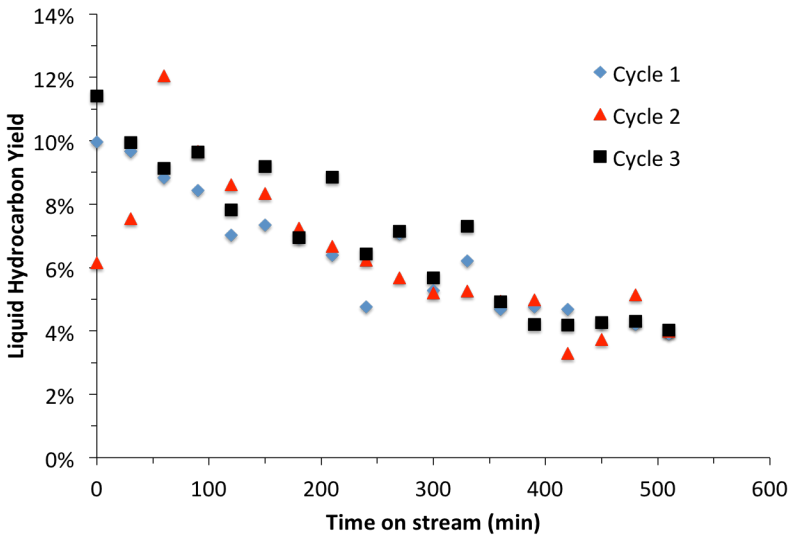

Figure 7.3. Liquid hydrocarbon yield from reacting o-cresol over 2% Raney NiCu (W/F = 80 min, 380 °C, 305 bar, feed solution (ambient conditions): 24.7 g/L o-cresol, 147 mL/L formic acid, balance DI H_2O, feed flow rate (ambient temperature) = 0.200 mL/min, 550 °C in situ H_2 catalyst reduction between runs).

7.1.2 Cu loading effects

This section elucidates the effect of Cu loading on the HDO selectivity of 1-40% Raney NiCu catalysts using H_2 (rather than formic acid) as the reductant to avoid the formation of CO. We performed these reactions in 4.1 mL batch mini-reactors to rapidly screen these catalysts.

Fig. 7.4 and table C.2 shows that at low Cu loading (e.g. 1 - 7%) the conversion of o-cresol was nearly 100%, and the selectivity to gas products, such as methane (55 - 68% yield), ethane (~1% yield), and CO_2 (15 – 30% yield), was high. Selectivity to liquid products was low. The liquid products were mainly oxygenated intermediates such as phenol (1.4 – 8.3% yield), cyclohexanone (0-2.7% yield), methylcyclohexanone (0.4-2.4% yield), and methylcyclohexanol (0 – 2.4% yield).

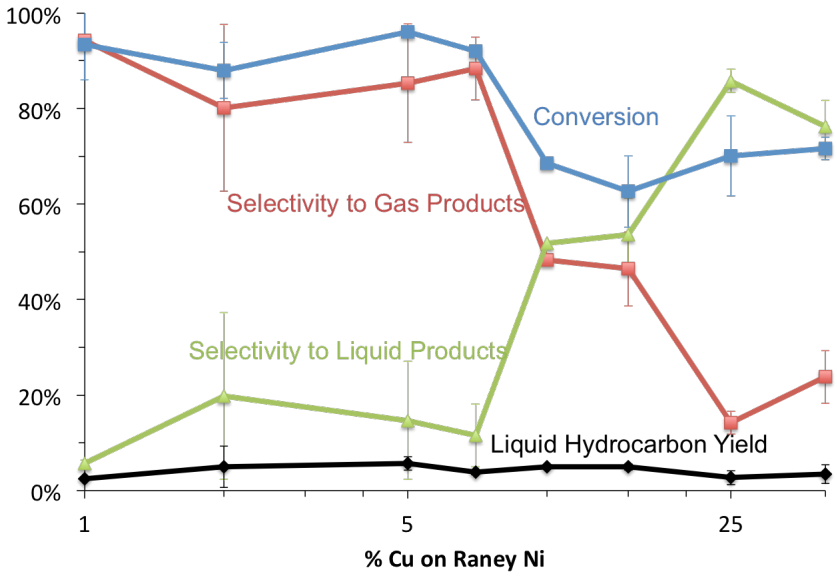

Figure 7.4. Effect of Cu loading for Raney NiCu catalysts on selectivity, conversion, and liquid hydrocarbon yield in 4.1 mL reactors (380 °C, 30 min, 20 mg catalyst, 20 mg of o-cresol, 0.67 mL DI H_2O, 19 bar H_2 (STP), w×t/m = 30 min, 17:1 H_2 to o-cresol).

There is a dramatic shift in product selectivities and conversion when the Cu content of the Raney NiCu catalyst increased beyond 7% Cu. Fig. 7.4 shows that the conversion of o-cresol drops beyond 7% Cu loading and remains relatively steady at ~70%. Also between 7 and 25% Cu, the product selectivities shift from forming gas to forming liquid products. Again, methane and CO_2 were the main gasses while the aforementioned oxygenated intermediate molecules were present in high yields (table C.2).

These results support the conclusion that Cu decreases the hydrocracking (C-C bond hydrogenolysis with H_2) activity of the catalyst. It is likely, on the low Cu loaded catalysts, that cyclohexanol, after forming from the hydrogenation of cyclohexanone, continues to react to form methane. This hypothesis is supported by literature showing that Ni is a more active hydrogenation and hydrocracking metal than Cu [2]. The lower overall activity of the high Cu loaded catalysts manifests in the decreased conversion observed. In contrast to the

conversion and liquid and gas product selectivities in fig. 7.4, the liquid hydrocarbon yield varied little as the Cu content of the catalysts is varied. The liquid hydrocarbon yield varied only from a low of 2.5 ± 0.2% for the 1% Raney NiCu catalyst to 5.6 ± 1.4% for the 5% Raney NiCu catalyst.

The goal of this work was to produce a non-noble metal catalyst that is active, selective, and stable for hydrothermal HDO because such a catalyst would result in high liquid hydrocarbon yield, while minimizing the formation of lower value gas products. The results above indicate that Cu doping the Raney Ni catalyst is itself, insufficient to achieve this goal because the addition of Cu results only in minimizing unwanted gas products and not in increasing the yield of the desired liquid hydrocarbon products.

7.1.3 Raney NiCu catalyst characterization

The reaction results presented in section 7.1.2 indicate that the addition of Cu to a Raney Ni catalyst has a dramatic effect on the product selectivities when o-cresol is reacted at 380 °C in supercritical water. This section elucidates the morphology of the Raney NiCu catalysts by discussing the results from titration, diffraction, and microscopy experiments used to characterize the catalysts.

Fig. 7.2 shows the results of CO TPD of both the unmodified Raney Ni and 10% Raney NiCu catalysts. Both spectra contain two major peaks at 75 and 405 °C. The Raney Ni spectrum contains one shoulder between 105 and 140 °C, while the Raney NiCu spectrum contains two shoulders, one between 105 and 115 °C, and the other, broader shoulder, between 145 and 210 °C. This second broad shoulder is an entirely new feature in the 10% Raney NiCu spectrum that was not observed in the Raney Ni spectrum. Both spectra were

integrated, and the 10% Raney NiCu catalyst adsorbed 1.7 times the CO of the Raney Ni catalyst. The new shoulder and the increased CO uptake suggest that a new phase is formed when the Raney Ni catalyst is doped with Cu, but the results do not provide direct evidence of the type of phase the Cu forms. Work by Wainwright, who produced bulk Raney NiCu alloys, also performed CO TPD of Raney Ni and an alloy Raney NiCu catalyst and found a similar shoulder over a similar temperature range, likely indicating that this observed shoulder is from an NiCu alloy [8]. We also examined a Cu standard (100 nm Cu particles) under the same reduction and TPD conditions and found no significant CO uptake because the Cu particles sintered. Therefore, it is likely that the Cu and Ni in the 10% Raney NiCu catalyst form an alloy due to the relatively high CO uptake observed.

Fig. 7.5 shows the XRD patterns of the 1-40% Raney NiCu catalysts. The dominant features of each diffraction pattern at low Cu loading (1-7%) are the Ni planes. As the Cu loading increases, a peak forms at the base of the Ni(111) peak in the 10% Raney NiCu catalyst. Further increases in Cu loading increase the size of this peak, identified as a $Ni_{0.5}Cu_{0.5}$, indicating the formation of an alloy of Ni and Cu. The 40% Raney NiCu catalyst shows the formation of a third peak in the (111) plane, identified as a Cu rich phase, $(Cu_{19}Ni)_{0.2}$. In addition to the (111) plane, one also observes the formation of the $Ni_{0.5}Cu_{0.5}$ and $(Cu_{19}Ni)_{0.2}$ phases in the (200) and (220) planes. These results indicate that Ni and Cu form an alloy under the synthesis and reduction conditions used, and that at low to moderate Cu loading, this alloy appears to be roughly equal parts Ni and Cu.

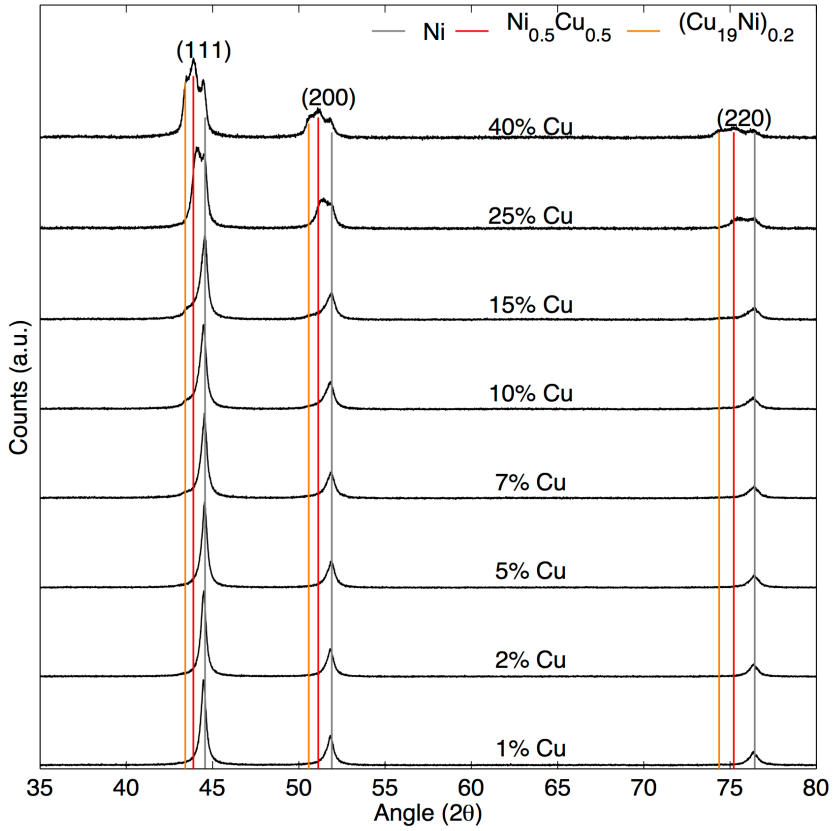

Figure 7.5. X-ray diffraction patterns of the Raney NiCu catalysts (passivated in 1% O_2 at 70 °C overnight, Cu Kα source, 40 kV, 15 mA, 1.25°/min).

Fig. 7.6 shows TEM and STEM images of the 10% Raney NiCu catalyst. Fig. 7.6a shows a TEM image of the catalyst particle examined. Fig. 7.6d shows the STEM image used to generate the elemental map. We calculated the x distance across Fig. 7.6d, using the scale bar from Fig. 7.6a and common points in both images, as 870 nm. Fig. 7.6b, c, e, and f show the elemental maps of Ni, Cu, Zn, and Al. One expects Ni, Cu, and Al to be present in the catalyst. Zn, on the other hand, (Fig. 7.6e) served as a control element to determine the amount of background signal one should expect. Examination of Fig. 7.6e indicates that the background signal is low compared to the signals obtained from the other elements. Fig. 7.6f shows that the Al appears to be segregated to both ends of the catalyst particle

examined, with relatively little Al present in the middle of the image. This segregation is likely a result of the leaching methods that are used to remove Al from the Ni matrix during the synthesis of Raney Ni.

Fig. 7.6b and c indicate that Ni and Cu appear to spread evenly across the catalyst surface. This finding likely indicates that the Cu added to the catalyst is not present in Cu islands, but rather is present in a NiCu alloy that is relatively evenly dispersed on the catalyst surface. This finding is also in agreement with the XRD and TPD results presented earlier. All of the catalyst characterization findings are consistent with the results of Huber and Shabacker who used a Sn doped Raney Ni catalyst for aqueous phase reforming reactions and found that the Sn incorporated in the Ni catalyst [9-11].

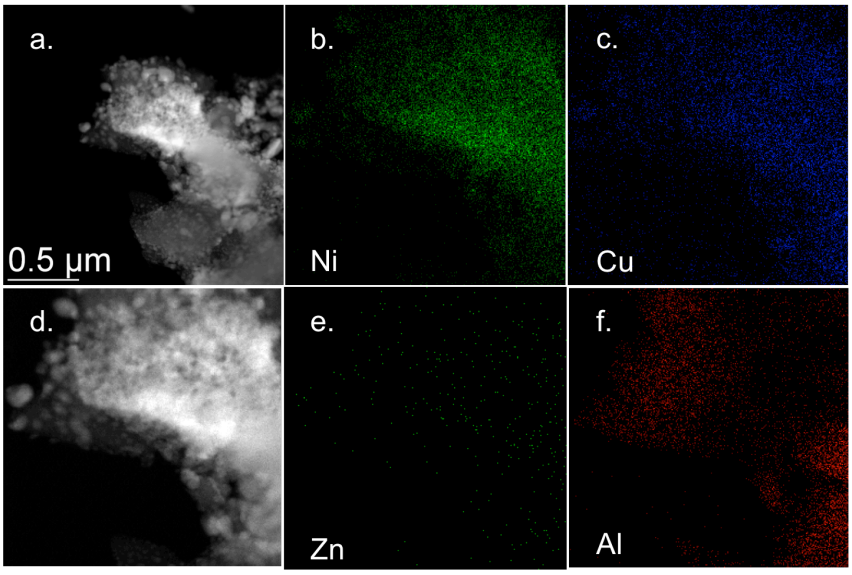

Figure 7.6. TEM and STEM elemental maps of 10% Raney NiCu. Fig. 7.6a. shows the original TEM image of the catalyst. Fig. 7.6d. shows the STEM image taken of the section of the catalyst used for the elemental map. Fig. 7.6b, c, e, and f. show the result from elemental maps of Ni, Cu, Zn, and Al respectively.

7.2 Improved Ni-based Hydrothermal HDO catalysts with the addition of acid sites

Section 7.1 showed that the addition of Cu to Ni catalysts suppresses gasification activity, but has little effect on the HDO activity of these catalysts. In short, the Raney NiCu catalysts are active for the hydrogenation of o-cresol, but are not sufficiently active for the C-O hydrogenolysis required for HDO. Recent research suggests that acid sites are essential for hydrothermal HDO reactions over Ni catalysts [12, 13]. Zhao et al. found that the Raney Ni 4200 and 2400 are active for HDO only when an additional acid catalyst, in this case Nafion supported on SiO_2, was added the reaction mixture [13]. Mortensen et al. found that the non-hydrothermal HDO of phenol occurred more rapidly on acidic supports such as ZrO_2 and Al_2O_3, leading these researchers to speculate that the HDO reaction actually occurred at the metal/support interface [12]. They also determined that Ni on non-acidic supports, such as carbon, were inactive for HDO.

This section elucidates the influence of added acidity on the product yields and selectivities by modifying the reaction system in three ways. First, we used the 10% Raney NiCu catalyst in an aqueous solution of HCl or H_2SO_4. Second, we synthesized Ni and NiCu catalysts on acidic supports that are known to be stable in a hydrothermal environment (e.g., Al_2O_3 and ZrO_2). Third, we further modified the Raney Ni catalyst by oxidizing some of the Al in the catalyst to Al_2O_3 by calcining the catalyst in air at 400 °C (see chapter 2). This calcined Raney Ni catalyst is a novel catalyst, that to the best of our knowledge, has never before been used for HDO. The only prior report we found of intentionally producing Al_2O_3 through calcination on a Raney Ni catalyst used the Al_2O_3 as a binder for an extruded catalyst [14].

7.2.1 Batch experiments with acidic Ni catalysts

We examined a variety of catalysts in 4.1 mL batch mini-reactors to quickly assess their activity for hydrothermal HDO under a variety of conditions. Table 7.1 summarizes these results and conditions used. These experiments used less catalyst (10 vs. 20 mg), more o-cresol (100 vs. 20 mg), and a lower H_2 to o-cresol molar ratio (6:1 vs. 17:1) than did the batch reactions that generated fig. 7.4. These reaction conditions were chosen primarily to prevent complete conversion. Table 7.1 indicates that the addition of HCl and H_2SO_4 had a negative effect on liquid hydrocarbon yield and conversion. We suspect, although we did not test this hypothesis, that the Cl and S poisoned the 10% Raney Ni catalyst and rendered the catalyst almost completely inactive.

Table 7.1 also summarizes the results of several active catalysts. The temporal variation of conversion and liquid hydrocarbon yield from these catalysts appear in fig. 7.7. Table 7.1 and fig. 7.7 reveal that the 10% Ni/ZrO_2 catalyst had a low liquid hydrocarbon yield and conversion, but a high selectivity to liquid products. The 10% Ni/Al_2O_3 catalyst showed the highest conversion, liquid hydrocarbon yield, and selectivity to liquid products. Last, the calcined Raney Ni catalyst had a high conversion, a relatively low liquid hydrocarbon yield, and a low selectivity to liquid products when compared to the 10% Ni/Al_2O_3 catalyst. Nonetheless, the calcined Raney Ni catalyst generally had higher liquid hydrocarbon yields than the 10% Raney NiCu catalyst. For the catalysts tested in fig. 7.7, the liquid hydrocarbons were cyclohexane, benzene, toluene and methylcyclohexane. The major oxygenated products were methylcyclohexanol, methylcyclohexanone, phenol, cyclohexanol, and cyclohexanone. The gas product was primarily methane with smaller amounts of CO_2. The yields of individual products are shown in table C.3.

Table 7.1. Summary of catalysts tested in 4.1 mL batch reactors (380 °C,15-180 min, 10 mg catalyst, 100 mg of o-cresol, 0.67 mL DI H_2O or DI water acid solution, 41 bar H_2 (STP), 6:1 H_2 to o-cresol, X= conversion, LH = liquid hydrocarbon, S_{liq} = selectivity to liquid products).

Catalyst	X	LH Yield	S_{liq}	Time (min)	W×t/m (min)
10% Raney NiCu	37-80%	0-7%	65-87%	15-45	1.5-4.5
10% Raney NiCu + HCl[1]	1-4%	0%	----	15-60	1.5-6.0
10% Raney NiCu + H_2SO_4[2]	0-5 %	0-1%	----	30-60	3.0-6.0
10% Ni/Al_2O_3	54-93%	12-35%	85-91%	30-150	0.15-1.5
10% Ni/ZrO_2	14-67%	0-8%	64-98%	15-180	0.3-1.8
Calcined Raney Ni	57-88%	3-12%	44-68%	15-60	1.5-6.0

[1]1.04 wt% HCl in DI water. [2]0.2 wt% H_2SO_4 in DI water

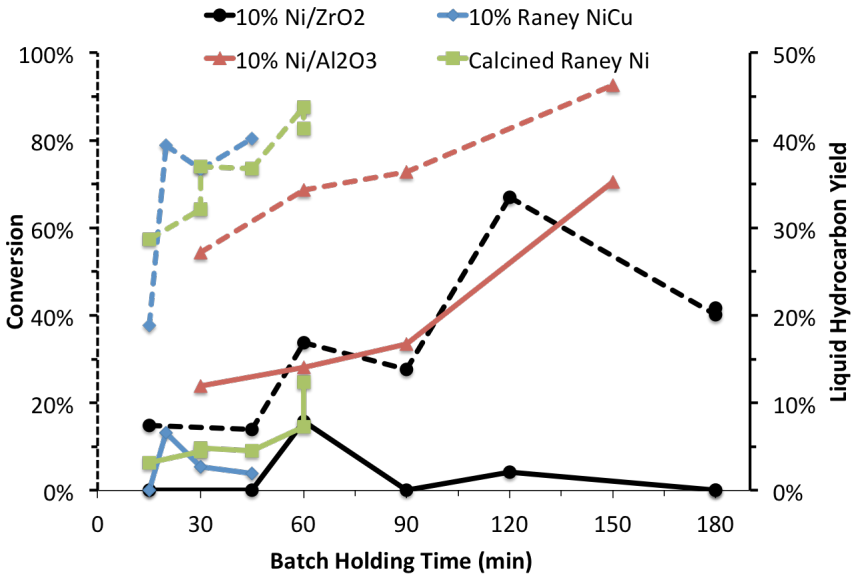

Figure 7.7. Conversion (dashed lines) and liquid hydrocarbon yield (solid lines) from Ni and NiCu catalysts in 4.1 mL batch reactors. Table 7.1 summarizes all of catalysts tested (380 °C, 10 mg catalyst, 100 mg of o-cresol, 0.67 mL DI H_2O, 41 bar H_2 (STP), 6:1 H_2 to o-cresol).

The high liquid hydrocarbon yield from the 10% Ni/Al_2O_3 catalyst and the increased liquid hydrocarbon yield from the calcined Raney Ni catalyst support the hypotheses by Mortensen et al. [12] and Zhao et al. [15] that acid sites, like those found in Al_2O_3, assist in

C-O hydrogenolysis, and therefore increase HDO activity. The results obtained with the calcined Raney Ni catalyst were especially encouraging because such a catalyst has not been studied previously for HDO. Furthermore, it is suspected that the liquid hydrocarbon yield, shown in fig. 7.7, was low due to the relatively high gasification activity of the catalyst (i.e., low selectivity to liquid products in Table 7.1), but in section 7.1 it was shown that Cu decreases the gasification activity of Raney Ni. Therefore, with these two tools, the addition of Cu and the addition of Al_2O_3, the activity and selectivity of Ni catalysts can be tuned.

7.2.2 Flow reactions

At this point, this work identified several catalysts that are active for hydrothermal HDO, but several challenges remain. The first challenge is to obtain a high liquid hydrocarbon yield (e.g., > 50%) with these catalysts, and the second challenge is to determine the stability of these catalysts under the harsh hydrothermal conditions. These challenges were addressed by performing a series of flow reactor experiments using the reactor shown in fig. 3.3 and described in detail in the methods chapter.

7.2.2.1 Calcined Raney Ni

Calcined Raney Ni was tested in the flow reactor, and fig. 7.8 shows the results. The conversion of o-cresol, at a W/F (mass of catalyst active metal/mass flow rate of o-cresol) of 12.7 min, is generally between 75 and 90%, and appears to decrease slightly with TOS. The liquid hydrocarbon yield was generally between 25 and 45% with the higher yields appearing at later TOS. The linear trend line fit to the liquid hydrocarbon yield data indicates an increasing liquid hydrocarbon yield with TOS. Fig. 7.8 also shows that the

yields of the two major liquid hydrocarbon products, methylcyclohexane and cyclohexane, appear relatively steady with TOS, if not increasing slightly. A variety of other minor liquid hydrocarbon products also formed, and in general had low individual yields (< 2%). The sum of these products, however, significantly increased the liquid hydrocarbon yield. These products include butane, 2-methylbutane, hexane, methylcyclopentane, 1,3-dimethylcyclopentane, ethylcyclopentane, toluene, and methylcyclohene (table C.4). These minor products indicate that this catalyst has a relatively high isomerization activity compared with the other catalysts examined.

Fig. 7.8 shows that the methane yield was between 20 and 40% during the reaction, indicating that this catalyst still retains significant gasification activity. This gasification activity also appears to be maintained with TOS indicating that this catalyst is unlikely to become more selective for liquid products, either oxygenated or hydrocarbons, without a modification to the catalyst.

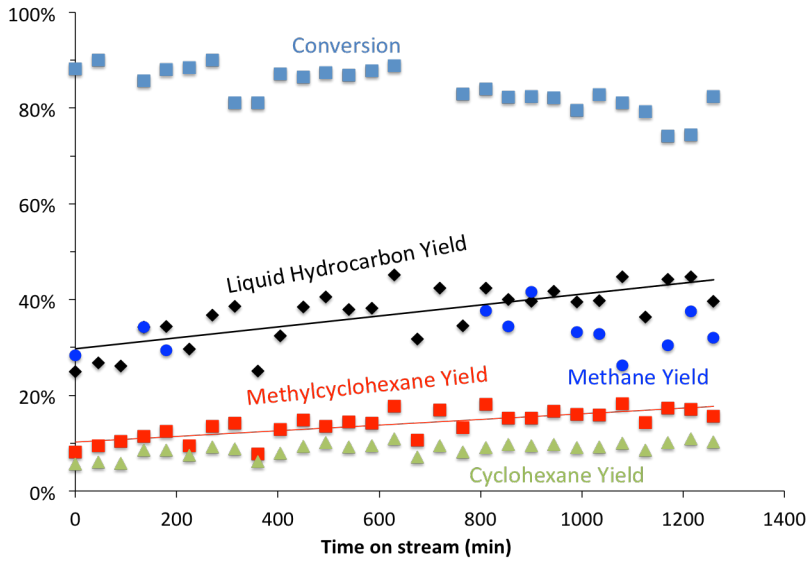

Figure 7.8. Results from reacting o-cresol over calcined Raney Ni (W/F = 12.7 min, T_{inlet} = 365 °C, T_{outlet} = 390 °C, 280 bar, feed flow rates (mL/min, ambient temperature): H_2O = 0.270, o-cresol = 0.030, internal standard solution =0.400, H_2 = 0.006 mol/min, H_2 to o-cresol molar ratio = 20:1, 550 °C in situ H_2 catalyst reduction).

Previous work revealed an increase in liquid hydrocarbon yield with TOS, similar to that in fig. 7.8, when using a Pt/C catalyst for the hydrothermal HDO of o-cresol. A potential cause of this increase in activity was reduction of the catalyst surface that had been oxidized during reactor startup [1]. Similarly, oxidation of the present Ni catalyst may have occurred during the reactor startup, and gradual re-reduction during the reaction led to increasing liquid hydrocarbon yields. Another possible cause of the increase in liquid hydrocarbon yield with TOS is an increase in the Al_2O_3 content of the Raney Ni catalyst caused by the oxidizing hydrothermal environment. Suchanek developed an Al_2O_3-H_2O phase diagram by subjecting γ-$Al(OH)_3$ and γ-AlOOH to a hydrothermal environment and showed that under conditions similar to those used in this reaction, α-Al_2O_3 is formed [16]. Therefore, it is also possible that the increase in liquid hydrocarbon yield observed in fig.

7.8 is due to an increasing concentration of acid Al_2O_3 sites adjacent to the Ni active metal, allowing for HDO reactions to occur more readily.

Previous work with Raney Ni, using formic acid as the H_2 source and similar reaction conditions, provided only very low yields of liquid hydrocarbons, 6.4%, at a very similar W/F of 12 min [1]. Therefore, the development of calcined Raney Ni represents a significant step forward in developing a low-cost, active, and stable catalyst for hydrothermal HDO.

7.2.2.2 Supported NiCu catalyst

Fig. 7.9 shows the results from reacting o-cresol over a 10%, 0.5% $NiCu/Al_2O_3$ catalyst at a W/F of 3.22 min using the same reaction conditions as above. We doped this catalyst with a small amount of Cu (0.5%) to suppress the gasification pathway.

Fig. 7.9 shows the conversion remained steady at ~100% throughout the 24 hr experiment. The liquid hydrocarbon yield was generally between 50 and 80%, with an average of 71 ± 19%. During this experiment the reaction pressure would occasionally drop to around 225 bar, for an unknown reason, before rebuilding to 280 bar. These occasional process upsets induced atypical scatter in the data collected. Nonetheless, the results clearly show a high average liquid hydrocarbon yield and no significant catalyst deactivation over the 24 hr reaction.

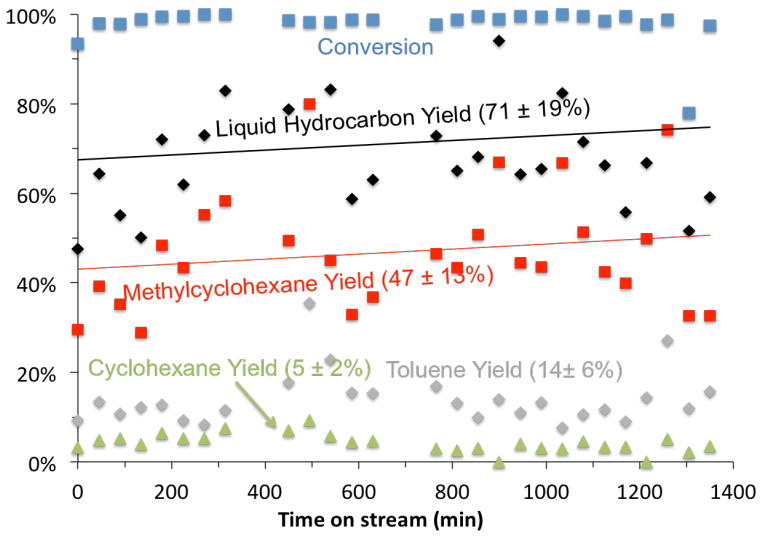

Figure 7.9. Results from reacting o-cresol over 10%, 0.5% $NiCu/Al_2O_3$ (W/F = 3.22 min, T_{inlet} = 365 °C, T_{outlet} = 390 °C, 280 bar, feed flow rates (mL/min, ambient temperature): H_2O = 0.270, o-cresol = 0.030, internal standard solution =0.400, H_2 = 0.006 mol/min, H_2 to o-cresol molar ratio = 20:1, 550 °C in situ H_2 catalyst reduction).

Fig. 7.9 also shows that the yields of the three major liquid hydrocarbon products: cyclohexane, toluene, and methylcyclohexane. These three products accounted for > 85% of the liquid hydrocarbon yield, but small yields of benzene (≤ 3%) and methylcyclohexene (≤ 2%) were also observed. This finding indicates that this supported catalyst is much less active for isomerization than the calcined Raney Ni catalyst.

The yields of oxygenated and gas products were generally low. The oxygenated products were phenol, cyclohexanone, cyclohexanol, 2-methylcyclohexanol, and 2-methylcyclohexanone, and the average yield for each oxygenated molecule was ≤ 2% (table C.5). The gas products were methane and CO_2 with average yields of 5 ± 2% and 3 ± 2%, respectively.

7.2.2.3 Calcined 5% Raney NiCu

The calcined Raney Ni catalyst tested in both batch and flow reactors showed very promising results because of the increased liquid hydrocarbon yield when compared with previous work [1]. Examination of the products revealed that this catalyst was still too active for gasification, because, as shown in fig. 7.8 and table C.4, between 20 and 40% of the carbon from o-cresol formed methane. Therefore, to suppress this gasification activity, we added 5% Cu to the calcined Raney Ni catalyst, and reacted o-cresol over this catalyst at a W/F of 19.9 min.

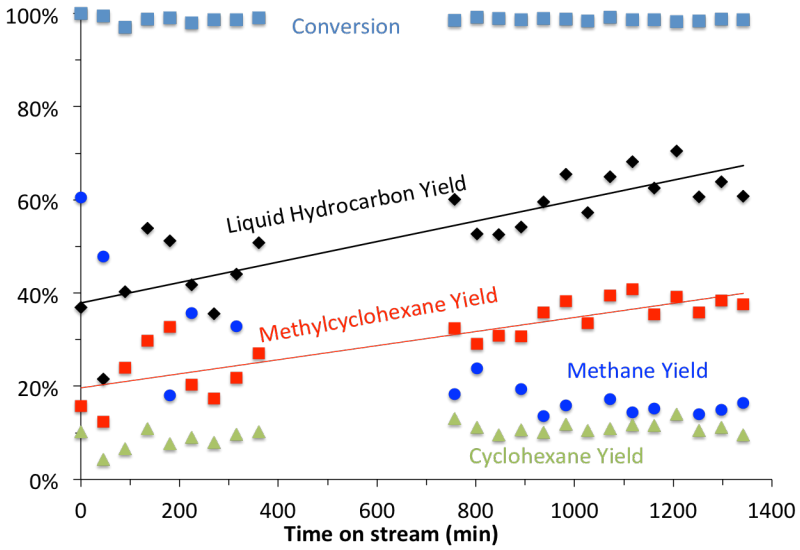

Figure 7.10. Results from reacting o-cresol over 5% calcined Raney NiCu (W/F = 19.9 min, T_{inlet} = 365 °C, T_{outlet} = 390 °C, 280 bar, feed flow rates (mL/min, ambient temperature): H_2O = 0.270, o-cresol = 0.030, internal standard solution =0.400, H_2 = 0.006 mol/min, H_2 to o-cresol molar ratio = 20:1, 550 °C in situ H_2 catalyst reduction).

Fig. 7.10 shows that the o-cresol was completely converted over the calcined 5% Raney NiCu catalyst throughout the reaction. The liquid hydrocarbon yield was ~40% early in the reaction and increased linearly to ~60% after 1200 min on stream. As with the calcined Raney Ni catalyst, the two major liquid hydrocarbon products were

methylcyclohexane and cyclohexane. The methylcyclohexane yield increased linearly with TOS from ~20 to ~40% while the cyclohexane yield remained steady at 10 ± 2% over the course of the reaction. The remaining liquid hydrocarbon and oxygenated products (table C.6) were the same as those observed with the calcined Raney Ni catalyst, and each product had a low yield (≤ 2%).

Fig. 7.10 also shows the methane yield from the calcined 5% Raney NiCu catalyst and indicates that at early TOS, the catalyst was active for gasification, but after 800 min on stream the gasification activity is lower and steady, producing methane in 17 ± 3% yield. This yield of methane compares favorably to the 34 ± 4% yield of methane observed with the calcined Raney Ni. Furthermore, this decrease in methane yield occurred even with an increase in W/F from 12.7 to 19.9 min. It is likely that this increase in selectivity toward liquid products, and more specifically liquid hydrocarbon products, in the calcined 5% Raney NiCu catalyst is due primarily to the decrease in the gasification activity of the calcined 5% Raney NiCu catalyst compared with the calcined Raney Ni catalyst. The reason for the increase in the liquid hydrocarbon yield with TOS is again not known with certainty, but we speculate that this increase is due to the same reasons discussed above for the calcined Raney Ni catalyst.

All three catalysts tested in the flow reactor, calcined Raney Ni, NiCu/Al_2O_3, and calcined 5% Raney NiCu, represent significant advances in hydrothermal HDO catalysts because each catalyst produced moderate to high yields of liquid hydrocarbons while minimizing the production of gaseous products. Furthermore, each catalyst appeared to be free of any rapid deactivation, suggesting the catalyst lifetime is significantly longer than the 24 hr time period tested. Last, these catalysts do not contain noble metals and do not

require the addition of a separate acid catalyst (i.e. Nafion or H_3PO_4) to produce liquid hydrocarbons. Both of these factors have significant commercial implications because the catalyst is inexpensive and additional separation steps are not necessary to remove a homogenous acid catalyst.

7.2.3 Catalyst characterization

We performed XRD on the Ni/Al_2O_3, $NiCu/Al_2O_3$ and calcined Raney Ni catalysts. Fig. 12 shows the XRD patterns of the γ-AlOOH, the calcined 10% Ni/AlOOH, the reduced 10% Ni/Al_2O_3, and the reduced 10%, 0.5% $NiCu/Al_2O_3$ catalysts. The calcined Ni/AlOOH catalyst diffraction pattern contains NiO, AlOOH, Al_2O_3 peaks, indicating that the AlOOH support is starting to convert to Al_2O_3. Reduction of the Ni/AlOOH catalyst converts the NiO to Ni and the remaining AlOOH to Al_2O_3. This outcome is evident by the absence of NiO and AlOOH peaks and presence of Ni and Al_2O_3 peaks in the reduced Ni/Al_2O_3 pattern. In the 10%, 0.5% $NiCu/Al_2O_3$ catalyst diffraction pattern, only NiCu and Al_2O_3 phases appear.. This result differs from the Raney NiCu catalysts where both Ni and NiCu phases were observed. This result is likely because both the Ni and Cu were impregnated on the catalysts at the same time, whereas with the Raney NiCu catalysts, the Cu was added on top of the base Raney Ni catalyst.

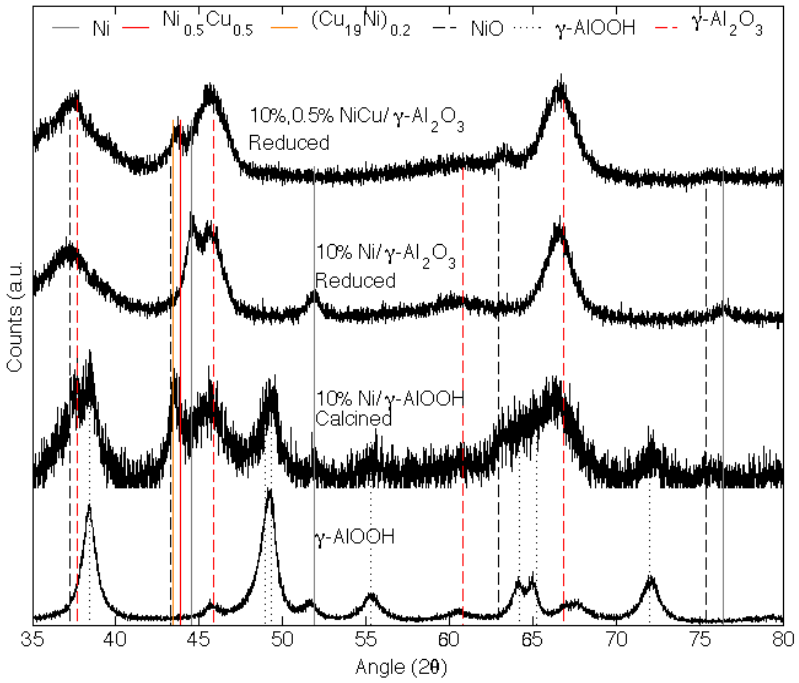

Figure 7.11. X-ray diffraction patterns of the 10% Ni/Al_2O_3 and 10%, 0.5% $NiCu/Al_2O_3$ catalysts (passivated in 1% O_2 at 70 °C overnight, Cu Kα source, 40 kV, 15 mA, 1.25°/min).

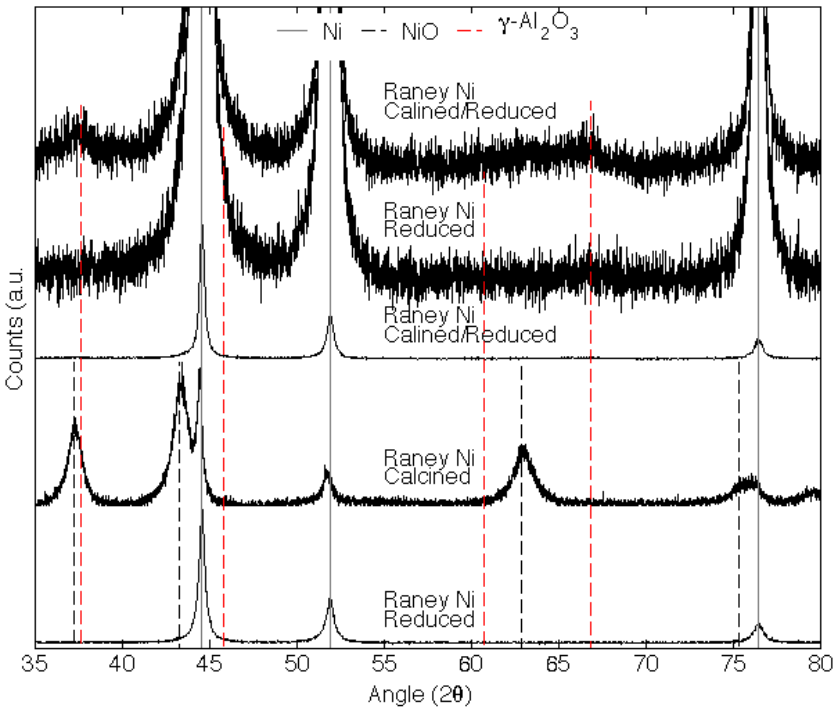

Figure 7.12. X-ray diffraction patterns of the Raney Ni catalysts (passivated in 1% O_2 at 70 °C overnight, Cu Kα source, 40 kV, 15 mA, 1.25°/min).

Fig. 7.12 shows the XRD patterns of the reduced Raney Ni, the calcined Raney Ni, and the calcined then reduced Raney Ni catalysts. The top two XRD patterns in fig. 7.12 zoom in on the baseline of the reduced Raney Ni and calcined/reduced Raney Ni patterns. The reduced Raney Ni pattern shows only Ni peaks as expected. Upon calcination, much of the Ni in the original catalyst is converted to NiO, which is evident by the appearance of NiO peaks in this pattern. Reduction of the calcined Raney Ni catalyst returns the catalyst, upon initial inspection, to a very similar XRD pattern as the reduced Raney Ni catalyst. The expanded patterns at the top of fig. 7.12, though, do indicate a slight difference between these catalysts. Upon careful inspection, one observes two new peaks at ~37 and ~ 67 ° in the calcined/reduced Raney Ni catalyst. These peaks correspond to γ-Al_2O_3 This

correspondence provides a strong indication that the calcination and reduction of the Raney Ni catalyst did result in the formation Al_2O_3, and provides further supporting evidence that it is the presence of Al_2O_3 that increases the HDO activity of these catalysts.

7.4. Conclusion

This chapter demonstrates two approaches for improving the hydrothermal HDO activity and selectivity of Ni catalysts, that when combined, provide the only known stable and high liquid hydrocarbon yield for non-noble metal catalysts. The first approach is to dope the Ni catalysts with Cu to reduce the gasification activity. Between 7 and 25 wt% Cu added to the Raney Ni catalyst shifts the selectivity of the catalyst from gas to liquid products. Unfortunately, this shift in selectivity did not increase the liquid hydrocarbon yield. The second approach is to add acid sites, as recent reports suggest that acid sites are important for the dehydration step in HDO [12, 13]. Acid sites were added via an acidic support (Al_2O_3) for Ni and NiCu catalysts, and via calcination of the Raney Ni catalyst to produce an Al_2O_3 phase within the catalyst. In flow reactor experiments, both the 10%, 0.5% NiCu/Al_2O_3 and the calcined 5% Raney NiCu catalysts produced liquid hydrocarbon yields over 60% and showed no activity loss over the 24 hr reaction. In particular the calcined 5% Raney NiCu catalyst represents an interesting hydrothermal HDO catalyst due to its novelty, activity, cost, and selectivity.

Acknowledgements

We thank Thomas Yeh for performing the TEM/STEM imaging and Erin Branton for assisting with the reaction experiments.

Appendix C: Supplementary data for chapter 7

Table C.1. Product yields from reacting o-cresol over 2% Raney NiCu using formic acid as the reductant. This data table corresponds to fig. 7.3.

TOS (min)	0	30	60	90	120	150	180	210	240	270	300	330	360	390	420	450	480	510
Molecule	**Yield**	**Yield**	**Yield**	**Yield**	**Yield**	**Yield**	**Yield**	**Yield**	**Yield**	**Yield**	**Yield**	**Yield**	**Yield**	**Yield**	**Yield**	**Yield**	**Yield**	**Yield**
Benzene	6.2%	5.8%	5.4%	4.7%	3.6%	3.8%	3.4%	3.0%	2.2%	3.2%	2.3%	2.4%	1.7%	1.6%	1.6%	1.4%	1.3%	1.2%
Methylcyclohexane	1.5%	1.5%	1.3%	1.4%	1.2%	1.3%	1.3%	1.2%	1.1%	1.4%	1.1%	1.6%	1.2%	1.3%	1.3%	1.1%	1.2%	1.1%
Ethylcyclopentane	0.0%	0.0%	0.0%	0.0%	0.0%	0.0%	0.0%	0.0%	0.0%	0.0%	0.0%	0.0%	0.0%	0.0%	0.0%	0.0%	0.0%	0.0%
Toluene	2.3%	2.4%	2.2%	2.4%	2.2%	2.2%	2.3%	2.1%	1.5%	2.4%	1.9%	2.2%	1.8%	1.9%	1.8%	1.7%	1.7%	1.6%
Methylcyclohexene	0.0%	0.0%	0.0%	0.0%	0.0%	0.0%	0.0%	0.0%	0.0%	0.0%	0.0%	0.0%	0.0%	0.0%	0.0%	0.0%	0.0%	0.0%
Cyclohexanol	0.0%	0.0%	0.0%	0.0%	0.0%	0.0%	0.0%	0.0%	0.0%	0.0%	0.0%	0.0%	0.0%	0.0%	0.0%	0.0%	0.0%	0.0%
Cyclohexanone	0.7%	1.1%	1.1%	1.5%	1.6%	1.7%	1.9%	2.0%	1.9%	2.4%	2.2%	2.4%	2.3%	2.5%	2.5%	2.4%	2.4%	2.3%
cis-2-methylcyclohexanol	0.0%	0.0%	0.0%	0.0%	0.5%	0.0%	0.6%	0.7%	0.7%	1.0%	1.0%	1.1%	1.1%	1.4%	1.5%	1.4%	1.4%	1.4%
trans-2-methylcyclohexanol	0.0%	0.0%	0.0%	0.0%	0.0%	0.0%	0.0%	0.0%	0.0%	0.0%	0.0%	0.0%	0.0%	0.4%	0.0%	0.0%	0.0%	0.0%
Methylcyclohexanone	1.3%	2.6%	2.3%	4.3%	5.2%	5.9%	7.1%	8.0%	7.7%	11.5%	10.1%	13.1%	13.0%	15.3%	15.6%	14.8%	16.4%	16.4%
Phenol	8.7%	13.2%	14.1%	17.9%	19.7%	20.8%	21.8%	22.9%	23.8%	25.3%	23.1%	24.4%	23.1%	22.8%	22.6%	21.5%	18.9%	19.5%
o-cresol (from rxn soln)	3.5%	6.2%	6.0%	9.9%	11.9%	13.3%	15.3%	17.5%	19.4%	21.5%	22.5%	24.6%	25.6%	28.4%	30.1%	27.7%	30.8%	30.5%
After Regeneration 1																		
Benzene	6.1%	4.0%	6.7%	4.2%	3.3%	2.7%	1.9%	1.7%	1.5%	1.2%	1.1%	1.0%	0.9%	0.9%	0.0%	0.0%	0.9%	0.0%
Methylcyclohexane	0.0%	1.3%	1.6%	2.3%	2.2%	2.4%	2.3%	2.2%	2.1%	2.0%	1.8%	1.9%	1.8%	1.8%	1.4%	1.7%	1.9%	1.9%
Ethylcyclopentane	0.0%	0.0%	0.0%	0.0%	0.0%	0.0%	0.0%	0.0%	0.0%	0.0%	0.0%	0.0%	0.0%	0.0%	0.0%	0.0%	0.0%	0.0%
Toluene	0.0%	2.2%	3.2%	3.2%	3.1%	3.2%	3.0%	2.7%	2.7%	2.5%	2.3%	2.4%	2.2%	2.3%	1.9%	2.0%	2.4%	2.1%
Methylcyclohexene	0.0%	0.0%	0.0%	0.0%	0.0%	0.0%	0.0%	0.0%	0.0%	0.0%	0.0%	0.0%	0.0%	0.0%	0.0%	0.0%	0.0%	0.0%
Cyclohexanol	0.0%	0.0%	0.0%	0.0%	0.0%	0.0%	0.0%	0.0%	0.0%	0.0%	0.0%	0.0%	0.0%	0.0%	0.0%	0.0%	0.0%	0.0%
Cyclohexanone	4.3%	4.7%	2.5%	3.5%	3.3%	3.3%	3.3%	3.2%	3.1%	3.0%	2.8%	3.0%	2.9%	2.9%	2.7%	2.7%	2.9%	2.8%
cis-2-methylcyclohexanol	3.1%	2.0%	0.5%	0.9%	0.9%	1.1%	1.6%	1.4%	1.6%	1.7%	1.8%	2.1%	2.1%	2.1%	2.2%	2.1%	2.7%	2.4%
trans-2-methylcyclohexanol	0.0%	0.6%	0.0%	0.0%	0.0%	0.0%	0.4%	0.0%	0.5%	0.5%	0.5%	0.6%	0.6%	0.6%	0.6%	0.6%	0.8%	0.6%
Methylcyclohexanone	14.5%	11.3%	3.7%	9.3%	9.7%	12.2%	15.0%	14.9%	16.0%	16.3%	16.9%	18.8%	18.8%	19.4%	18.6%	18.8%	21.5%	20.1%
Phenol	11.2%	18.9%	20.9%	25.0%	24.5%	22.6%	19.3%	19.2%	18.2%	16.5%	15.8%	15.5%	14.6%	13.6%	12.4%	11.7%	10.9%	11.1%
o-cresol (from rxn soln)	53.5%	33.2%	13.1%	26.7%	28.1%	32.9%	39.1%	37.8%	39.4%	40.1%	41.2%	44.9%	43.8%	44.8%	44.0%	42.6%	47.9%	45.0%
After Regeneration 2																		
Benzene	4.4%	3.4%	2.7%	2.5%	1.8%	1.9%	1.3%	1.6%	1.3%	1.3%	0.0%	0.0%	0.0%	0.0%	0.0%	0.0%	0.0%	0.0%
Methylcyclohexane	3.3%	3.2%	3.0%	3.5%	2.9%	3.6%	2.7%	3.8%	2.4%	3.0%	2.9%	3.8%	2.4%	2.0%	2.0%	2.1%	2.1%	2.0%
Ethylcyclopentane	0.0%	0.0%	0.0%	0.0%	0.0%	0.0%	0.0%	0.0%	0.0%	0.0%	0.0%	0.0%	0.0%	0.0%	0.0%	0.0%	0.0%	0.0%
Toluene	3.7%	3.3%	3.4%	3.6%	3.1%	3.7%	2.9%	3.4%	2.7%	2.9%	2.8%	3.5%	2.5%	2.2%	2.1%	2.1%	2.2%	2.0%
Methylcyclohexene	0.0%	0.0%	0.0%	0.0%	0.0%	0.0%	0.0%	2.4%	0.0%	0.0%	0.0%	2.9%	2.0%	1.7%	1.8%	2.1%	2.0%	2.1%
Cyclohexanol	0.0%	0.0%	0.0%	0.0%	0.0%	0.0%	0.0%	0.0%	0.0%	0.0%	0.0%	0.0%	0.0%	0.0%	0.0%	0.0%	0.0%	0.0%
Cyclohexanone	3.4%	3.7%	3.8%	4.0%	3.6%	3.7%	3.5%	3.5%	3.2%	3.2%	3.2%	3.3%	3.0%	2.8%	2.9%	2.9%	2.9%	2.7%
cis-2-methylcyclohexanol	1.2%	1.7%	1.9%	2.1%	2.1%	2.4%	2.6%	3.1%	2.3%	2.8%	2.8%	3.1%	3.1%	3.1%	3.2%	3.4%	3.2%	3.5%
trans-2-methylcyclohexanol	0.0%	0.0%	0.0%	0.5%	0.5%	0.5%	0.6%	0.7%	0.0%	0.6%	0.6%	0.7%	0.7%	0.7%	0.7%	0.7%	0.7%	0.7%
Methylcyclohexanone	11.2%	14.0%	15.3%	17.2%	16.5%	19.0%	18.8%	21.3%	16.6%	20.0%	20.7%	23.2%	21.1%	20.2%	21.0%	21.6%	21.7%	21.7%
Phenol	17.5%	14.0%	12.1%	12.6%	11.2%	10.0%	9.5%	10.2%	9.9%	8.4%	8.1%	6.9%	7.2%	6.5%	6.2%	6.5%	6.0%	5.6%
o-cresol (from rxn soln)	35.6%	39.2%	42.2%	43.4%	42.8%	44.5%	46.3%	47.4%	43.4%	47.3%	47.6%	48.4%	47.6%	47.1%	47.5%	48.3%	48.1%	48.1%

Table C.2. Product yields from reacting o-cresol over Raney NiCu with H_2 as the reductant. This data table corresponds to fig. 7.4.

Catalyst	1% Raney NiCu		2% Raney NiCu			5% Raney NiCu			7% Raney NiCu			10% Raney NiCu	15% Raney NiCu			25% Raney NiCu			40% Raney NiCu		
Molecule	**Yield**	**Yield**	**Yield**	**Yield**	**Yield**	**Yield**	**Yield**	**Yield**	**Yield**	**Yield**	**Yield**	**Yield**	**Yield**	**Yield**	**Yield**	**Yield**	**Yield**	**Yield**	**Yield**	**Yield**	**Yield**
CH4	60.0%	75.7%	52.9%	53.7%	38.8%	75.0%	71.0%	55.2%	43.6%	60.3%	55.6%	77.2%	19.9%	15.4%	15.6%	0.1%	8.7%	8.2%	6.3%	12.6%	10.5%	15.4%
CO2	19.1%	22.0%	16.6%	18.3%	12.2%	15.2%	27.8%	18.1%	44.1%	13.6%	19.9%	30.0%	7.8%	4.1%	4.7%	42.3%	3.0%	2.0%	0.7%	1.8%	3.5%	6.4%
C2H6	1.1%	1.2%	1.0%	0.0%	0.6%	1.3%	1.6%	1.2%	1.1%	1.1%	1.2%	1.4%	0.5%	0.0%	0.4%	0.0%	0.0%	0.0%	0.0%	0.0%	0.0%	0.0%
Cyclohexane	0.0%	0.0%	0.0%	0.0%	0.0%	0.0%	0.0%	0.0%	0.0%	0.0%	0.0%	0.0%	0.0%	0.0%	0.0%	0.0%	0.0%	0.0%	0.0%	0.0%	0.0%	0.0%
Benzene	2.6%	2.4%	3.4%	2.2%	9.5%	2.9%	4.3%	5.5%	7.1%	3.6%	4.3%	3.5%	5.0%	5.5%	5.0%	4.3%	4.4%	2.2%	1.5%	5.7%	2.8%	1.9%
Methylcyclohexane	0.0%	0.0%	0.0%	0.0%	0.0%	0.0%	0.0%	0.0%	0.0%	0.0%	0.0%	0.0%	0.0%	0.0%	0.0%	0.0%	0.0%	0.0%	0.0%	0.0%	0.0%	0.0%
Toluene	0.0%	0.0%	0.0%	0.0%	1.9%	0.0%	0.0%	0.0%	0.0%	0.0%	0.0%	0.0%	0.0%	0.0%	0.0%	0.0%	0.0%	0.0%	0.0%	0.0%	0.0%	0.0%
Cyclohexanol	0.0%	0.0%	0.0%	0.0%	3.7%	0.0%	0.0%	0.0%	2.1%	2.3%	0.0%	1.2%	6.9%	8.5%	5.8%	9.0%	22.0%	22.8%	14.3%	20.2%	15.5%	9.9%
Cyclohexanone	0.0%	0.0%	1.7%	3.1%	4.7%	1.3%	0.0%	1.1%	2.8%	2.5%	0.0%	0.0%	1.5%	1.7%	1.9%	2.2%	5.5%	8.5%	2.7%	4.6%	6.7%	6.1%
cis-2-methylcyclohexanol	0.0%	1.8%	0.0%	0.0%	5.1%	1.4%	0.0%	0.0%	0.0%	1.6%	0.0%	0.0%	0.9%	0.9%	1.5%	3.1%	4.5%	4.3%	5.1%	5.7%	2.0%	1.1%
trans-2-methylcyclohexanol	0.0%	0.0%	0.0%	0.0%	3.1%	0.0%	0.0%	0.0%	0.0%	1.0%	0.0%	0.0%	0.9%	1.0%	1.5%	2.6%	3.8%	3.4%	6.0%	4.9%	1.8%	1.0%
Methylcyclohexanone	0.0%	1.3%	0.0%	0.0%	7.1%	2.3%	0.0%	0.0%	1.2%	3.4%	0.0%	0.0%	1.4%	1.3%	2.4%	3.5%	6.9%	8.9%	8.4%	8.1%	5.1%	4.0%
Phenol	2.7%	0.0%	3.4%	5.1%	8.8%	2.2%	0.0%	3.2%	21.8%	3.3%	2.5%	4.0%	13.8%	9.4%	9.1%	9.6%	10.5%	14.1%	13.1%	5.9%	20.6%	26.6%
o-cresol	11.9%	1.4%	7.7%	20.3%	12.2%	8.0%	4.6%	2.9%	4.2%	9.0%	8.1%	6.9%	31.4%	42.7%	40.7%	28.8%	26.5%	23.9%	39.5%	28.9%	30.3%	25.7%

Table C.3. Product yields from reacting o-cresol over various catalysts with H_2 as the reductant. This data table corresponds to fig. 7.7 and table 7.1.

Catalyst	10% Raney NiCu				10% Ni/ZrO2						10% Ni/Al2O3						No Cat			10% Raney NiCu + HCl					10% Raney NiCu + H2SO4					Oxi/Cal Raney 2800				
Time (min)	15	20	30	45	15	45	60	90	120	180	30	60	90	150	60	60	60	15	30	45	60	60	15	30	45	60	60	15	30	30	45	60	60	60
Molecule	Yield	Yield	Yield	Yield	Yield	Yield	Yield	Yield	Yield	Yield	Yield	Yield	Yield	Yield	Yield	Yield	Yield	Yield	Yield	Yield	Yield	Yield	Yield	Yield	Yield	Yield	Yield	Yield	Yield	Yield	Yield	Yield	Yield	Yield
CH4	11.3%	11.0%	7.9%	8.1%	0.3%	0.3%	0.9%	0.8%	1.2%	0.8%	0.5%	4.6%	7.5%	6.9%	11.4%	0.0%	0.0%	0.0%	0.0%	0.0%	0.0%	0.0%	0.0%	0.0%	0.0%	0.0%	0.0%	12.0%	18.6%	18.3%	20.4%	31.9%	33.8%	
CO2	5.2%	1.0%	0.7%	0.3%	0.0%	2.9%	0.6%	0.0%	0.0%	0.0%	0.0%	0.0%	0.3%	0.2%	0.2%	0.0%	0.0%	0.0%	0.0%	0.0%	0.0%	0.0%	0.0%	0.0%	0.0%	0.0%	0.0%	1.7%	3.2%	2.7%	3.1%	7.5%	4.9%	
C2H6	0.0%	0.0%	0.0%	0.0%	0.0%	0.0%	0.0%	0.0%	0.0%	0.0%	0.0%	0.0%	0.0%	0.0%	0.1%	0.0%	0.0%	0.0%	0.0%	0.0%	0.0%	0.0%	0.0%	0.0%	0.0%	0.0%	0.0%	0.2%	0.4%	0.4%	0.4%	0.7%	0.7%	
Cyclohexane	0.0%	1.2%	0.0%	0.0%	0.0%	0.0%	0.7%	0.0%	0.0%	0.0%	0.0%	2.7%	1.7%	6.2%	0.0%	0.0%	0.0%	0.0%	0.0%	0.0%	0.0%	0.0%	0.0%	0.0%	0.0%	0.0%	0.0%	3.2%	3.9%	4.2%	4.0%	6.5%	11.1%	
Benzene	0.0%	3.3%	2.0%	1.4%	0.0%	0.0%	0.7%	0.0%	0.0%	0.0%	0.0%	3.2%	7.4%	12.8%	0.0%	0.0%	0.0%	0.0%	0.0%	0.0%	0.0%	0.0%	0.0%	0.0%	0.0%	0.0%	0.0%	0.0%	0.0%	0.0%	0.0%	0.0%	0.0%	
Methylcyclohexane	0.0%	0.6%	0.0%	0.0%	0.0%	0.0%	0.0%	0.0%	0.0%	0.0%	0.0%	2.4%	1.6%	6.1%	0.0%	0.0%	0.0%	0.0%	0.0%	0.0%	0.0%	0.0%	0.0%	0.0%	0.0%	0.0%	0.0%	0.0%	0.0%	0.0%	0.0%	0.0%	0.0%	
Ethylcyclopentane	0.0%	0.0%	0.0%	0.0%	0.0%	1.8%	0.0%	0.0%	0.9%	0.0%	0.0%	3.6%	3.3%	5.0%	10.1%	0.0%	0.0%	0.0%	0.0%	0.0%	0.0%	0.0%	0.0%	0.0%	0.0%	0.0%	0.0%	0.0%	0.0%	0.0%	0.0%	0.0%	0.0%	
Toluene	0.0%	1.4%	0.7%	0.5%	0.0%	3.6%	0.0%	1.2%	0.0%	0.0%	0.0%	3.6%	3.3%	5.0%	10.1%	0.0%	0.0%	0.0%	0.0%	0.0%	0.0%	0.0%	0.0%	0.0%	0.0%	0.0%	0.0%	0.0%	0.5%	0.6%	0.5%	0.8%	1.3%	
Methylcyclohexene	0.0%	0.0%	0.0%	0.0%	0.0%	1.8%	0.0%	0.0%	0.0%	0.0%	0.0%	0.0%	0.0%	0.0%	0.0%	0.0%	0.0%	0.0%	0.0%	0.0%	0.0%	0.0%	0.0%	0.0%	0.0%	0.0%	0.0%	0.0%	0.0%	0.0%	0.0%	0.0%	0.0%	
Cyclohexanol	1.7%	12.5%	13.7%	11.1%	0.0%	1.5%	2.0%	3.2%	1.9%	1.1%	6.3%	9.7%	9.4%	8.5%	0.0%	0.0%	0.0%	0.0%	0.0%	0.0%	0.0%	0.0%	0.5%	0.5%	0.6%	0.0%	0.0%	5.3%	4.1%	6.9%	7.4%	4.7%	4.6%	
Cyclohexanone	3.7%	10.2%	10.6%	9.5%	0.0%	1.1%	0.9%	1.5%	0.8%	0.6%	2.0%	4.6%	3.8%	4.6%	0.0%	0.0%	0.0%	0.0%	0.0%	0.0%	0.0%	0.0%	0.0%	0.0%	0.0%	0.0%	0.0%	2.3%	2.5%	2.9%	3.3%	2.4%	1.3%	
cis-2-methylcyclohexanol	2.7%	10.6%	10.6%	9.3%	2.1%	8.1%	12.3%	17.0%	10.7%	11.8%	9.0%	6.6%	8.6%	4.5%	0.0%	0.0%	0.0%	0.0%	0.0%	0.0%	0.0%	0.0%	0.0%	0.0%	0.0%	0.0%	0.0%	2.2%	0.9%	2.5%	1.3%	0.5%	0.7%	
trans-2-methylcyclohexanol	1.4%	5.6%	6.1%	4.9%	1.3%	1.1%	3.7%	7.6%	9.3%	6.7%	5.8%	4.0%	5.3%	2.4%	0.0%	0.0%	0.0%	0.0%	0.0%	0.0%	0.0%	0.0%	0.0%	0.0%	0.0%	0.0%	0.0%	2.1%	0.8%	2.0%	1.0%	0.5%	0.7%	
2-methylcyclohexanone	10.4%	15.8%	16.3%	15.0%	2.7%	2.5%	13.2%	14.4%	21.1%	12.5%	12.0%	12.7%	14.8%	8.4%	0.0%	0.0%	0.0%	0.0%	0.0%	0.0%	0.0%	0.0%	0.0%	0.0%	0.0%	0.0%	0.0%	5.4%	3.0%	6.6%	3.3%	2.0%	1.8%	
2-methylcyclohexanone	0.0%	0.0%	0.0%	0.0%	1.2%	0.7%	0.0%	0.0%	0.0%	0.0%	0.0%	0.0%	0.0%	0.0%	0.0%	0.0%	0.0%	0.0%	0.0%	0.0%	0.0%	0.0%	0.0%	0.0%	0.0%	0.0%	0.0%	0.0%	0.0%	0.0%	0.0%	0.0%	0.0%	
Phenol	10.8%	2.6%	3.9%	3.1%	0.0%	0.0%	0.0%	0.0%	0.0%	0.0%	0.0%	3.4%	2.8%	3.3%	0.0%	0.0%	0.0%	0.0%	0.0%	0.0%	0.0%	0.0%	0.0%	0.0%	0.0%	0.0%	0.0%	8.9%	10.3%	11.1%	12.8%	14.4%	9.3%	
o-cresol (from rxn soln)	62.3%	21.2%	26.6%	19.6%	85.1%	86.1%	66.3%	72.4%	33.1%	59.9%	58.3%	45.6%	31.3%	27.2%	7.4%	99.8%	93.2%	95.3%	96.3%	99.2%	97.4%	97.7%	98.9%	97.6%	111.0%	93.9%	95.0%	94.0%	42.6%	35.8%	26.0%	26.4%	12.5%	17.4%
2,5-dimethylphenol	1.0%	0.0%	0.0%	0.0%	0.0%	0.0%	0.0%	0.0%	0.0%	0.0%	0.0%	0.0%	0.0%	0.0%	0.0%	0.0%	0.0%	0.0%	0.0%	0.0%	0.0%	0.0%	0.0%	0.0%	0.0%	0.0%	0.0%	0.0%	0.0%	0.0%	0.0%	0.0%	0.0%	

Table C.4. Product yields from reacting o-cresol over calcined Raney Ni with H_2 as the reductant. This data table corresponds to fig. 7.8. Average C balance = 94 ± 13%.

TOS (min)	0		45		90		135		180		225		270		315		360		405		450		495		540		585		630		675		720		765		810		855		900		945		990		1035		1080		1125		1170		1215		1260	
Molecule	**Yield**		**Yield**		**Yield**		**Yield**		**Yield**		**Yield**		**Yield**		**Yield**		**Yield**		**Yield**		**Yield**		**Yield**		**Yield**		**Yield**		**Yield**		**Yield**		**Yield**		**Yield**		**Yield**		**Yield**		**Yield**		**Yield**		**Yield**		**Yield**		**Yield**		**Yield**		**Yield**		**Yield**		**Yield**		**Yield**	
CH4	28.3%	----	----	----	34.3%	29.4%	----	----	----	----	----	----	----	----	----	----	----	----	----	----	----	----	----	----	----	----	----	----	----	----	----	37.7%	34.3%	41.6%	----	----	33.2%	32.8%	26.3%	----	----	30.5%	37.5%	32.1%						
CO2	0.0%	----	----	----	3.9%	3.8%	----	----	----	----	----	----	----	----	----	----	----	----	----	----	----	----	----	----	----	----	----	----	----	----	----	0.0%	0.0%	0.0%	----	5.7%	1.2%	3.5%	----	0.0%	0.0%	0.0%	0.0%						
C2H6	0.5%	----	----	----	0.5%	0.0%	----	----	----	----	----	----	----	----	----	----	----	----	----	----	----	----	----	----	----	----	----	----	----	----	----	0.0%	0.0%	0.0%	----	0.0%	0.0%	0.0%	----	0.0%	0.0%	0.5%	0.0%						
Butane	0.3%	0.2%	0.4%	0.7%	0.7%	0.3%	0.4%	0.2%	1.1%	0.4%	0.0%	0.3%	0.8%	0.5%	0.9%	0.8%	0.5%	0.6%	0.7%	0.5%	0.7%	0.6%	0.6%	0.6%	0.6%	0.6%	0.6%	0.6%	0.6%	0.6%	0.6%	0.7%	0.5%	0.6%	0.6%	0.6%	0.5%	0.6%	0.6%	0.6%	0.6%	0.6%	0.8%	0.6%						
2-methylbutane	0.3%	0.3%	0.4%	0.7%	0.4%	0.4%	0.4%	0.3%	0.8%	0.4%	0.2%	0.3%	0.8%	0.4%	0.8%	0.4%	0.2%	0.3%	0.8%	0.4%	0.4%	0.4%	0.5%	0.5%	0.5%	0.5%	0.5%	0.5%	0.5%	0.5%	0.5%	0.5%	0.4%	0.4%	0.4%	0.4%	0.4%	0.4%	0.4%	0.4%	0.5%	0.4%	0.4%	0.6%	0.5%	0.3%						
Unknown	0.8%	0.8%	0.8%	0.8%	1.4%	1.1%	1.4%	1.1%	1.1%	1.1%	1.1%	1.4%	1.4%	1.1%	1.4%	0.9%	0.8%	1.1%	1.1%	1.3%	1.6%	1.6%	1.1%	1.2%	1.3%	1.2%	1.3%	1.2%	1.2%	1.1%	1.1%	0.9%	1.1%	1.1%	1.0%	1.0%	1.0%	1.0%	1.2%	0.9%	1.3%	1.2%	0.9%	0.5%	0.3%						
Unknown	0.8%	0.8%	0.8%	0.8%	1.3%	1.1%	1.1%	1.1%	1.1%	1.1%	1.1%	1.1%	1.3%	0.9%	0.9%	0.7%	1.0%	1.4%	0.9%	1.0%	1.4%	0.9%	0.9%	0.9%	1.0%	1.0%	1.1%	1.1%	1.2%	0.9%	0.9%	0.8%	0.9%	0.8%	0.8%	0.8%	0.8%	0.8%	0.9%	0.7%	1.0%	1.0%	0.7%	0.5%	0.3%						
Hexane	1.1%	1.1%	1.0%	1.7%	1.7%	1.5%	1.5%	1.4%	1.5%	1.8%	1.2%	1.1%	1.4%	1.9%	1.4%	1.5%	1.7%	1.6%	1.5%	1.7%	1.8%	1.7%	1.7%	1.8%	1.7%	1.7%	1.7%	1.6%	1.5%	1.4%	1.4%	1.5%	1.4%	1.4%	1.4%	1.5%	1.3%	1.4%	1.5%	1.2%	1.7%	1.6%	1.4%	0.6%	0.3%						
Methylcyclopentane	1.0%	1.0%	1.1%	1.7%	1.7%	1.5%	1.3%	1.7%	1.8%	1.1%	1.4%	1.7%	1.9%	1.4%	1.7%	1.7%	1.7%	2.1%	1.3%	1.7%	1.5%	1.8%	1.8%	1.8%	1.7%	1.6%	1.8%	1.8%	1.8%	1.8%	1.8%	1.8%	1.8%	1.8%	1.7%	1.6%	1.7%	1.9%	1.8%	1.9%	1.8%	1.9%	1.8%	0.7%	0.4%						
Cyclohexane	5.7%	6.0%	5.8%	8.6%	8.6%	8.5%	7.4%	9.2%	8.7%	6.1%	7.9%	9.3%	10.2%	9.2%	9.4%	10.9%	7.1%	9.4%	9.0%	9.7%	9.4%	9.7%	9.1%	9.2%	9.9%	8.6%	10.0%	10.8%	10.2%	9.3%	9.2%	9.3%	9.2%	9.2%	9.2%	9.2%	9.2%	9.2%	9.2%	9.2%	9.2%	9.2%	9.2%	9.2%	9.2%						
Benzene	0.0%	0.0%	0.0%	0.0%	0.0%	0.0%	0.0%	0.0%	0.0%	0.0%	0.0%	0.0%	0.0%	0.0%	0.0%	0.0%	0.0%	0.0%	0.0%	0.0%	0.0%	0.0%	0.0%	0.0%	0.0%	0.0%	0.0%	0.0%	0.0%	0.0%	0.0%	0.0%	0.0%	0.0%	0.0%	0.0%	0.0%	0.0%	0.0%	0.0%	0.0%	0.0%	0.0%	0.0%	0.0%						
3-methylhexane	0.5%	0.6%	0.6%	0.5%	0.5%	0.7%	0.7%	0.7%	0.7%	0.7%	0.5%	0.5%	0.7%	0.8%	0.5%	0.7%	0.6%	0.7%	0.7%	0.7%	0.6%	0.5%	0.5%	0.5%	0.5%	0.5%	0.5%	0.5%	0.5%	0.5%	0.5%	0.5%	0.5%	0.5%	0.5%	0.5%	0.5%	0.5%	0.5%	0.5%	0.5%	0.5%	0.5%	0.5%	0.5%						
1,3-dimethylcyclopentane	0.5%	0.6%	0.6%	0.6%	0.7%	0.8%	0.6%	0.8%	0.8%	0.8%	0.7%	0.7%	0.8%	0.8%	0.8%	0.8%	0.7%	0.8%	0.8%	0.8%	0.8%	0.8%	0.8%	0.8%	0.8%	0.8%	0.8%	0.8%	0.8%	0.8%	0.8%	0.8%	0.8%	0.8%	0.8%	0.8%	0.8%	0.8%	0.8%	0.8%	0.8%	0.8%	0.8%	0.8%	0.8%						
1,3-dimethylcyclopentane	0.6%	0.7%	0.7%	0.9%	0.9%	0.9%	0.7%	0.9%	0.9%	1.0%	0.6%	0.8%	1.0%	0.9%	1.0%	1.1%	0.7%	1.0%	1.0%	1.0%	0.9%	1.0%	0.9%	0.9%	1.0%	0.9%	1.0%	1.0%	1.0%	1.0%	1.0%	1.0%	1.0%	1.0%	1.0%	1.0%	1.0%	1.0%	1.0%	1.0%	1.0%	1.0%	1.0%	1.0%	1.0%						
Methylcyclohexane	8.2%	9.4%	10.4%	11.4%	12.4%	9.4%	13.5%	14.2%	7.7%	12.9%	14.8%	13.5%	14.5%	14.2%	17.7%	10.6%	17.0%	13.3%	18.1%	15.2%	15.2%	16.6%	15.9%	15.9%	18.3%	14.3%	17.3%	17.1%	15.6%	14.8%	14.5%	14.8%	14.5%	14.2%	17.7%	10.6%	17.0%	13.3%	18.1%	15.2%	15.2%	16.6%	15.9%	15.9%	18.3%	14.3%	17.3%	17.1%	15.6%						
Ethylcyclopentane	0.3%	0.4%	0.4%	0.4%	0.5%	0.4%	0.5%	0.6%	0.4%	0.5%	0.6%	0.5%	0.5%	0.5%	0.5%	0.5%	0.5%	0.7%	0.5%	0.7%	0.5%	0.6%	0.6%	0.7%	0.7%	0.6%	0.7%	0.7%	0.7%	0.6%	0.6%	0.6%	0.6%	0.6%	0.7%	0.7%	0.7%	0.5%	0.7%	0.7%	0.6%	0.7%	0.7%	0.7%	0.7%	0.7%	0.7%	0.7%	0.5%						
3-methylcyclohexene	0.9%	1.0%	0.5%	0.7%	0.9%	0.8%	1.0%	0.8%	0.7%	0.9%	1.1%	1.0%	1.1%	1.1%	1.2%	0.8%	1.2%	1.1%	1.4%	1.3%	1.3%	1.3%	1.3%	1.3%	1.5%	1.2%	1.4%	1.4%	1.2%	1.2%	1.1%	1.2%	1.1%	1.1%	1.2%	1.2%	1.2%	1.1%	1.4%	1.2%	1.2%	1.3%	1.2%	1.2%	1.5%	1.2%	1.4%	1.4%	1.2%						
Toluene	2.1%	2.1%	1.5%	1.9%	2.2%	2.2%	2.2%	2.0%	2.2%	2.0%	2.3%	2.3%	2.1%	2.2%	2.2%	2.4%	2.6%	1.9%	1.7%	2.2%	2.1%	2.1%	2.1%	2.0%	2.0%	2.1%	2.4%	2.5%	1.8%	2.1%	2.1%	2.1%	2.1%	2.1%	2.2%	2.2%	2.2%	2.1%	2.2%	2.1%	2.1%	2.1%	2.1%	2.1%	2.0%	2.1%	2.4%	2.5%	1.8%						
1-methylcyclohexene	1.8%	1.9%	1.1%	1.5%	1.8%	1.6%	2.0%	1.7%	1.4%	1.8%	2.2%	2.0%	2.2%	2.2%	2.5%	1.6%	2.6%	2.2%	2.8%	2.6%	2.6%	2.8%	2.7%	2.6%	3.1%	2.4%	2.8%	2.9%	2.7%	2.2%	2.2%	2.2%	2.2%	2.2%	2.5%	1.6%	2.6%	2.2%	2.8%	2.6%	2.6%	2.8%	2.7%	2.6%	2.8%	2.4%	2.8%	2.9%	2.7%						
Cyclohexanol	0.0%	0.0%	0.0%	0.0%	0.0%	0.0%	0.0%	0.0%	0.0%	0.0%	0.0%	0.0%	0.0%	0.0%	0.0%	0.0%	0.0%	0.0%	0.0%	0.0%	0.0%	0.0%	0.0%	0.0%	0.0%	0.0%	0.0%	0.0%	0.0%	0.0%	0.0%	0.0%	0.0%	0.0%	0.0%	0.0%	0.0%	0.0%	0.0%	0.0%	0.0%	0.0%	0.0%	0.0%	0.0%	0.0%	0.0%	0.0%	0.0%						
Cyclohexanone	0.4%	0.4%	0.0%	0.3%	0.3%	0.3%	0.4%	0.4%	0.3%	0.4%	0.4%	0.4%	0.4%	0.4%	0.4%	0.4%	0.5%	0.4%	0.4%	0.4%	0.4%	0.4%	0.4%	0.5%	0.4%	0.5%	0.5%	0.5%	0.6%	0.4%	0.4%	0.4%	0.4%	0.4%	0.4%	0.4%	0.5%	0.4%	0.4%	0.4%	0.4%	0.4%	0.4%	0.5%	0.4%	0.5%	0.5%	0.5%	0.4%						
cis-2-methylcyclohexanol	0.8%	1.3%	0.3%	0.7%	1.0%	1.0%	1.4%	0.6%	0.4%	0.9%	1.2%	1.2%	1.1%	1.3%	1.5%	0.9%	0.8%	0.5%	0.8%	0.8%	0.6%	0.9%	1.0%	0.9%	0.9%	0.9%	0.9%	0.9%	1.1%	1.1%	1.2%	1.1%	1.2%	1.3%	1.5%	1.3%	1.3%	1.2%	1.5%	1.3%	1.3%	1.3%	1.3%	1.3%	1.3%	1.5%	1.2%	1.4%	1.2%						
trans-2-methylcyclohexanol	0.0%	0.2%	0.0%	0.0%	0.0%	0.0%	0.0%	0.2%	0.0%	0.0%	0.0%	0.0%	0.2%	0.2%	0.2%	0.2%	0.2%	0.0%	0.0%	0.0%	0.0%	0.0%	0.0%	0.2%	0.0%	0.0%	0.0%	0.0%	0.0%	0.0%	0.0%	0.0%	0.0%	0.0%	0.0%	0.0%	0.0%	0.0%	0.0%	0.0%	0.0%	0.0%	0.0%	0.0%	0.0%	0.0%	0.0%	0.0%	0.0%						
2-methylcyclohexanone	3.3%	3.7%	1.7%	2.5%	3.1%	3.2%	3.5%	2.6%	2.7%	2.9%	3.6%	3.6%	3.5%	3.7%	3.7%	3.1%	3.5%	3.0%	3.1%	3.6%	3.7%	3.5%	3.5%	3.7%	3.5%	3.7%	3.7%	3.8%	3.9%	4.2%	3.3%	3.9%	4.2%	4.1%	4.2%	4.2%	4.2%	4.2%	4.2%	4.2%	4.2%	4.2%	4.2%	4.2%	4.2%	4.2%	4.2%	4.2%	4.2%						
2-methylcyclohexanone	0.0%	0.0%	0.0%	0.0%	0.0%	0.0%	0.0%	0.0%	0.0%	0.0%	0.0%	0.0%	0.0%	0.0%	0.0%	0.0%	0.0%	0.0%	0.0%	0.0%	0.0%	0.0%	0.0%	0.0%	0.0%	0.0%	0.0%	0.0%	0.0%	0.0%	0.0%	0.0%	0.0%	0.0%	0.0%	0.0%	0.0%	0.0%	0.0%	0.0%	0.0%	0.0%	0.0%	0.0%	0.0%	0.0%	0.0%	0.0%	0.0%						
Phenol	0.0%	0.0%	0.0%	0.0%	0.0%	0.0%	0.0%	0.0%	0.0%	0.0%	0.0%	0.0%	0.0%	0.0%	0.0%	0.0%	0.0%	0.0%	0.0%	0.0%	0.0%	0.0%	0.0%	0.0%	0.0%	0.0%	0.0%	0.0%	0.0%	0.0%	0.0%	0.0%	0.0%	0.0%	0.0%	0.0%	0.0%	0.0%	0.0%	0.0%	0.0%	0.0%	0.0%	0.0%	0.0%	0.0%	0.0%	0.0%	0.0%						
o-cresol (from rxn soln)	11.8%	10.0%	19.2%	14.3%	11.9%	11.6%	9.9%	18.9%	18.8%	12.8%	13.5%	12.6%	13.1%	12.2%	11.2%	25.0%	22.6%	17.1%	15.9%	17.7%	17.6%	17.8%	20.5%	17.2%	18.8%	20.7%	25.8%	25.6%	17.6%	13.5%	12.6%	13.5%	12.6%	12.8%	13.1%	12.2%	11.2%	25.0%	22.6%	17.1%	15.9%	17.7%	17.6%	17.8%	20.5%	17.2%	18.8%	20.7%	25.8%	25.6%	17.6%					
2,5-dimethylphenol	0.0%	0.0%	0.0%	0.0%	0.0%	0.0%	0.0%	0.0%	0.0%	0.0%	0.0%	0.0%	0.0%	0.0%	0.0%	0.0%	0.0%	0.0%	0.0%	0.0%	0.0%	0.0%	0.0%	0.0%	0.0%	0.0%	0.0%	0.0%	0.0%	0.0%	0.0%	0.0%	0.0%	0.0%	0.0%	0.0%	0.0%	0.0%	0.0%	0.0%	0.0%	0.0%	0.0%	0.0%	0.0%	0.0%	0.0%	0.0%	0.0%	0.0%	0.0%	0.0%				

Table C.5. Product yields from reacting o-cresol over 10%, 0.5% NiCu/Al2O3 with H_2 as the reductant. This data table corresponds to fig. 7.9. Average C balance = 88 ± 23%.

TOS (min)	0	45	90	135	180	225	270	315	450	495	540	585	630	765	810	855	900	945	990	1035	1080	1125	1170	1215	1260	1305	1350
Molecule	**Yield**	**Yield**	**Yield**	**Yield**	**Yield**	**Yield**	**Yield**	**Yield**	**Yield**	**Yield**	**Yield**	**Yield**	**Yield**	**Yield**	**Yield**	**Yield**	**Yield**	**Yield**	**Yield**	**Yield**	**Yield**	**Yield**	**Yield**	**Yield**	**Yield**	**Yield**	**Yield**
CH4	5.7%	-----	7.9%	4.8%	4.9%	-----	4.9%	4.5%	2.5%	10.1%	7.3%	-----	4.7%	-----	3.9%	2.7%	3.7%	-----	3.1%	3.0%	4.0%	-----	5.3%	8.6%	7.1%	-----	5.8%
CO2	3.8%	-----	4.1%	0.9%	3.0%	-----	2.6%	2.4%	1.3%	8.7%	0.6%	-----	3.5%	-----	2.8%	2.1%	4.1%	-----	2.3%	2.3%	0.0%	-----	3.2%	2.9%	7.5%	-----	1.4%
C2H6	0.0%	-----	0.0%	0.0%	0.0%	-----	0.0%	0.0%	0.0%	0.0%	0.0%	-----	0.0%	-----	0.0%	0.0%	0.0%	-----	0.0%	0.0%	0.0%	-----	0.0%	0.0%	0.0%	-----	0.0%
Butane	0.0%	0.0%	0.0%	0.0%	0.0%	0.0%	0.0%	0.0%	0.0%	0.0%	0.0%	0.0%	0.0%	0.0%	0.0%	0.0%	0.0%	0.0%	0.0%	0.0%	0.0%	0.0%	0.0%	0.0%	0.0%	0.0%	0.0%
2-methylbutane	0.0%	0.0%	0.0%	0.0%	0.0%	0.0%	0.0%	0.0%	0.0%	0.0%	0.0%	0.0%	0.0%	0.0%	0.0%	0.0%	0.2%	0.0%	0.0%	0.0%	0.0%	0.0%	0.0%	0.0%	0.0%	0.0%	0.0%
Unknown	0.0%	0.0%	0.2%	0.6%	0.3%	0.3%	0.3%	0.4%	0.3%	0.3%	0.4%	0.3%	0.3%	0.2%	0.0%	0.0%	0.0%	0.0%	0.0%	0.0%	0.3%	0.2%	0.0%	0.0%	0.3%	0.0%	0.2%
Unknown	0.0%	0.0%	0.0%	0.0%	0.0%	0.0%	0.0%	0.0%	0.0%	0.0%	0.0%	0.0%	0.0%	0.0%	0.0%	0.0%	0.0%	0.0%	0.0%	0.0%	0.0%	0.0%	0.0%	0.0%	0.0%	0.0%	0.0%
Hexane	0.0%	0.0%	0.0%	0.0%	0.2%	0.0%	0.0%	0.3%	0.2%	0.2%	0.2%	0.0%	0.0%	0.3%	0.0%	0.0%	0.4%	0.0%	0.0%	0.0%	0.0%	0.5%	0.3%	0.0%	0.3%	0.0%	0.2%
Methylcyclopentane	0.3%	0.5%	0.4%	0.5%	0.6%	0.5%	0.6%	0.8%	0.7%	0.9%	0.8%	0.5%	0.6%	0.0%	0.2%	0.3%	6.1%	0.3%	0.4%	0.4%	0.5%	0.4%	0.0%	0.0%	0.7%	0.0%	0.5%
Cyclohexane	3.2%	4.8%	5.3%	3.9%	6.4%	5.3%	5.2%	7.6%	7.0%	9.3%	5.8%	4.5%	4.7%	3.0%	2.5%	3.1%	0.0%	4.0%	3.1%	3.0%	4.5%	3.3%	0.0%	5.1%	2.1%	3.6%	
Benzene	2.3%	3.5%	0.0%	3.0%	0.0%	0.0%	0.0%	0.0%	0.0%	0.0%	5.9%	3.2%	3.2%	2.2%	1.7%	0.0%	0.0%	0.0%	2.2%	0.0%	0.0%	2.4%	0.0%	6.2%	3.2%	4.8%	
3-methylhexane	0.0%	0.0%	0.0%	0.0%	0.0%	0.0%	0.0%	0.0%	0.0%	0.4%	0.0%	0.0%	0.0%	0.0%	0.0%	0.0%	0.0%	0.0%	0.0%	0.0%	0.0%	0.0%	0.0%	0.0%	0.0%	0.2%	
1,3-dimethylcyclopentane	0.0%	0.0%	0.0%	0.0%	0.0%	0.0%	0.0%	0.0%	0.0%	0.5%	0.0%	0.0%	0.0%	0.0%	0.0%	0.0%	0.0%	0.0%	0.0%	0.0%	0.0%	0.0%	0.0%	0.0%	0.0%	0.0%	
1,3-dimethylcyclopentane	0.0%	0.0%	0.0%	0.0%	0.0%	0.0%	0.0%	0.0%	0.0%	0.5%	0.0%	0.0%	0.0%	0.0%	0.0%	0.0%	0.0%	0.0%	0.0%	0.0%	0.0%	0.0%	0.0%	0.0%	0.0%	0.0%	
Methylcyclohexane	29.6%	39.2%	35.3%	28.9%	48.4%	43.4%	55.3%	58.3%	49.5%	80.0%	45.0%	33.0%	36.8%	46.5%	43.4%	50.8%	66.9%	44.5%	43.5%	66.8%	51.4%	42.4%	39.9%	49.9%	74.3%	32.7%	32.7%
Ethylcyclopentane	2.0%	2.0%	2.4%	1.1%	2.6%	2.7%	3.3%	3.5%	2.4%	3.1%	1.9%	1.5%	1.7%	2.7%	2.9%	3.2%	4.1%	3.0%	2.5%	4.1%	3.4%	3.2%	2.7%	2.6%	3.2%	1.0%	1.1%
3-methylcyclohexene	0.0%	0.0%	0.0%	0.0%	0.0%	0.0%	0.0%	0.0%	0.0%	0.0%	0.0%	0.0%	0.0%	0.0%	0.0%	0.0%	0.6%	0.0%	0.0%	0.0%	0.0%	0.5%	0.0%	0.0%	0.0%	0.0%	0.0%
Toluene	9.2%	13.4%	10.7%	12.2%	12.8%	9.3%	8.3%	11.6%	17.7%	35.5%	22.8%	15.4%	15.3%	17.0%	13.2%	10.0%	14.0%	11.1%	13.3%	7.7%	10.6%	11.7%	8.9%	14.3%	27.1%	11.9%	15.7%
1-methylcyclohexene	1.0%	0.9%	1.0%	0.0%	0.8%	0.6%	0.0%	0.5%	0.9%	0.9%	0.4%	0.3%	0.5%	1.1%	1.1%	0.8%	1.8%	1.3%	0.5%	0.4%	0.9%	1.6%	0.6%	0.0%	0.7%	0.8%	0.3%
Cyclohexanol	1.1%	0.7%	0.8%	0.3%	0.3%	0.4%	0.3%	0.4%	0.4%	0.4%	0.7%	0.6%	0.6%	0.7%	0.8%	0.3%	0.4%	0.0%	0.0%	0.0%	0.2%	0.5%	0.4%	0.0%	0.5%	0.6%	0.3%
Cyclohexanone	1.2%	0.7%	0.8%	0.3%	0.3%	0.4%	0.0%	0.3%	0.5%	0.5%	0.9%	0.6%	0.7%	0.8%	0.8%	0.3%	0.7%	0.4%	0.4%	0.0%	0.4%	1.0%	0.4%	0.0%	0.9%	1.4%	0.6%
cis-2-methylcyclohexanol	3.7%	2.6%	2.6%	1.0%	1.3%	1.3%	1.0%	1.0%	1.4%	1.7%	1.0%	0.8%	0.9%	2.4%	2.6%	1.1%	1.4%	0.6%	0.2%	0.0%	0.5%	1.2%	1.0%	2.8%	0.6%	0.7%	0.2%
trans-2-methylcyclohexanol	1.5%	1.0%	1.0%	0.4%	0.4%	0.4%	0.4%	0.4%	0.4%	0.6%	0.4%	0.3%	0.3%	0.9%	0.9%	0.3%	0.3%	0.0%	0.0%	0.0%	0.0%	0.2%	0.3%	0.0%	0.0%	0.0%	0.0%
2-methylcyclohexanone	4.9%	3.1%	3.5%	1.2%	1.6%	1.5%	0.8%	1.1%	2.1%	2.5%	1.6%	1.4%	1.5%	3.0%	3.0%	1.3%	2.8%	1.3%	0.7%	0.3%	1.1%	3.0%	1.2%	3.2%	1.3%	2.1%	0.5%
2-methylcyclohexanone	0.0%	0.0%	0.0%	0.0%	0.0%	0.0%	0.0%	0.0%	0.0%	0.0%	0.0%	0.0%	0.0%	0.0%	0.0%	0.0%	0.0%	0.0%	0.0%	0.0%	0.0%	0.0%	0.0%	0.0%	0.0%	0.0%	0.0%
Phenol	1.2%	0.0%	0.0%	0.0%	0.0%	0.0%	0.0%	0.0%	0.0%	0.0%	0.4%	0.0%	0.0%	0.7%	0.0%	0.0%	0.0%	0.0%	0.0%	0.0%	0.0%	0.0%	0.0%	0.0%	0.0%	8.7%	1.4%
o-cresol (from rxn soln)	6.5%	2.0%	2.1%	1.1%	0.5%	0.3%	0.0%	1.4%	1.7%	1.8%	1.2%	1.1%	2.2%	1.2%	0.4%	1.0%	0.4%	0.5%	0.0%	0.3%	1.5%	0.3%	2.3%	1.2%	22.0%	2.5%	
2,5-dimethylphenol	0.0%	0.0%	0.0%	0.0%	0.0%	0.0%	0.0%	0.0%	0.0%	0.0%	0.0%	0.0%	0.0%	0.0%	0.0%	0.0%	0.0%	0.0%	0.0%	0.0%	0.0%	0.0%	0.0%	0.0%	0.0%	0.5%	0.0%

Table C.6. Product yields from reacting o-cresol over calcined 5% Raney NiCu with H_2 as the reductant. This data table corresponds to fig. 7.9. Average C balance = 86 ± 6%.

TOS (min)	0		45		90		135		180		225		270		315		360		757		802		847		892		937		982		1027		1072		1117		1162		1207		1252		1297		1342
Molecule	**Yield**		**Yield**		**Yield**		**Yield**		**Yield**		**Yield**		**Yield**		**Yield**		**Yield**		**Yield**		**Yield**		**Yield**		**Yield**		**Yield**		**Yield**		**Yield**		**Yield**		**Yield**		**Yield**		**Yield**		**Yield**		**Yield**		**Yield**		**Yield**	
CH4	60.5%	47.9%	-----	-----	18.0%	35.7%	-----	32.9%	-----	18.3%	23.8%	-----	19.4%	13.6%	15.8%	-----	17.2%	14.3%	15.2%	-----	14.0%	14.9%	16.4%																						
CO2	1.9%	3.7%	-----	-----	0.8%	2.5%	-----	1.9%	-----	0.5%	1.7%	-----	0.9%	0.0%	0.0%	-----	0.0%	1.4%	0.9%	-----	0.0%	0.0%	0.0%																						
C2H6	0.6%	0.4%	-----	-----	0.0%	0.0%	-----	0.0%	-----	0.0%	0.0%	-----	0.0%	0.0%	0.0%	-----	0.0%	0.0%	0.0%	-----	0.0%	0.0%	0.0%																						
Butane	0.6%	0.3%	0.3%	0.0%	0.3%	0.6%	0.2%	0.5%	0.3%	0.5%	0.2%	0.3%	0.3%	0.2%	0.3%	0.3%	0.3%	0.3%	0.4%	0.4%	0.2%	0.3%	0.0%																						
2-methylbutane	0.6%	0.2%	0.2%	0.0%	0.2%	0.4%	0.2%	0.4%	0.2%	0.3%	0.0%	0.0%	0.0%	0.0%	0.0%	0.0%	0.0%	0.0%	0.0%	0.0%	0.0%	0.0%	0.0%																						
Unknown	1.3%	0.5%	0.5%	0.0%	0.7%	0.9%	0.6%	0.9%	0.8%	1.1%	0.7%	0.7%	0.8%	0.8%	0.9%	0.8%	0.8%	0.8%	1.0%	1.0%	0.7%	0.8%	0.6%																						
Unknown	1.0%	0.3%	0.4%	0.6%	0.4%	0.7%	0.5%	0.7%	0.5%	0.5%	0.4%	0.3%	0.4%	0.4%	0.4%	0.3%	0.3%	0.4%	0.4%	0.4%	0.3%	0.4%	0.3%																						
Hexane	1.1%	0.4%	0.5%	0.8%	0.6%	0.8%	0.6%	0.8%	0.6%	0.9%	0.7%	0.7%	0.7%	0.7%	0.9%	0.8%	0.8%	0.9%	0.9%	0.9%	0.4%	0.4%	0.3%																						
Methylcyclopentane	1.6%	0.6%	1.0%	1.6%	1.2%	1.4%	1.1%	1.4%	1.5%	2.0%	1.5%	1.5%	1.6%	1.5%	1.8%	1.6%	1.8%	1.8%	1.8%	1.8%	1.6%	1.8%	1.5%																						
Cyclohexane	10.2%	4.3%	6.6%	10.9%	7.7%	9.0%	7.9%	9.6%	10.2%	13.1%	11.2%	9.6%	10.7%	10.0%	11.9%	10.5%	10.9%	11.7%	11.6%	14.0%	10.5%	11.1%	9.5%																						
Benzene	0.5%	0.0%	0.0%	0.0%	0.0%	0.0%	0.0%	0.0%	0.0%	0.0%	0.0%	0.0%	0.0%	0.0%	0.0%	0.0%	0.0%	0.0%	0.0%	0.0%	0.0%	0.0%	0.0%																						
3-methylhexane	0.0%	0.0%	0.0%	0.6%	0.4%	0.4%	0.3%	0.4%	0.4%	0.4%	0.4%	0.3%	0.4%	0.4%	0.4%	0.3%	0.4%	0.4%	0.4%	0.4%	0.0%	0.0%	0.0%																						
1,3-dimethylcyclopentane	0.5%	0.0%	0.4%	0.7%	0.6%	0.5%	0.4%	0.5%	0.5%	0.7%	0.5%	0.5%	0.6%	0.6%	0.6%	0.4%	0.4%	0.0%	0.7%	0.8%	0.6%	0.7%	0.6%																						
1,3-dimethylcyclopentane	0.5%	0.0%	0.5%	0.9%	0.7%	0.5%	0.5%	0.5%	0.6%	0.8%	0.7%	0.8%	0.7%	0.7%	0.6%	0.6%	0.7%	0.8%	0.8%	0.9%	0.7%	0.8%	0.7%																						
Methylcyclohexane	15.8%	12.4%	24.0%	29.7%	32.7%	20.4%	17.3%	21.7%	27.1%	32.4%	29.1%	30.9%	30.7%	35.8%	38.2%	33.5%	39.4%	40.8%	35.5%	39.2%	35.8%	38.3%	37.6%																						
Ethylcyclopentane	0.7%	0.7%	1.5%	1.7%	1.9%	1.2%	1.1%	1.3%	1.5%	1.8%	1.6%	1.8%	1.8%	2.1%	2.2%	1.9%	2.2%	2.3%	2.0%	2.3%	2.1%	2.2%	2.2%																						
3-methylcyclohexene	0.0%	0.0%	0.0%	0.4%	0.0%	0.0%	0.0%	0.0%	0.4%	0.0%	0.0%	0.4%	0.0%	0.6%	0.6%	0.6%	0.7%	0.8%	0.7%	0.6%	0.7%	0.7%	0.6%																						
Toluene	2.7%	1.7%	3.3%	4.8%	2.6%	4.1%	3.9%	4.3%	4.5%	4.6%	4.3%	3.6%	4.4%	3.6%	4.3%	4.2%	3.8%	4.3%	4.2%	5.3%	4.2%	4.1%	3.7%																						
1-methylcyclohexene	0.0%	0.0%	0.9%	1.3%	1.0%	0.9%	0.8%	1.0%	1.4%	1.1%	1.3%	1.4%	1.4%	2.0%	2.0%	2.0%	2.0%	2.6%	2.2%	2.2%	2.4%	2.1%	2.6%																						
Cyclohexanol	0.0%	0.3%	0.4%	0.4%	0.4%	0.4%	0.3%	0.4%	0.4%	0.7%	0.6%	0.6%	0.6%	0.6%	0.7%	0.8%	0.6%	0.8%	0.7%	0.8%	0.8%	0.7%	0.7%																						
Cyclohexanone	0.0%	0.3%	0.7%	0.5%	0.3%	0.6%	0.5%	0.5%	0.6%	0.7%	1.4%	2.0%	2.0%	1.8%	1.8%	2.6%	2.0%	1.9%	1.9%	2.3%	2.2%	2.0%	2.2%																						
cis-2-methylcyclohexanol	0.2%	0.9%	2.1%	1.4%	2.5%	1.1%	1.0%	1.1%	1.3%	2.0%	0.3%	0.5%	0.5%	0.3%	0.4%	0.7%	0.4%	0.3%	0.4%	0.5%	0.4%	0.4%	0.4%																						
trans-2-methylcyclohexanol	0.0%	0.3%	0.6%	0.3%	0.8%	0.3%	0.2%	0.2%	0.3%	0.6%	2.2%	2.8%	2.8%	3.1%	3.0%	3.4%	3.0%	3.7%	3.4%	3.6%	3.7%	3.2%	3.7%																						
2-methylcyclohexanone	0.3%	0.9%	2.8%	2.3%	2.4%	1.9%	1.7%	2.1%	2.4%	2.7%	0.0%	0.0%	0.0%	0.0%	0.0%	0.0%	0.0%	0.0%	0.0%	0.0%	0.0%	0.0%	0.0%																						
2-methylcyclohexanone	0.0%	0.0%	0.0%	0.0%	0.0%	0.0%	0.0%	0.0%	0.0%	0.0%	0.0%	0.0%	0.0%	0.0%	0.0%	0.0%	0.0%	0.0%	0.0%	0.0%	0.0%	0.0%	0.0%																						
Phenol	0.0%	0.0%	1.4%	0.0%	0.0%	0.0%	0.0%	0.0%	0.0%	0.0%	0.0%	0.0%	0.0%	0.0%	0.0%	0.0%	0.0%	0.0%	0.0%	0.0%	0.0%	0.0%	0.0%																						
o-cresol (from rxn soln)	0.0%	0.5%	3.0%	1.2%	1.0%	2.0%	1.3%	1.3%	0.9%	1.5%	0.8%	1.1%	1.3%	1.1%	1.2%	1.6%	0.9%	1.4%	1.4%	1.7%	1.6%	1.1%	1.3%																						
2,5-dimethylphenol	0.0%	0.0%	0.0%	0.0%	0.0%	0.0%	0.0%	0.0%	0.0%	0.0%	0.0%	0.0%	0.0%	0.0%	0.0%	0.0%	0.0%	0.0%	0.0%	0.0%	0.0%	0.0%	0.0%																						

References

1. J. G. Dickinson, P. E. Savage, J. Mol. Catal. A: Chem. (2013)
2. D. C. Elliott, L. J. Sealock Jr, E. G. Baker, Ind. Eng. Chem. Res. 32, (1993) 1542-1548.
3. S. Sitthisa, T. Pham, T. Prasomsri, T. Sooknoi, R. G. Mallinson, D. E. Resasco, J. Catal. 280, (2011) 17-27.
4. C. A. Mullen, A. A. Boateng, N. M. Goldberg, I. M. Lima, D. A. Laird, K. B. Hicks, Biomass Bioenerg. 34, (2010) 67-74.
5. A. B. Ross, P. Biller, M. L. Kubacki, H. Li, A. Lea-Langton, J. M. Jones, Fuel 89, (2010) 2234-2243.
6. S. J. Choe, H. J. Kang, S. Kim, S. Park, D. H. Park, D. S. Huh, Bull. Korean Chem. Soc. 26, (2005) 1682.
7. M. P. Andersson, F. Abild-Pedersen, I. N. Remediakis, T. Bligaard, G. Jones, J. Engbæk, O. Lytken, S. Horch, J. H. Nielsen, J. Sehested, J. Catal. 255, (2008) 6-19.
8. M. S. Wainwright, R. B. Anderson, J. Catal. 64, (1980) 124-131.
9. G. W. Huber, J. W. Shabaker, J. A. Dumesic, Science 300, (2003) 2075.
10. J. W. Shabaker, G. W. Huber, J. A. Dumesic, J. Catal. 222, (2004) 180-191.
11. J. W. Shabaker, D. A. Simonetti, R. D. Cortright, J. A. Dumesic, J. Catal. 231, (2005) 67-76.
12. P. M. Mortensen, J. D. Grunwaldt, P. A. Jensen, A. D. Jensen, ACS Catal. 3, (2013) 1774-1785.
13. C. Zhao, Y. Kou, A. A. Lemonidou, X. Li, J. A. Lercher, Chemical Communications 46, (2010) 412-414.
14. W. C. Cheng, L. J. Czarnecki, C. J. Pereira, Ind. Eng. Chem. Res. 28, (1989) 1764-1767.
15. C. Zhao, S. Kasakov, J. He, J. A. Lercher, J. Catal. 296, (2012) 12-23.
16. W. L. Suchanek, J. Am. Ceram. Soc. 93, (2010) 399-412.

Chapter 8

Conclusions, Impacts, and Future Work

Chapters 4-7 provide the details of the work completed during this dissertation. Significant progress was achieved on several fronts, and with this progress, new questions have arisen and several promising areas of research have been uncovered.

8.1. Conclusions

In chapter 4, we performed a detailed analysis of the composition of bio-oil, and determined the effect of solvent. In this study, we collected and analyzed the gas, crude bio-oil, dissolved aqueous solids, and insoluble residual solids product fractions arising from the hydrothermal liquefaction of *Nannochloropsis* sp. at 350 °C for 60 min. Most of the carbon and hydrogen in the algal biomass appears in the crude bio-oil product, as desired. A majority of the original nitrogen appears as ammonia in the aqueous phase. We also determined how the solvent used to recover the crude bio-oil affected the yields and compositions of the product fractions. We used both non-polar solvents (hexadecane, decane, hexane, cyclohexane) and polar solvents (methoxycyclopentane, dichloromethane, and chloroform). Hexadecane and decane provided the highest gravimetric yields of bio-oil (39 ± 3 wt % and 39 ± 1 wt % respectively), but these crude bio-oils had a lower carbon content (69 wt % for decane) than did those recovered with polar solvents such as chloroform (74 wt %) and dichloromethane (76 wt %). We quantified the amount of 19

different individual molecular components in the crude bio-oil for the first time. Fatty acids were the most abundant components, but some aromatic and S- and N-containing compounds were also quantified. This work, and the work of others [1], identified that cyclic and aromatic molecules were often the carriers of S, N, and O in HTL bio-oils.

Using the above information about the oxygen-containing molecules in HTL bio-oils, we next shifted our focus to the hydrothermal HDO of benzofuran, a model compound chosen for its heterocyclic and aromatic characteristics. In chapter 5, we examined the hydrothermal HDO of benzofuran over a Pt/C catalyst. The Pt/C catalyst was chosen because, at the time, noble metals on carbon supports were the only known active and stable catalysts for hydrothermal HDO [2-7]. We examined the effect of batch-holding time, water loading, hydrogen loading, and catalyst loading on the reaction products. Increasing the water loading or decreasing the hydrogen loading decreased the selectivity to aromatic deoxygenated products (e.g. ethylbenzene) and increased the selectivity to hydrogenated deoxygenated products (e.g. ethylcyclohexane). Combining the results from these benzofuran experiments with results obtained in separate experiments with the reaction intermediates as the starting reagents allowed for the development of the hydrothermal HDO reaction network for benzofuran. The reaction network provided a foundation for a quantitative kinetic model that correlated the experimental results. The model showed that the experimental results were consistent with benzofuran having an inhibitory effect on the deoxygenation of ethylphenol to ethylbenzene. Furthermore, the kinetic model provided industrially relevant information because it provided an accurate fit to reaction data collected under a variety of reaction conditions, including reactions that achieved a high conversion and high yield of liquid hydrocarbons.

In chapter 6, we desired to develop an active and stable non-noble metal catalyst for the hydrothermal HDO of o-cresol, another model oxygenated bio-oil molecule, because of the high cost of noble metals. We determined the stability, activity, and selectivity of Pt/C, $Ni/SiO_2Al_2O_3$, Raney Ni 2800, and 10% Raney NiCu for the hydrothermal HDO of o-cresol at 380 °C. We also demonstrate the feasibility of using a renewable chemical, formic acid, for the in situ production of the H_2 needed for HDO. Pt/C, Raney Ni, and Raney NiCu were stable in supercritical water, but only Pt/C and Raney NiCu were selective to deoxygenated products. The Raney NiCu catalyst provided a 3.4 fold increase in yield of liquid hydrocarbons when compared with the Raney Ni catalyst by decreasing the C-C bond hydrogenolysis (i.e., gasification) activity. The Raney NiCu catalyst was stable throughout the 24 hr time on stream that was examined and was a promising catalyst for further study and optimization. This finding is significant because it provided an avenue for reducing the cost of stable and active HDO catalysts for hydrothermal HDO of bio-oils, as Ni is ~3000 times less expensive than Pt.

Chapter 7 expanded on the work with Raney NiCu in chapter 6 and explored the effect of Cu loading on the reaction products and selectivities. Raney Ni catalysts doped with greater than 10 wt% Cu showed a significant reduction in gasification activity, and produced a higher yield of liquid products than the unmodified Raney Ni catalyst. Adding Cu did not, however, increase the yield of the desired HDO products, liquid hydrocarbons. The addition of acid sites to the catalysts, by supporting Ni and NiCu on Al_2O_3 and by calcining the Raney Ni to produce Al_2O_3 within the catalyst, however, did significantly increase the HDO activity of the catalysts such that yields of liquid hydrocarbons exceeded 60%. Two catalysts, a novel calcined 5% Raney NiCu catalyst and a $NiCu/Al_2O_3$ catalyst,

produced the highest liquid hydrocarbon yields to date (~70%) for stable, non-noble-metal, hydrothermal HDO catalysts.

8.2. Impacts

This dissertation contains several findings of significance. First, in chapter 4, we provided the first account where the composition of all of the product fractions from HTL of microalgae were analyzed. Furthermore, we showed that the choice of solvent and workup procedures had an effect on the bio-oil yield from the HTL of microalgae. This is an important finding, as it is necessary to realize that small differences in bio-oil yield may not be the result of the HTL processing conditions or microalgae species used, but rather a function of the post reaction work up used. This work also provided further information on the molecular composition of the microalgal bio-oil by identifying light ends with GC/MS and heavy products with EI MS. Identification of these fractions of bio-oil may spur future research that seeks to turn them into useful fuels and chemicals.

Second, in chapter 5, we performed the first hydrothermal HDO study of benzofuran. Within this study, we determined the reaction network and associated kinetics for HDO. The kinetic analysis was performed over a wide range of conversions and yields, thereby providing industrially relevant information to future researchers. Furthermore, we showed that the liquid hydrocarbon selectivity (i.e., aromatic or hydrodrogenated) can be altered by changing both the water and hydrogen loading in the reactor. Both of these methods provide future researchers a further means of tailoring the reaction conditions to produce desired products.

Third, in chapters 6 and 7, we developed the first stable non-noble metal hydrothermal HDO catalysts. In particular, we identified and developed two catalysts, a calcined 5% Raney NiCu catalyst and a 10%, 0.5% NiCu/Al_2O_3 catalyst, that achieved a high (~70%) and stable yield of liquid hydrocarbons over a 24 hr TOS reaction. The development of low-cost catalysts such as these is essential to producing fungible liquid transportation fuels from bio-oils. Furthermore, beyond the simple identification of these active and stable catalysts, we also developed two techniques for tuning the reaction selectivity for hydrothermal HDO: the addition of Cu and the addition of acid sites (i.e., Al_2O_3). With this knowledge, future researchers can use these techniques to tune the reaction selectivity to meet their needs.

8.3. Future work

The discussion above shows the significant progress made during this dissertation. Below we discuss the areas of research that may be fruitful for future researchers to pursue.

At the present time, the calcined 5% Raney NiCu catalytic surface is not well understood, and progress could be made in this area with further catalyst characterization and reaction studies. For example, characterization techniques such as N_2 physisorption to obtain the Brunauer-Emmet-Teller (BET) surface area and temperature programmed reduction (TPR) may reveal how the surface of the catalysts changes when the synthesis steps such as calcination or Cu addition are performed. Further, the nature and quantity of the acid sites on the calcined Raney Ni catalyst should be probed using techniques such as NH_3 TPD and pyridine adsorbed infrared (IR) spectroscopy [8]. In particular, pyridine IR spectroscopy distinguishes between Brønsted acid sites and Lewis acid sites, and these

results, combined with further reaction results may provide insights into the exact reaction mechanism for HDO. Often such insights can spur further development of more active catalysts.

Beyond the titration experiments discussed above, several other ex situ characterization techniques would also provide new insights into the calcined Raney Ni and Raney NiCu catalysts. At present, we have several characterization techniques that indicate that the Ni and Cu in Raney NiCu catalysts form an alloy. The exact nature of this interaction it is unclear, however. Mossbauer spectroscopy and x-ray photoelectron spectroscopy (XPS) would elucidate this interaction further by revealing the coordination number of the Cu atoms in the alloy, and by revealing changes in coordination number that may occur with increasing Cu content in the catalysts.

The experiments described above are all ex situ characterization experiments, and they would reveal little about the morphology of the catalyst surface under reaction conditions. With the construction of a proper reaction cell, it should possible to perform x-ray absorption spectroscopy (XAS) on the catalyst during a hydrothermal HDO reaction. This technique should provide insights as to the oxidation state and morphology of the catalyst surface during the reaction. Further, in situ Raman spectroscopy could provide information on the organic species present in the reaction. This technique would provide insights on short-lived chemical species and, potentially, the transition state of the rate-limiting step in the HDO reaction. These results cannot be obtained with the current techniques employed because the reaction products are not analyzed until they leave the reactor, making the detection of short-lived chemical species impossible. These characterization results, when combined with experimental reaction results could allow

future researchers to find even more active catalysts and explain, at a mechanistic level, why these catalysts are active.

Aside from the characterization studies discussed above, numerous reaction and synthesis experiments need to be performed. In chapter 7, we discussed the two techniques developed for tuning the activity and selectivity of the Raney Ni catalysts: The addition of the acid sites and the addition of Cu. Ideally, both of these parameters should tuned to obtain a high HDO activity and selectivity. These experiments would require the in-house synthesis of Raney Ni catalysts to control the Al content of the catalysts. Once the Al content of the Raney Ni is closely controlled, then a study of the conversion of Al to Al_2O_3 should be performed to understand the calcination conditions necessary to fully or partially convert Al to Al_2O_3. In fact, it may be easier to use a hydrothermal environment, instead of calcination in air, to perform this conversion [9].

Al_2O_3 could also be added to the catalyst by means that may provide more control over the deposition, such as atomic layer deposition (ALD) [10-12]. We performed Al_2O_3 ALD on a 10% Raney NiCu catalyst and tested the catalyst using the 4.1 mL batch reactors. We did not see a significant increase in the production of liquid hydrocarbons when compared to the uncoated 10% Raney NiCu. Unfortunately, we did not have time to pursue this technique in great detail, but it may still provide significant results. Future experiments could use this technique and vary the number Al_2O_3 layers deposited, the dosage time, and the post ALD calcination conditions. All of these variables have been shown to affect the morphology of the deposited Al_2O_3 [10-12].

Along with the tuning of the Cu and Al_2O_3 content of the catalysts, it would be useful to use several active catalysts for the hydrothermal HDO of other common oxygen-

containing bio-oil compounds such as free fatty acids and guaiacols. Such a study could provide useful information about the kinetics of the HDO for these molecules. Furthermore, these studies may elucidate the catalyst deactivation mechanisms that may arise. Last, these catalysts should be tested with bio-oil feeds to assess their activity and stability under industrial conditions. Such work may provide information as to the feasibility of using these catalysts, and potential causes of deactivation.

Beyond the use of Cu, other dopant metals could be used to change the selectivity of the Raney Ni catalyst. For example, Re has been shown to have an affinity of -OH functional groups and help increase the dehydration activity of the catalysts [13], and Sn has been shown to modify the activity of Raney Ni [14]. We encourage future researchers to examine these metals and others to find more active and stable hydrothermal HDO catalysts.

The reaction experiments and catalyst characterization described above may help future researchers understand why certain catalysts are active, but these techniques do not have a predictive ability to determine if a catalyst will be active prior to testing. In order to rationally design catalysts, we must fully understand the reaction on the catalyst surface and have a method to screen through possible catalysts prior to synthesizing them. Great strides have been made recently with density functional theory (DFT) that are making this rational catalyst design possible. We suggest that future researchers develop DFT models for common oxygen-containing bio-oil compounds on catalysts, such as those discussed above, that are known to be active. It is essential that these models account for the effect water adsorbed to the surface, because, as we showed in chapter 5, water can affect the reaction products. Work has already begun and this field [15], and we suggest that future researchers devote significant effort in this area as it has great potential.

References

1. A. B. Ross, P. Biller, M. L. Kubacki, H. Li, A. Lea-Langton, J. M. Jones, Fuel 89, (2010) 2234-2243.
2. J. Fu, X. Lu, P. E. Savage, Energy Environ. Sci. 3, (2010) 311-317.
3. J. Fu, X. Lu, P. E. Savage, ChemSusChem 4, (2011) 481-486.
4. C. Zhao, Y. Kou, A. A. Lemonidou, X. Li, J. A. Lercher, Angew. Chem. 121, (2009) 4047-4050.
5. C. Zhao, Y. Kou, A. A. Lemonidou, X. Li, J. A. Lercher, Chemical Communications 46, (2010) 412-414.
6. C. Zhao, J. He, A. A. Lemonidou, X. Li, J. A. Lercher, J. Catal. 280, (2011) 8-16.
7. C. Zhao, J. A. Lercher, ChemCatChem 4, (2012) 64-68.
8. C. Zhao, Y. Yu, A. Jentys, J. A. Lercher, Appl. Catal. B: Environ. 132, (2013) 282-292.
9. W. L. Suchanek, J. Am. Ceram. Soc. 93, (2010) 399-412.
10. C. P. Canlas, J. Lu, N. A. Ray, N. A. Grosso-Giordano, S. Lee, J. W. Elam, R. E. Winans, R. P. Van Duyne, P. C. Stair, J. M. Notestein, Nature chemistry (2012)
11. H. Feng, J. Lu, P. C. Stair, J. W. Elam, Catal. Lett. 141, (2011) 512-517.
12. J. Lu, B. Liu, J. P. Greeley, Z. Feng, J. A. Libera, Y. Lei, M. J. Bedzyk, P. C. Stair, J. W. Elam, Chem. Mater. 24, (2012) 2047-2055.
13. E. L. Kunkes, D. A. Simonetti, R. M. West, J. C. Serrano-Ruiz, C. A. Gärtner, J. A. Dumesic, Science 322, (2008) 417.
14. G. W. Huber, J. W. Shabaker, J. A. Dumesic, Science 300, (2003) 2075.
15. M. Salciccioli, Y. Chen, D. G. Vlachos, The Journal of Physical Chemistry C 114, (2010) 20155-20166.